PALEOENVIRONMENTAL RECONSTRUCTION OF PREHISTORIC SUBMERGED SHORELINES AND COASTAL ENVIRONMENTS AT LIMAN TEPE/ KLAZOMENAI, TURKEY

By

GILLIAN M. KREZOSKI, B.A.

A thesis submitted to the School of Graduate Studies in partial fulfillment of the requirements for the degree Master of Science

McMaster University

MASTER OF SCIENCE (2006) McMaster University

Department of Geography and Earth Science Hamilton, Ontario

TITLE: Paleoenvironmental Reconstruction of Pre-Historic Submerged Shorelines and Coastal Environments at Liman Tepe/ Klazomenai, Turkey

AUTHOR: Gillian M. Krezoski, B.A. (University of Wisconsin, Eau Claire)

SUPERVISOR: Dr. Joe I. Boyce

NUMBER OF PAGES: xvii, + 139 pages

Abstract

Rising post-glacial sea levels since the last glacial maximum have dramatically changed the configuration of coastal areas worldwide. On the western Anatolian coast of Turkey, rising Holocene sea levels and tectonic subsidence have drowned large areas of coastal and terrestrial landscapes that were once occupied by Neolithic peoples. These submerged landscapes have high potential for well-preserved Neolithic sites, but to date few systematic attempts have been made to investigate the prehistoric underwater archaeology. Further exploration for these sites is dependent on an improved understanding of the coastal paleogeography, sea level history and shoreline positions during prehistory.

In this study, detailed coastal geoarchaeological investigations were conducted at Liman Tepe/Klazomenai, a long-occupied (Chalcolithic-Roman Age) coastal settlement near Izmir, Turkey, to reconstruct changes in the prehistoric coastal environments and to document coastal impacts associated with the construction of a Hellenistic causeway structure. Detailed sedimentological (lithofacies, grain size, magnetic susceptibility, loss on ignition), geochemical (trace metals) and micropaleontological analysis was conducted on five cores extracted from the Bay of Izmir. Core data were integrated with the results of a detailed marine geophysical survey (bathymetry, side-scan sonar, chirp seismic profiling) to reconstruct the shoreline positions from the Late Neolithic (ca. 4000 BC) to the present.

The core results identified five distinct lithostratigraphic units (Units A-E), recording the development of transgressive barrier-lagoonal system prior to ca. 3800 BC

and progradation of the coast during a subsequent high-stand phase after ca. 2800 BC. The transgressive barrier-lagoonal system is represented by a fining-upwards sequence of pebbly foreshore deposits (Unit E) overlain by laminated, organic-rich muds deposited in shallow wetland and lagoonal environments (Units C,D). The transition from beach to lagoonal sediments is represented in seismic profiles by a basin-wide, high-amplitude seismic reflector. Mapping of the reflector surface identifies the beach deposits as a linear, northeast-trending beach barrier ridge. ^{14}C dating of organics from Unit E yielded a Late Neolithic Age (3860 +/- 120 cal BC) for the beach deposits.

At the top of the lagoonal sequence a sharp transition to muddy silt lithofacies (Unit B) with abundant *Posidonia Oceanica* fragments records sediment accumulation with a sheltered embayment formed by construction of a causeway commissioned by Alexander the Great (334 BC). The onset of causeway construction (Phase 3) is indicated by a shift to coarser mean grain size, the appearance of pottery and masonry and abundant olive pits which yielded a ^{14}C date of 450 ± 70 cal BC, confirming the early Hellenistic age for the causeway. The causeway construction dramatically altered the coastal sediment budget, contributing to accelerated sedimentation and rapid progradation of the coastline. An increase in the abundances of *Bolivinid* and *Rodalinid* genera below the causeway construction horizon indicates increasing eutrophication of coastal waters as Archaic populations increased at Klazomenai. The detailed record of changing coastal environments and shoreline configurations obtained through this study provide important baseline data for future underwater archaeological exploration at Liman Tepe/Klazomenai.

Acknowledgements

Funding for this research was provided by an NSERC grant to Dr. Joe Boyce. Additional funds for the final research project were provided by a United Nations Bursary – Hamilton chapter. Special thanks to Ankara University (Turkey) and Haifa University (Israel) for providing logistical support, including transportation, boats, student helpers, housing and food.

Primary thanks go to Dr. Joe Boyce, a thoughtful and thorough individual who bestowed much appreciated knowledge of coring and data interpretation upon me. Dr. Boyce is also an excellent writer with a knack for conveying research in a consistent and clear manner. Many thanks for pushing me in the right direction with my writing.

A second thanks is directed at Dr. Eduard Reinhardt who provided lab space and equipment for core storage, cutting, preparation and analysis. This project would not have been feasible without his equipment and aide. Also thank you for providing a micropaleontology course where we (the students) were able to hash out how to identify, pick and count the little critters.

As mentioned before, thank you to Ankara University, specifically Hayat Erkanal, the director of the archaeological excavation at Liman Tepe. Vasif Sahoglu was also key in the interpretation and supply department; he worked tirelessly to make sure we had what we needed in a timely manner. Also, thank you to the Turkish students, Kamil and Guliz, who provided coring help on a small Zodiac boat during long, hot, 8+ hour days.

Haifa University was also important for providing transportation and Scuba-diving support for this project as well. Thank you to Michal Artzy, director of the

Interuniversity Department of Marine Sciences out of Eilat, Israel. A special thanks to the Israeli workers as well, including Beverly Goodman, for providing culture and fun. A special thanks to Amit for driving and coring support.

Back in Canada, I am surrounded by a spectacular group of friends and colleagues, including my lab-mate Lisa Sonnenburg. Lisa has a spectacular memory, and if I tell her anything she can pull it out of her brain with no problem. I often found myself asking her questions about my project from 2 years prior and her reminding me about specific aspects and procedures. Lisa is also a great friend and I will truly miss her after my time at McMaster University is done. She is always welcome to share my office wherever in the world I end up.

Also, thanks very much to Jessica Pilarczyk, who provided micropaleontology support. Jessica was very good at pointing me in the right direction, both in school and in life. Thanks also to Jeremy Gabriel for being the geophysical data monkey and helping make my thesis viable. In addition, thanks to all the other graduate students in the department for making life interesting. Thanks also go to Duncan Findlay and Andrew Kingston (my rock and fossil-hunting buddy), who together provided a very entertaining first year of my thesis.

A special thanks goes to my family, especially my mother, Sue, who took the time to run my trace metal samples at her work, the University of Wisconsin, Milwaukee. Thanks to my limnologist father, John for being ever so excited when I chose this career path. A final thanks goes to Brian King, who took the time to point at my computer whenever I strayed and order me back to writing. It worked!

Table of Contents

List of Illustrations, Charts and Tables

Chapter 1: Introduction

Chapter 2: Paleogeographic Reconstruction of Submerged Pre-Historic Shorelines and Coastal Environments at Liman Tepe, Western Turkey.

Chapter 4: Conclusion

Appendices:

Preface

McMaster University copyright regulations require a report of writings submitted in theses that will also be used in professional publications. The following section lists these details and outlines contributions provided by various co-authors on the papers:

Chapter 2: Paleogeographic Reconstruction of Submerged Pre-Historic Shorelines and Coastal Environments at Liman Tepe, Western Turkey will be submitted after a final round of editing to *Marine Geology*. This author collected all the sedimentological data and completed all sedimentological analysis and interpretation for the project. Dr. Joe Boyce assisted with core collection as well as collected seismic, bathymetry, and side-scan sonar data. This author was involved in interpreting the data and correlating it with sedimentological analysis with the aide of Dr. Boyce. Dr. Boyce also provided funding of the paper through his NSERC research grant. Jeremy Gabriel processed the seismic geophysical data for a final class project at McMaster University. Other authors on the paper provided logistical support, including transportation, equipment, lodgings and food.

Chapter 3: Coastal sediment record of the construction of Alexander the Great's causeway at Klazomenai, Turkey will be submitted after a final round of editing to the *Journal of Archaeological Sciences*. Again this author collected all sedimentological data and completed analysis and interpretations. This author also conducted research into the background of the site. Dr. Joe Boyce provided assistance for the data collection and interpretation, and funding with his NSERC research grant.

All other authors provided logistical support, including transportation, equipment, lodgings and food.

Chapter 1: Introduction

1.1 Background and Rationale

Since the end of the last glacial maximum (LGM), approximately 20,000 years ago, sea levels have risen approximately 120-130 m to modern-day levels (Lambeck and Chappell, 2001). Sea levels rose slowly (ca. 6 m per 1000 years) during the early post-glacial, speeding up ~15,000 years ago (ca. 10 m per 1000 years) and finally decelerating during the mid-Holocene as ice sheets disappeared entirely (ca. 7000 years ago) (Fleming, 1998). At 7,000 years before present, sea levels began to reach modern levels, adding an average of 3-5 m total since then (Fleming, 1998). These post-glacial changes in sea level dramatically altered the configuration of coastlines worldwide and inundated many coastal landscapes that were once occupied by prehistoric peoples.

In the last three decades there has been a growing recognition of the tremendous archaeological potential of submerged prehistoric landscapes and the importance of coastal paleoenvironmental change (Fleming et al., 1998; Bergman et al., 2003; Flemming, 2004; Flatman et al., 2005;). The first systematic investigations of the prehistoric underwater archaeological sites were conducted in northwestern Europe and the Mediterranean since the 1970's (Flatman et al., 1998). Much early work, particularly in Denmark and the United Kingdom, was conducted in connection with economic exploration of the seabed (i.e. for petroleum resources, fisheries) and led to rapid expansion of underwater archaeology as a discipline. Later in the 1990's, the systematic swath mapping of the European shelf and Baltic Sea with multi-beam sonar led to discovery of new prehistoric sites, many with well-preserved cultural materials (Firth,

2004; Gron and Skaarup, 2004; Flemming, 2004; Momber, 2004). Many sites were found in close proximity to drowned Pleistocene shorelines and other relict coastal landforms (e.g. estuaries). Similar approaches, employing geophysical remote sensing and paleogeographic mapping, have led to the discovery of submerged Paleoindian and Archaic sites in North America (Fedje and Christiansen, 1999; Faught, 2002; Bell and Renouf, 2003). These studies account for only a fraction of the vast, prehistoric shelf areas that were flooded by post-glacial sea level rise and much remains to be explored.

Archaeologists have long recognized the importance of landscapes and environmental change but it is only recently that geological studies have become an important component of archaeological site investigations. Pioneering work by Kraft (1975; 1980; 1977) demonstrated that the coastal configuration and geomorphology of many long-occupied sites in the Aegean have changed dramatically during the Holocene. At ancient Ephesus, for example, rapid alluvial sedimentation in the Kucuk Menderes valley in-filled the city's harbour basin, moving the shoreline over 10 km west since Classical times. Relative sea level rise had a similar impact at Troy, causing rapid aggradation of the Scamander floodplain and infilling of Troia Bay. During the past 5500 years, the shoreline has prograded 5 km to the north of the ancient city, explaining the large discrepancy between ancient descriptions of Troy and its modern setting (Kraft, 1975; 1980; 2003). These results, while not surprising to geologists, demonstrated to the archaeological community the rapid rate at which geological processes can re-shape coastlines and the importance of understanding paleogeography.

In the following decades, geoarchaeology emerged as a distinct sub-discipline, encompassing the study archaeological sites and materials using a broad range of geoscience techniques. Recent work in coastal geoarchaeology has focused on the reconstruction of sea levels and coastal environments using the sediment record from ancient harbour basins (Stiros et al., 1996, 1998; Marriner et al., 2006; Stanley et al., 2006; Goodman, 2006; Reinhardt and Raban, 2008). Ancient harbours can provide an important archive of coastal environmental changes as they often contain long, continuous sediment records and architectural features that can be used as sea-level reference markers (i.e. paved surfaces). Recent geoarchaeological investigations in Tyre's ancient harbour on the Lebanese coast, for example, have documented impacts of human engineering interventions on the coastline and have allowed the paleogeography of the ancient harbour to be reconstructed (Marriner et al., 2005; Marriner et al., 2007). Other work in Mediterranean coast of Israel has documented changing environments in Caesarea's Roman harbor and its submergence and destruction as result of co-seismic subsidence and an ancient tsunami impact (Reinhardt and Raban, 1999; Reinhardt et al., 2006a). Coastal geoarchaeological reconstructions have also been employed to determine the long-term impacts of ancient engineering structures (i.e. causeways, breakwaters) on coastal depositional systems (Millet et al., 2007; Marriner et al., 2007).

A developing area of application in coastal geoarchaeology is the predictive mapping of submerged prehistoric sites (Quinn et al., 2000; Reinhardt et al., 2006b; Sonnenburg and Boyce, 2008). Predictive modeling has been employed with success in terrestrial archaeology for determining the site distributions; most models incorporate a

broad range of paleoenvironmental factors (e.g. proximity to shorelines, water bodies, slope gradients, habitat types) that are statistically weighted according to their importance in determining settlement location (Conolly and Lake, 2006; Chapman, 2006). It has been well demonstrated in North America for instance, that the locations of raised Pleistocene shorelines and relict river terraces are excellent predictors of Paleoindian and Archaic site distribution (Boyd, 2007; Karrow et al., 2007). Geomorphic data have also been employed in the exploration for underwater prehistoric sites (Fedje and Christiansen, 1999; Faught, 2004) but statistical numerical modeling using a wide range of site determinants has not yet been attempted.

One of the major constraints on the use of predictive modeling techniques in underwater archaeological exploration is that the relative sea-level history for a site must be known in some detail. As shown by Lambeck (1995) and Lambeck and Purcell (2005) relative sea level change is a function of least three regionally varying components – eustacy (water volume transfers between ice masses and oceans), glacio-hydro-isostacy (isostatic effects due to fore-bulge development and hydrostatic loading) and tectonics (vertical crustal motions). As a result, prediction of shoreline positions using generalized eustatic sea-level curves and coastal bathymetry data are likely to simplistic and would be of limited use for site modeling. This is particularly true for tectonically-active areas such as the Aegean basin (Figure 1.2) where a complex interplay of these three factors has resulted in regionally-varying rates of relative sea level rise (Lambeck, 1995, 2005; Lambeck and Bard, 2000). Regional differences in sea level history are well documented from several coastal sites in Greece and western Turkey (van Andel and Lianos, 1983;

Stiros et al., 1996; Lambeck, 1996). These data show that some coastal areas have undergone net uplift while others have experienced subsidence, or no apparent net change in sea level. Lambeck (1995) attributed these regional variations in the Aegean to isostatic adjustment of the crust and local tectonic motions.

As a result of rapid tectonic subsidence and a long history of human settlement, many areas of the Aegean coastlines of Greece and western Turkey have a high archaeological potential for underwater prehistoric archaeology. This is particularly the case for large segments of the Anatolian coastline of western Turkey (Figure 1.1), which has experienced relatively rapid rates of coastal subsidence during the Holocene in connection with regional extension. The region lies within the Aegean extensional province, a zone of active crustal stretching and normal faulting produced by the westward extrusion of the Anatolian plate into the Aegean back-arc basin (Ocakoglu, 2005) (Figure 1.2). Regional extension has been ongoing since the Oligocene and is manifested by the development large fault-bounded graben and horst structures (Brinkman, 1976; Bozkurt and Sozbilir, 2004).

The Bay of Izmir region is of archaeological importance as it contains a large number of prehistoric archaeological sites, including the long-occupied Chalcolithic-Bronze Age settlements at Liman Tepe, Bakla Tepe, Panzatepe and the recently discovered site of Bağlararası (Saholgu, 2007; Erkanal, 2008; Saholgu, 2008). These sites have been under investigation since the 1990's as part of the Izmir Regional Excavations and Research Project (IRERP) under the direction of Dr. Hayat Erkanal of Ankara University. Most of

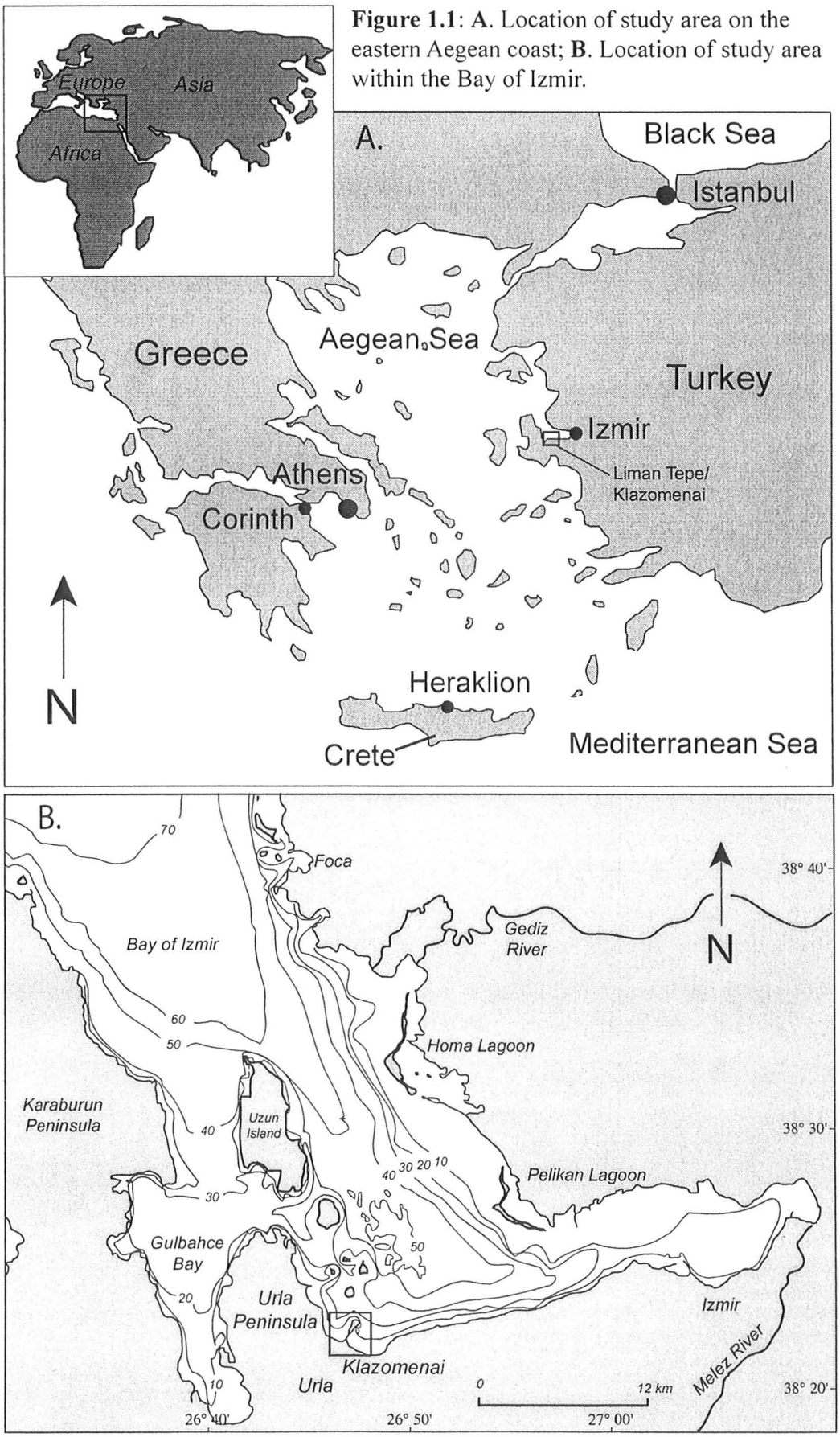

Figure 1.1: **A**. Location of study area on the eastern Aegean coast; **B**. Location of study area within the Bay of Izmir.

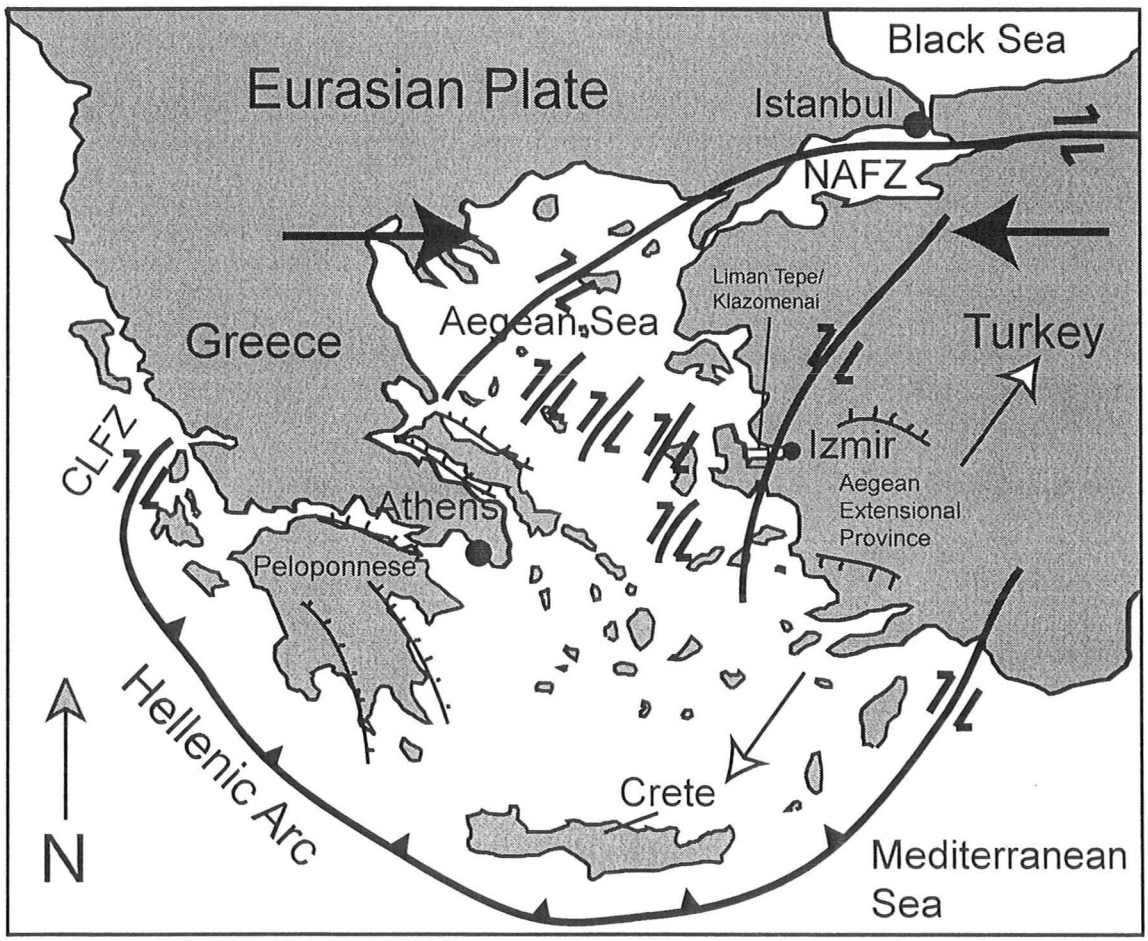

Figure 1.2: Tectonic setting of Turkey and the Aegean Sea (modified from Ocakoglu et al., 2005). NAFZ: Northern Anatolian Fault Zone; CFLZ: Cephalonia–Lefkada Fault Zone. Liman Tepe/Klazomenai lies at the edge of the Aegean extensional province.

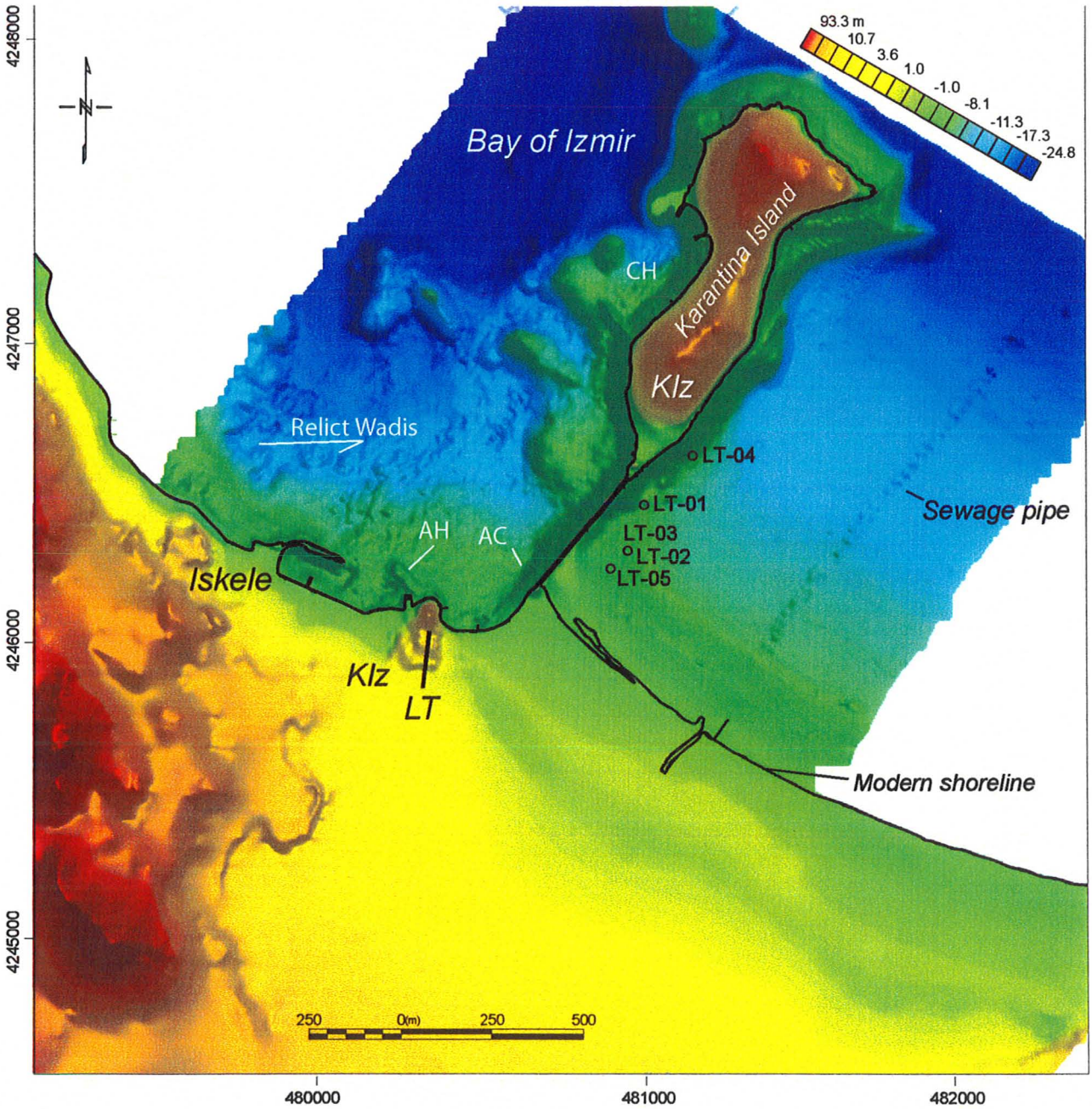

Figure 1.3: Digital elevation model (m) for study area showing generalized topographic relief and detailed bathymetry. Locations of archaeological sites also indicated: Klz - Klazomenai, LT - Liman Tepe, AH - Archaic harbour; AC - Alexander's causeway, CH - Classical Harbour, LT-01 - Core locations.

the coastal sites are of Chalcolithic-Late Bronze Age and very few Neolithic sites with a clear coastal context have been discovered.

Liman Tepe is a well-fortified, Early Bronze-age settlement located on the south shore of the Bay of Izmir (Figure 1.3). Excavations have uncovered pottery evidence indicating the presence of Neolithic peoples in the area; however a Neolithic settlement has not been discovered (Erkanal, 2008). The regional subsidence of the coastline around the Bay of Izmir, indicates that Neolithic sites if present, are likely submerged and lying at some distance seaward of the Bronze Age land site in shallow water.

In this thesis, the paleoenvironmental record of coastal environmental changes at Liman Tepe was investigated using detailed multi-proxy geoarchaeological study of 6 sediment cores extracted from the Bay of Izmir (Figure 1.3). Sedimentological and micropaleontogical data from core samples were used to identify changes in depositional environments and to document changes relative sea levels at Liman Tepe. The core data were combined with detailed bathymetry and seismic data taken within a 4 km^2 area around the site to identify the prehistoric shorelines and to reconstruct the Late Neolithic coastal paleogeography. The resulting paleogeographic maps identify a series of prehistoric shorelines that have been radiocarbon dated to the Late Neolithic period. The integrated core and geophysical data also provided a basis for investigating changes in the coastal environments stemming from a causeway barrier constructed by Alexander the Great during the early Hellenistic period (ca. 4^{th} c BC). The causeway was constructed to defend the Ionian port city of Klazomenai, which was founded on the site Liman Tepe during the Archaic period, against Persian attack.

1.2 Objectives

The overall objective of this thesis is to document changes in coastal depositional environments and shoreline positions at Liman Tepe/Klazomenai during the Late Neolithic (ca. 4000 BC) to present. Previous work has established the coastal environments that existed during the main Early to Late Bronze Age occupation of the site (Goodman, 2006; Goodman et al., in press) but little is known about the configuration of the coastline when the first Neolithic peoples settled here. The presence of Neolithic and Chalcolithic cultures is indicated by scattered pottery remains on land but no Neolithic settlement to date with a clearly coastal context has been located. The generally low visibility of Late Neolithic coastal sites in the region probably reflects both a bias towards the study of terrestrial sites and major changes in the coastal configuration during prehistory. A major emphasis is to reconstruct the shoreline positions during the Late Neolithic in order to provide the baseline data for future predictive modeling and exploration for submerged prehistoric sites.

A second major objective of the thesis is to document the human impacts on the coast that resulted from the growth of the city of Klazomenai. The construction of the Alexander causeway in 334 BC had major impact on the coastal depositional environments. This thesis aims to document these changes and to better resolve how the coastal sediment budget and depositional systems were altered by the causeway construction.

The detailed objectives are to:

1. Reconstruct the changes in the coastal paleogeography and shoreline positions at Liman Tepe/ Klazomenai from the Late Neolithic to present (~ 6000 years).
2. Better resolve the timing of the construction of the Alexander causeway at Klazomenai and its impact on the natural coastal environment and depositional processes.
3. Determine which geoarchaeological methods and proxies (coring, sediment, physical and magnetic properties, geophysical remote sensing, geochemistry) are most useful for reconstructing coastal environments.

1.3 Study Area

This study area is located about 40 km to the southwest of the city of Izmir, in western Turkey (Figure 1.1). Geoarchaeological studies and geophysical investigations were conducted within a 4 km^2 area including the modern Port of Iskele and nearby Karantina Island. The area includes two significant archaeological sites – the Bronze-age settlement at Liman Tepe and Classical port city of Klazomenai (Figure 1.3).

1.3.1 Geological Setting

The study area lies within the Aegean extensional province of western Turkey, which is defined by a series of major west-east trending graben structures formed during late Oligocene-Miocene extensional faulting (Brinkman, 1976; Bozkurt and Sozbilir, 2004 – Figure 1.2). The Bay of Izmir lies over a major fault-bounded extensional basin

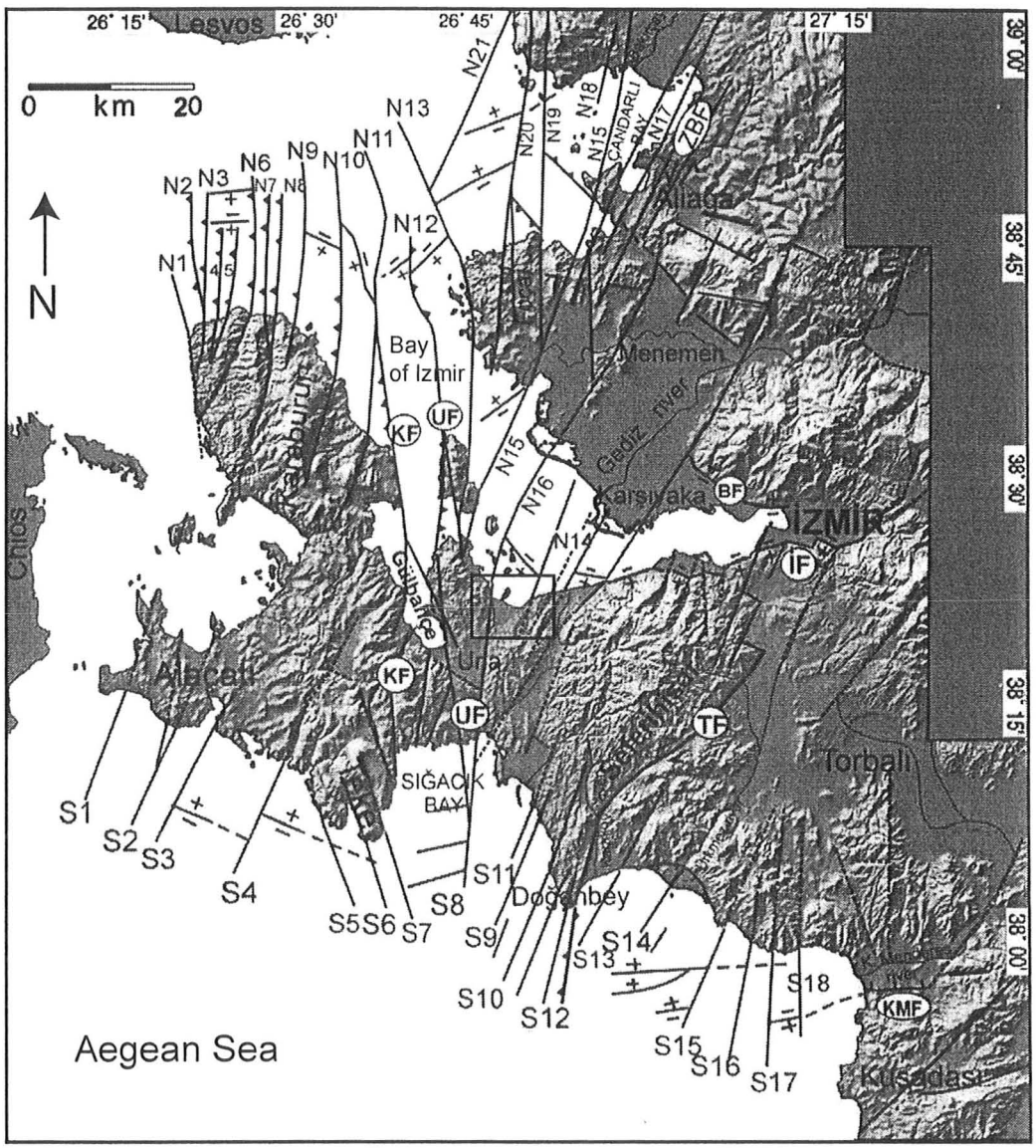

Figure 1.4: Mapped faults in the Bay of Izmir and surrounding region (from Ocakoglu et al., 2005) The Bay of Izmir lies within a graben structure that has experienced tectonic motion throughout the Holocene. Rectangle indicates study area. N and S labels are identified fault structures according to Ocakoglu et al., 2005.

(Izmir Graben) that is associated with modern-day seismicity and active tectonic subsidence. The Bay is underlain by a number of N-S trending normal and strike-slip faults that divide the Bay into a series of graben and half-graben structures (Ocakoglu, 2005) (Figure 1.4). Recent seismic activity was recorded with a > 5 magnitude (Richter Scale) earthquake offshore of Izmir in 2005.

The basement rock consists of Cretaceous schists overlain by Neogene marls, shales and limestones (Ocakoglu et al., 2005). The Neogene sediments form the local bedrock below the Liman Tepe and Karantina Island. The sedimentary rocks are locally interbedded with Neogene volcanics (tuffs, lavas) that form the coastal highlands on the south shore of the Bay of Izmir (Figure 1.5).

The Neogene sedimentary cover rocks are overlain by thin Pleistocene and Holocene marine sediments within the Bay of Izmir (Aksu et al., 1987). The upper part of the marine sediment sequence at Liman Tepe consists of modern marine muds, silts overlying older Holocene lagoonal and terrestrial sediments deposited during lowered phases of sea level (Goodman et al., in press). The marine sediment thickness is greater on the eastern side of Karantina Island owing to its more sheltered location behind the Alexander causeway.

The causeway construction (334 BC) effectively shut-down the natural east-west longshore transport of sediment along the coast, creating a sheltered embayment with more rapid sediment accumulation to the east of the island. The sediment accumulation on the western side of Karantina Island has been much less extensive, as indicated by the presence of bedrock outcrops and relict wadi and shoreline features on the modern seabed

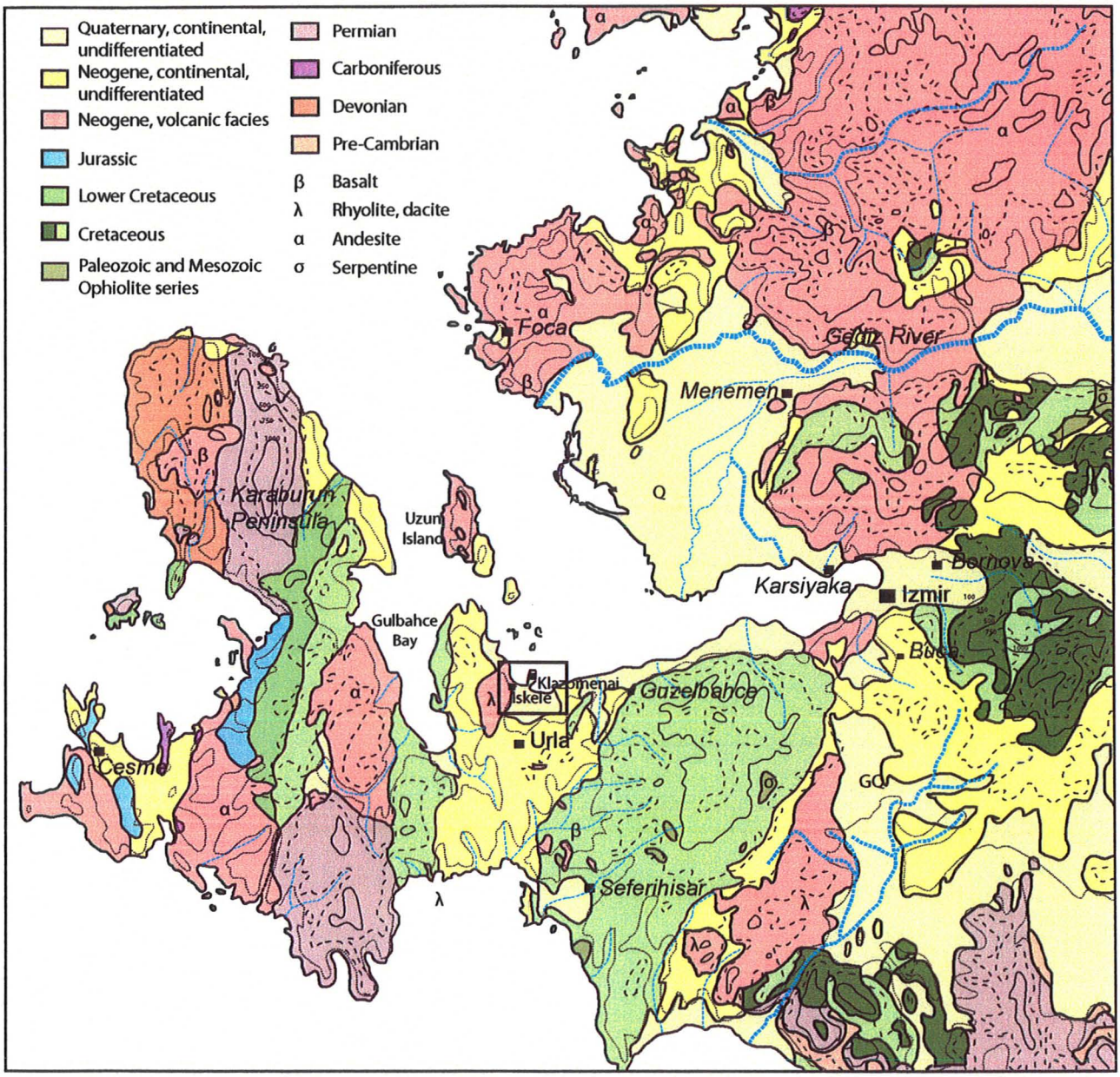

Figure 1.5: Geologic map of lands surrounding the Bay of Izmir. Modified from the Institute of Mineral Research and Exploration – Ankara (1964). Rectangle indicates study area.

(Boyce et al., in review). The relict shoreline features record early Holocene low-stand phases when sea levels were more than 10 m below present.

1.3.2 Bay of Izmir: Physical Setting

The Gediz River is the dominant geomorphological feature in the Bay of Izmir. The Gediz Delta has prograded through the late Quaternary, infilling the southeastern end of the Gediz Graben, an E –W trending half-graben system that has been active throughout the late Pliocene (Hakyemez et al., 1999 – Figure 1.6A). The main sediment source in the study area is poorly-sorted alluvial sediments from the Gediz River and erosion of the surrounding coastal highlands (Duman et al., 2004 – Figure 1.6).

The dominant wind pattern in the Bay of Izmir is from the north to northwest and blows Aegean waters along the southern coast into the Bay, creating localized gyre systems (Ivanov et al. 1998; Sayin, 2003). The gyres create an east-west transport direction of sediments along the southern shores of the Bay away from Izmir. A second, wind-dominated current system moves eastward along the western shoreline of the Karaburun Peninsula, however little deposition occurs on the western side of the causeway due to a lack of sediment supply (Sayin, 2003). These characteristics are evident in the construction of various harbours on the south shore of the Bay of Izmir. Most modern harbours have an arcuate breakwater that open to the east, preventing siltation by sediment transported by westerly currents.

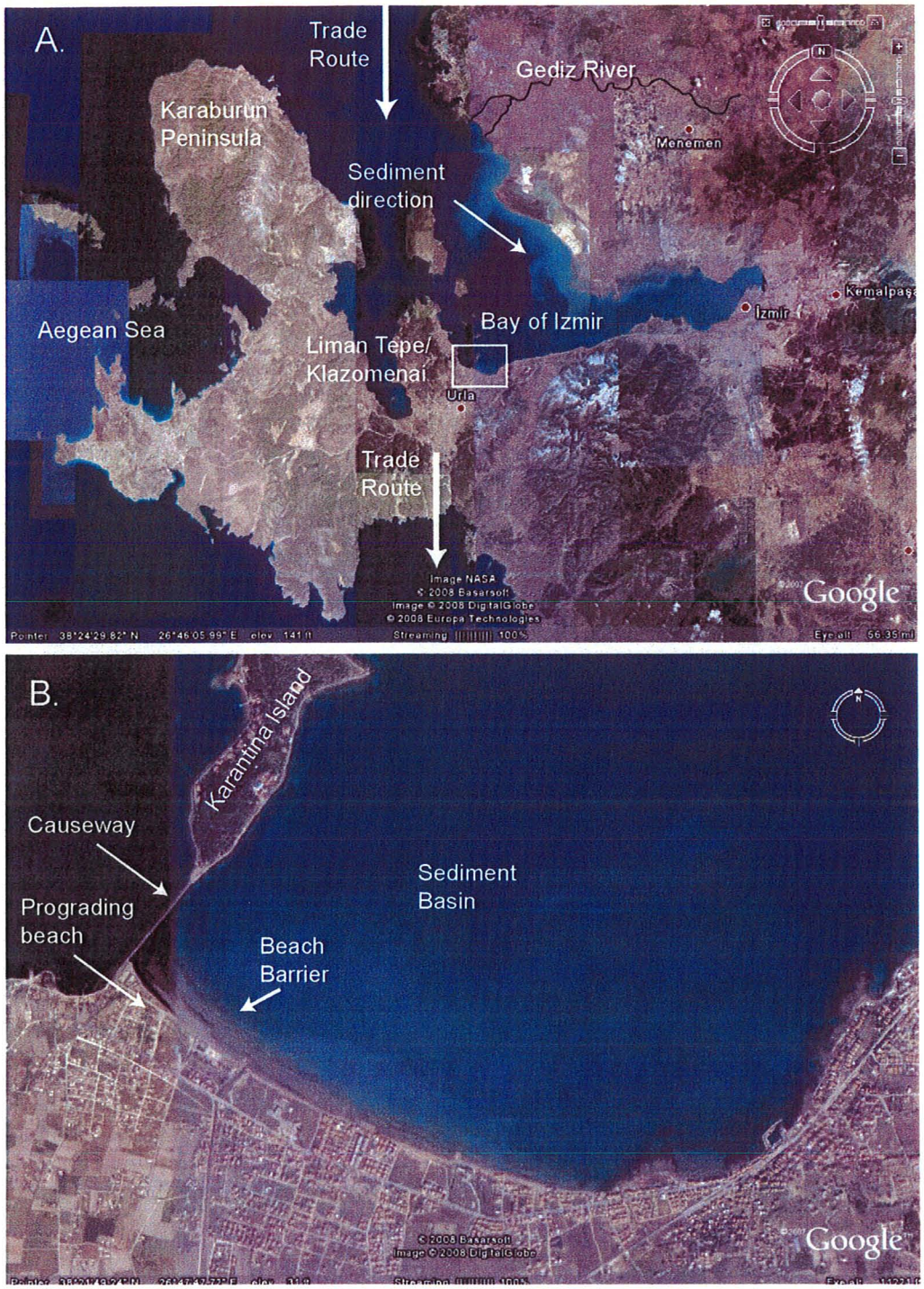

Figure 1.6: Aerial images of study area (courtesy of Google Maps #325519188). **A**. Bay of Izmir showing outflow from the Gediz River. Sediments are carried by currents south-west along the northern shore of the Bay. **B**. A view of the causeway and sediment basin forming by prograding beach barriers to the east of the structure.

Within the study area, the modern harbour at Iskele is oriented in this fashion but the adjacent Archaic mole structure at Liman Tepe opens westward. This may indicate that the easterly longshore sediment transport was dominant prior to the construction of the causeway. A second Classical-age harbor on the eastern side of Karantina Island, opens to the north, also avoiding the eastern sediment supply. When the causeway was constructed, the sediment from the east rapidly prograded the coastline on the east side of the structure (Figure 1.7A, B).

1.3.3 Archaeological Setting

The coastal settlement at Liman Tepe was established in the late Neolithic period (8,000 – ~3,500 BC) and early Chalcolithic (3,500 – 2,800 BC) (Goodman, 2006). The settlement grew and eventually took over a small hill located next to the modern shoreline during the Bronze Age (2800 – 1200 BC). The Bronze-age city, Liman Tepe, literally "Harbour Hill', had a well-defined urban character with a monumental architecture and well fortified walls.

Previous studies have shown that this site was ideal – it provided a landscape that created a sheltered marina and was located at a thin portion of land that connects the Karaburun Peninsula with the rest of Turkey (Sahoglu, 2005). Ancient traders wishing to sail along the Turkish coastline would be delayed for days having to go around the peninsula, while the Liman Tepe settlement provided a perfect location to offload goods and transport them quickly over-land.

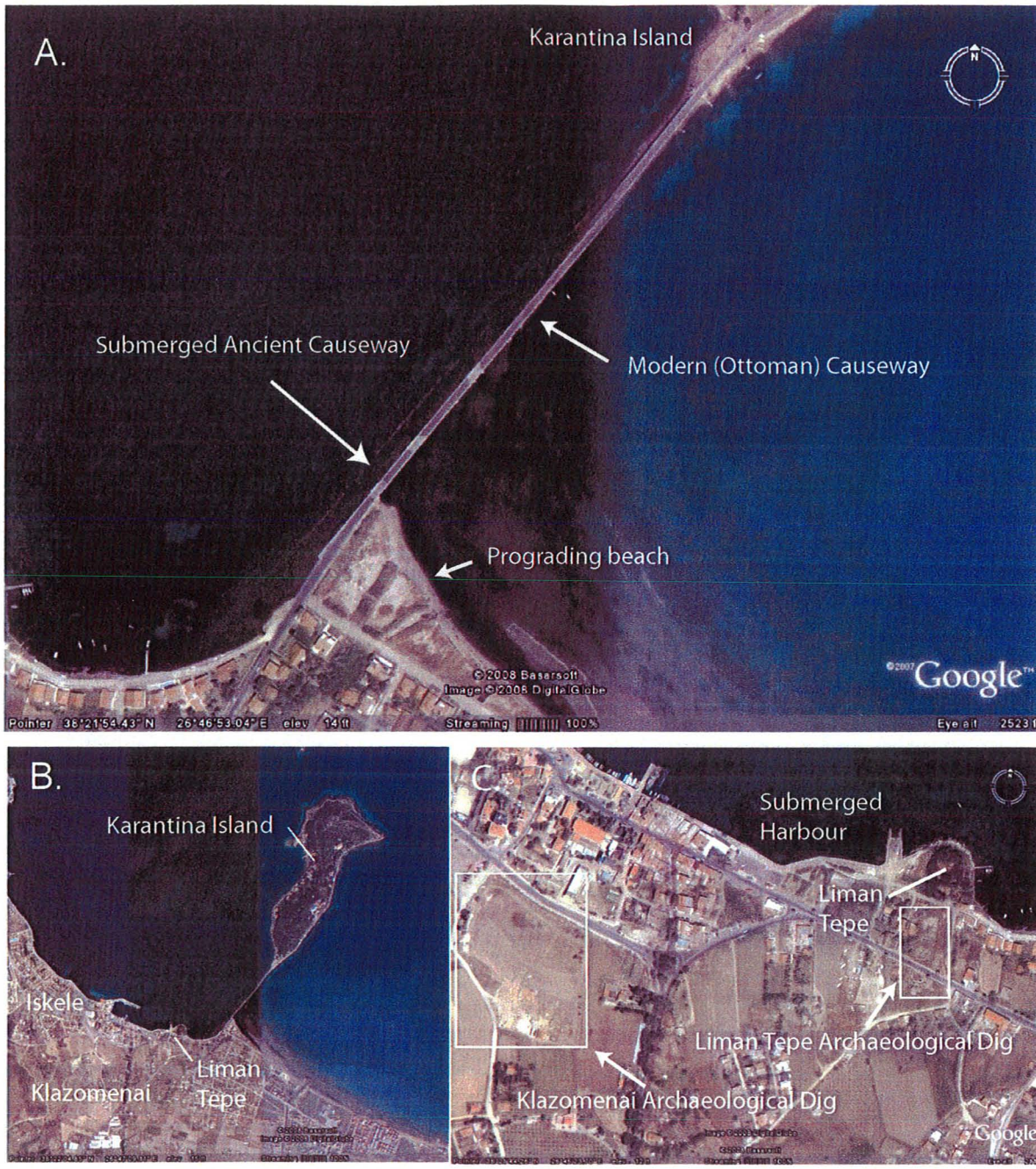

Figure 1.7: Aerial images of archaeological sites in the study area (courtesy of Google Maps #325519188) **A**. A close view of Alexander's and the modern Causeway structures. **B**. A view of the area noting submerged location of modern Iskele harbour and Liman Tepe/Klazomenai land sites. **C**. Archaeological digs on land, both Klazomenai (left) and Liman Tepe (right) are being worked by Ege and Ankara Universities (respectively). No work has been done on the actual causeway structure.

The settlement was later re-colonized by Greek settlers in the 9th century BC and later became known as 'Klazomenai'. The area expanded during the Classical and Roman periods, becoming a thriving port dealing in the trades of olive products and the trans-shipment of goods from Anatolia (Ersoy, 1993). Klazomenai was one of the 12 cities (Dodecapolis) of the Ionian League, a confederation of Ionian city states in western Anatolia that joined in a political alliance (Herodotus, 5th c BC) (Figure 1.8). Klazomenai was of strategic importance as an access point to two major river valleys, the Gediz to the north and the Kucuk Menderes to the south that led to the interior of Anatolia and to major trade centers connecting with Mesopotamia (Sahoghlu, 2005). Persian encroachment during the 6th and 5th centuries BC prompted a move by the Klazomenains to the nearby Karantina Island (Ersoy, 1993). Alexander the Great, upon defeating the Persians, ordered the shoreline to be secured and a causeway was built to connect the island city to the mainland (Pausanius, 2nd c BC). This causeway drastically altered the near-shore currents and a small sediment basin formed that can still be seen today (ca. 334 BC; Figure 1.7; 1.9).

1.4 Historical background of Klazomenai

References to Klazomenai (also Clazomenai) in Greek and Macedonian history books are, in general, scarce. Historian Pausanias provides background to the settlement of the city in his *Guide to Greece,* written in the 2nd century BC. The city was settled by a contingent of Greeks displaced from the Peloponnese in the 9th c BC. Klazomenai was one of a politically allied citied western shoreline of Ionia (Turkey) called the Dodecapolis (Herodotus, 5th c BC; Figure 1.8).

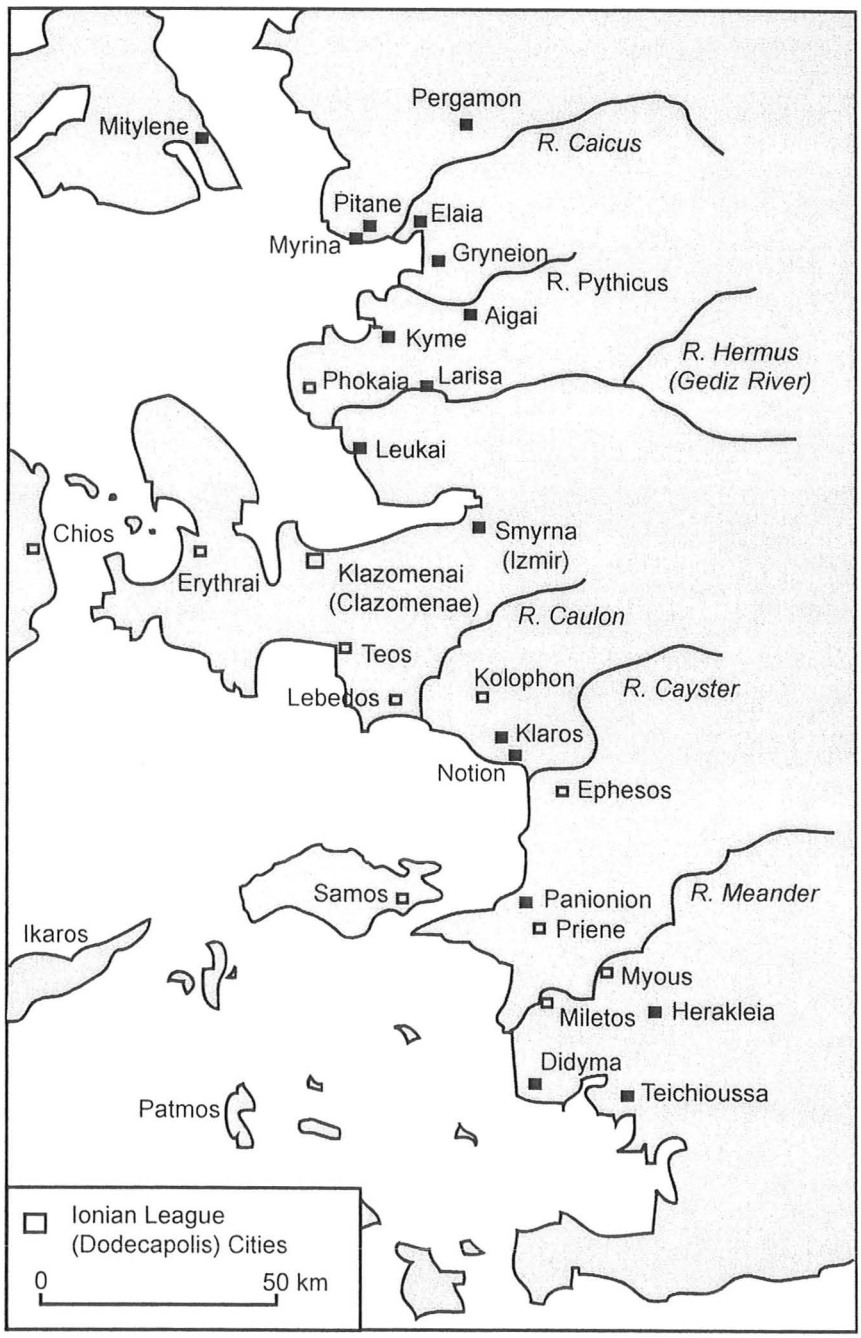

Figure 1.8: Map of Ionia showing locations of ancient cities (Pausanius 2nd c BC). Klazomenai was one of 12 cities united in culture and politics known as the Ionian 'Dodecapolis' (Herodotus, 5th c. BC).

Figure 1.9: **A**. View of bay on west side of the Alexander Causeway (center) Karantina Island (Left) and the mainland (right) looking west from Liman Tepe. **B**. Image from the south end of causeway looking north to Karantina Island. The ruins of the Roman causeway renovation parallels the modern structure. **C**. View of Liman Tepe and the modern port of Iskele.

1.5 Alexander the Great

In 334 BC, Alexander the Great of Macedon crossed the Hellespont and entered Anatolia. Meeting the Persian troops at the Battle of Granicus, the Macedonians won and continued to push into Anatolia via Sardis, eventually arriving in Ephesus (Figure 1.10). From Ephesus, Alexander ordered his general Parmenion to travel to the surrounding countryside to receive Ionian submission. This included the construction of the causeway from the mainland to the island of Klazomenai in order to thwart the Persian fleet from landing on the island (Green 1991). Historians Pliny and Pausanius (2nd century BC) both record the connection of the island to the mainland after the battle of Granicus (334 BC). In southern Lebanon, Alexander ordered the construction of two more causeways, the most notable in Tyre. Alexander moved on to construct the Heptastadion in Alexandria and spread his country's knowledge and culture throughout the east.

Despite the abundant historical record of Alexander the Great's campaigns, ancient historians wrote about his exploits, including the Klazomenaian causeway, at least two centuries after his death. There is no record corresponding to the actual construction timeline, and therefore this study aims to use multi-proxy sedimentological analysis as well as radiocarbon dating in order to confirm the causeway's 4th c. BC construction.

Figure 1.10: Alexander the Great's campaign in Anatolia and Syria (334-331 BC). The causeway at Klazomenai was built following battle of Granicus (334 BC).

1.6 Previous Work

Excavations at Liman Tepe have been conducted by the archaeologists of Ankara University since the early 1990's as part of the large Izmir Regional Excavations and Research Project (IRERP) (Erkanal, 2008). The land excavations have uncovered extensive Chalcolithic and Early Bronze-age occupation phases and also evidence for a harbour structure. The harbour has been investigated since 2002 by a team from Haifa University out of Israel. The excavations had led to the discovery of large pithoi and abundant Bronze-age pottery materials which indicate the importance maritime trade at Liman Tepe. The harbour basin included a protective breakwater (mole structure) that was constructed during the Archaic period (ca. 6-7th c. BC). The mole now lies submerged at a depth of ~1.5 m below present sea level.

Goodman (2006) investigated the Bronze Age coastal depositional environments at Liman Tepe using land cores from the archaeological site and marine cores from the harbour basin. Goodman identified two main depositional phases: a transgresssive systems tract that was formed during mid-Holocene sea level rise, and a subsequent high-stand systems tract that formed as sea level rise decelerated after ca. 2800 BC. The high stand led to the development of an extensive beach barrier complex with back barrier lagoon and wetland environments (Goodman et al., in press).

The Classical archaeology of ancient Klazomenai is being investigated by researchers from Ege University, under the direction of Dr. Y. Ersoy. Excavations on Karantina Island have found evidence for one of the earliest known olive pressing plants.

Cultural Period	Beginning Date (BC)*	Ending Date (BC)	Beginning Date (yBP)	Ending Date (yBP)
Neolithic	8,000	3,500	10,000	5,500
Chalcolithic	3,500	2,800	5,500	4,800
Bronze Age	2,800	1,200	4,800	3,200
Iron Age - Dark Ages	1,200	1,000	3,200	3,000
Iron Age - Geometric	1,000	700	3,000	2,700
Iron Age - Archaic	700	450	2,700	2,450
Iron Age - Classical/ Hellenistic	450	114	2,450	2,114
Roman	114	400 AD**	2,114	1,600

*BC: Before Christ
** AD: Anno Domini - After Christ

Figure 1.11: Archaeological time periods for western Aegean in years BC/AD and years Before Present (yBP) (after Manning, 1995; Warren and Hankey, 1989; Renfrew, 1972 and Goodman, 2006).

Chapter 2: PALEOGEOGRAPHIC RECONSTRUCTION OF SUBMERGED PREHISTORIC SHORELINES AND COASTAL ENVIRONMENTS AT LIMAN TEPE, WESTERN TURKEY

G.M. Krezoski, J.I. Boyce, E.G. Reinhardt, J. Gabriel

School of Geography and Earth Sciences, McMaster University, Hamilton, ON

H. Erkanal, V. Sahoglu

Department of Humanities, Ankara University, Ankara, Turkey

B.N. Goodman

Haifa University, Haifa, Israel

For submission to Marine Geology

Abstract:

Liman Tepe is a long-occupied prehistoric coastal settlement located on the southern shore of the Bay of Izmir in western Turkey. The configuration of the submerged mid-Holocene (ca. 5-6 Ka) coastline was investigated at Liman Tepe to guide the search for underwater Neolithic archaeological sites. Shoreline features were mapped on the shallow shelf area (4 km^2) using a single-beam (200 kHz) echosounder and chirp (18-24 kHz) sub-bottom seismic profiler. Changes in the coastal paleoenvironments were determined by detailed sedimentological (lithofacies, grain size, magnetic susceptibility) and micropaleontological analyses of five marine sediment cores.

The sediment cores revealed a sequence of poorly-sorted pebbly shoreface deposits containing abundant shell and coralline fragments (Unit E shell hash) overlain by marine muds and silts (Units D-B) deposited in lagoonal/wetland and low-energy shallow marine environments. The contact between the pebbly sands and mud sequence is represented in seismic profiles by a high amplitude reflection that is continuous basin-wide. The reflector surface (top of Unit E) shows a number of northwest-trending ridges and terrace features that are interpreted as buried paleoshorelines. ^{14}C dating of shell materials from uppermost buried beach ridge yielded a Late Neolithic age of 3860 +/- 120 cal BC. The laminated mud sequence (Unit C, D) overlying the beach deposits record the development of a shallow back-barrier wetland/lagoon. The lagoonal sediments transition at 60-80 cm in the core to sandy, organic-rich muds containing abundant organic fragments (Unit B). Organic (plant) materials from just below Unit B yielded a ^{14}C date at 450 +/- 70 cal BC. The transition is interpreted as the onset of construction of

the Alexander causeway (~ 4th c BC) connecting the mainland with Karantina Island. Following the causeway construction, the shoreline on the east side of the island prograded rapidly covering older barrier/lagoonal sequences with a > 1 m mud drape.

2.1 Introduction

Since the end of the Last Glacial Maximum (LGM ~20,000 Ka.) ocean levels have risen approximately 125 m to the present-day levels (Fleming, 1998). In the Mediterranean, sea-level rise throughout the Holocene is the reason most human settlements on coastal locations are no longer accessible. Sites associated with cultures during the Neolithic (~8,000-3,500 BC) and earlier have been inundated. Because of this, studies completed in the past three decades have addressed the question of local sea-level curves (Lambeck, 1995; 1996) Using these curves, geologists can re-create shoreline environments at archaeological sites and determine the geomorphology of landscapes based on changing erosional and depositional rates (Kraft, 2003). In the Aegean, this task is made more difficult by the active tectonism of the area caused by movement of the Anatolian plate between the European and African plates.

Prior to the past decade, the underwater realm has gone relatively unexplored due to the belief that artifacts would be poorly preserved and surveys expensive to run (Bailey, 2004). Recent advances in remote sensing and sedimentological analysis have proven the opposite, with submerged sites found in better condition than similar land excavations (Quinn, 2000; Bailey, 2004). With these new techniques, the submerged archaeological world has become accessible, with many pioneering studies providing a

wealth of information from submerged archaeological sites in the North Sea (Flemming, 2004).

The Bay of Izmir in the eastern Aegean Sea (western Turkey shoreline), is the location of a long-occupied archaeological site (Liman Tepe/Klazomenai) known for its major contributions to the understanding of the ancient Anatolian trade network (Sahoglu, 2005). The bay is an arm of an E-W trending horst and graben system that has developed throughout the Holocene (Gediz Graben). The dominating sediment source to the bay is the Gediz River, north of the study site, and the major wind direction travels from the North/Northwest.

Recent geoarchaeological evidence at the site has documented changes in coastal environments during the main Bronze-Age (2800 - 1200 BC) phase of occupation characterized by a beach-barrier/back lagoon system proximal to the modern-day shoreline (Goodman, 2006). Evidence of older settlements has been discovered at the site (pottery) but no sites have been found on land. In this study the configuration of the pre-Bronze-age shorelines were reconstructed using detailed geophysical and sedimentological analyses in order to assist in the exploration for older inundated Neolithic shorelines (8,000-3,500 BC). Bathymetric and seismic surveys identified a series of relict shorelines, the most recent at approximately 10 m below modern sea-levels that has been dated to approximately 3860 BC corresponding to the Late Neolithic age.

This study also examines geomorphologic changes at the study site due to changing sea-levels in an attempt to determine possible locations of Neolithic occupation

sites. It was discovered that the Bronze-age beach barrier was the youngest in a series of (now submerged) relict shorelines that were preserved by rapid inundation. The relict shorelines are buried to the east of the causeway by sediments after ca. 2800 BC, when the depositional environment changed from transgressive shoreline to progradational beach-barrier system. The accretion was likely further accelerated during the Hellenistic period by the construction of Alexander's causeway in the 4th c BC.

2. 2 Study Area

The study area is located on southern shore of the Bay of Izmir, Turkey, about 40 km southwest of the city of Izmir (Figure 2.1A). The area lies within the geologically active Aegean extensional province in western Turkey, formed from the movement of the Anatolian plate between the European and African plates (Ocakoglu et al., 2005). The Bay is a fault-bounded graben structure bordered to the north and south by the Gediz and Kucuk Menderes Grabens respectively. The Gediz River is a major sediment source in the Bay of Izmir and has prograded seaward over 400 km^2 since the Pleistocene (Erinc, 1978). Localized gyres of water masses within the Bay transport sediment toward Liman Tepe from the east (Figure 2.1A; B – Sayin 2003). Smaller, localized sediment sources are derived from erosion of the nearby volcanic highlands.

Differences in deposition within the study area can be seen in the bathymetry map. To the west of the causeway the sea-bottom has a rugged topography with relict shorelines and wadi systems that record a drowned terrestrial landscape. On the eastern side, the bottom topography smooth due to much thicker accumulation of Holocene sediments (Figure 2.1C).

The Bay of Izmir is associated with several tectonically active fault systems including several major west-east trending faults and a number of minor north-south fracture systems that are oriented perpendicular to the direction of basin extension (Ocakoglu et al., 2005). Regionally, bedrock consists of Cretaceous sedimentary rocks (exposed in highlands), Neogene volcanics and sediments (rhyolites and andesites; limestones and sandstones) (Ocakoglu et al., 2005; Brinkman, 1972). Neogene limestones form the local bedrock at Liman Tepe, and are overlain by unconsolidated Quaternary sediment layers of variable thicknesses.

Archaeologically the area is of great importance, preserving a major Bronze-age settlement Liman Tepe and later Classical and Roman-age Klazomenai. Liman Tepe figured prominently in the Bronze Age as trading port of the Anatolian Trade Network (Sahoglu, 2002). Recent evidence has demonstrated that Liman Tepe may have eclipsed its contemporary, Troy in terms of its economic importance during the Bronze Age (Erkanal, 2008; Sahoglu, 2008). The city of Klazomenai was also an important olive producing centre and shipping port during the Hellenistic and Classical periods.

2.4 Methods

2.4.1 Geophysical survey

A detailed bathymetric and sub-bottom seismic study was conducted in a 4 km^2 area around Karantina Island to map the location of relict shoreline features (Figure 2.2). Bathymetry data were acquired using a 200 kHz Knudsen single-beam echosounder with nominal 50-75 line spacings along north-south and east-west transects (Figure 2.2).

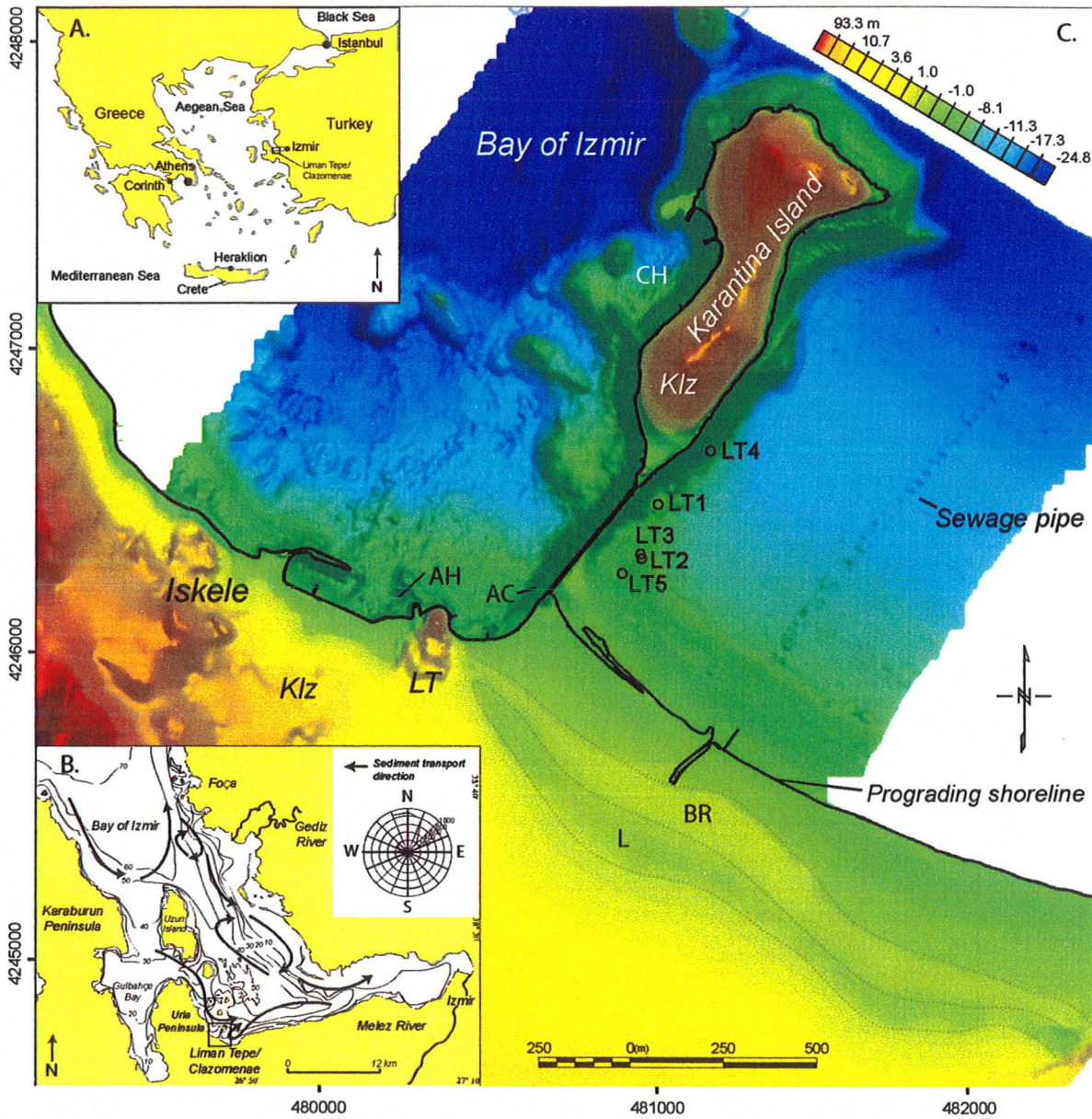

Figure 2.1: **A**. Location of Liman Tepe study area in western Turkey. **B**. Dominant wind and current patterns in Bay of Izmir (after Sayin, 2003). Predominant longshore transport direction is west-east with localized transport from the east due to clockwise circulation of water in the eastern end of the Bay of Izmir. **C**. Digital elevation and bathymetric model for coastal plain and inshore areas around Liman Tepe. Bathymetry map from Boyce et al., (In review). Land topography based on 1:5000 Turkish land survey maps. Klz = Klazomenai, LT = Liman Tepe, AH = Archaic-age harbour, CH = Classical-age harbour, AC = Alexander Causeway. Bronze-age relict barrier (BR) and back-barrier lagoon (L) identified by Goodman (2006) are also visible in topography.

Bathymetry data were processed according to the methods outlined by Sonnenburg and Boyce (2008). The corrected bathymetry data were integrated with land elevations obtained from 1:5000 topographic maps and interpolated using a kriging algorithm to create digital elevation model (Figure 2.1).

Sub-bottom seismic profiles were acquired at 75-100 m line spacing using a Knudsen swept frequency (18-24 kHz) chirp echosounder. The penetration depth of the high-frequency chirp source was limited to < 2 m across much of the survey area by the presence of reflective (sandy) bottom sediments. To the east of Karantina Island, greater penetration of up to 6 m was achieved due to the dominantly silty bottom sediments. The processing of the seismic profiles included the application of automatic gain control (AGC) to equalize trace amplitudes, band-pass filtering (pass band 15-30 kHz) and depth-conversion of the two-way travel times using an estimated sediment velocity of 1550 ms^{-1}. The reflector surfaces in each profile were then digitized and the calculated depths interpolated to create maps of the reflector surface relief and isochore thickness.

2.4.2 Sediment Coring and Physical Properties

Five sediment cores were collected on the eastern side of the causeway using 20 ft aluminum irrigation tubes and percussion coring methods (Figure 2.2). Cores were split into 1 m sections and placed in cold storage (4-6 degrees C) until split for analysis. Sedimentary characteristics, including grain texture and visual size, horizon changes,

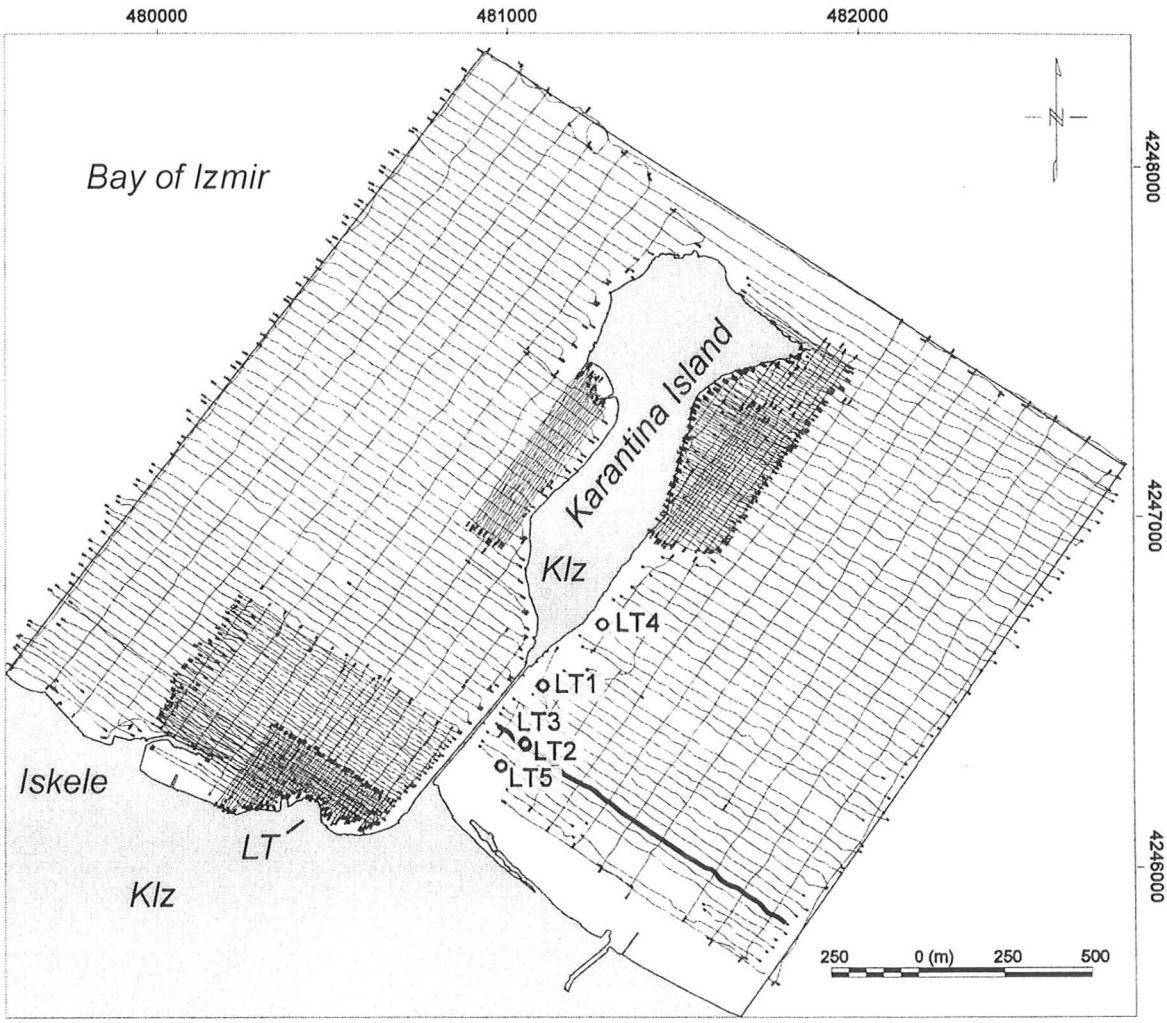

Figure 2.2: Core locations and geophysical survey tracklines. Bathymetry and sub-bottom chirp seismic data were acquired at 50-75 m line spacings and side-scan sonar acquired at 100 m spacings for 100% coverage. Klz: Klazomenai, LT: Liman Tepe. Highlighted W-E seismic track-line to the east of the causeway is presented in Figure 2.7.

organics and carbonates were logged, digitized, and plotted to depth (Figure 2.3).

Radiocarbon dates were obtained on four samples in order to constrain the sediment ages: two from LT-04 (olive pits, 76-77 cm depth; plant organics 171-172 cm depth) and two from LT-01 (plant organics 84-85 cm and plant material at 99-101 depths) for radiocarbon (AMS) dating.

Grain size samples (5 cm^3) were taken every 5 cm in each core and processed according to van Hengstum et al. (2007). Samples were treated with a 10% Hydrochloric Acid (HCL) solution and a 40% Hydrogen Peroxide (H_2O_2) solution in order to remove carbonate and organic populations, respectively. Samples were treated with a 1% Sodium Carbonate (Na_2CO_3) and heated to 85 degrees C for 2 hours in order to remove the organic silica content (diatoms) (Conley and Schelske, 2001). Samples were allowed to evaporate into a paste, then mixed and run three times for particle size averages on a Beckman 250 LS Coulter Counter using the Fraunhofer optical model. Results (mean μm) were plotted down-core and compared to lithology. Results were converted to phi scale and displayed using a minimum curvature grid in Geosoft's Oasis Montaj in order to create a visual surface plot (van Hengstum, 2007; Beierle et al, 2002).

Magnetic susceptibility was performed on the cores in order to determine ease of magnetization of sediments using a Bartington MS2F probe. The probe was placed every 5mm along the spine (back 2 cm removed) of archived cores and measurements corrected for drift every 5 to 7 measurements. Trends were plotted downcore using Oasis Montaj geophysical software and plotted to compare with lithology.

2.4.3 Micropaleontological Analysis

Foraminifera have been employed in a number of previous studies to as indicators of changes in salinity, water depth and trophic conditions in marine environments (Scott et al., 2001). In this study the down-core trends in foraminifera abundance were investigated to assist in the interpretation of depositional environments. Foraminifera abundances were determined on ca. 5 cm^3 sediment samples taken at 10-30 cm intervals from core LT-04. Samples were separated using a 500 μm and 63 μm sieves, dried and split into aliquots. Each aliquot was then counted until a minimum of ca. 300 specimens were identified to the genus level according to Cimerman and Langer (1991). The relative abundance of each genus was determined then plotted to depth (Figure 2.4). The representative foraminifera were photographed using a scanning electron microscope (SEM) to aid in the identification (Figure 2.5). A Q-mode cluster analysis was performed using Ward's sorting method and Shannon diversity index calculated using the PAST statistical software package (Davis, 2002 Hammer et al., 2001; Figure 2.6).

2.5 Results

2.5.1 Core Lithostratigraphy

Unit E: Pebbly shell hash facies.

This lowermost unit in cores LT-01 and LT-04 consists of a pebbly shell hash. The shell hash has a matrix of coarse pebbly sand with abundant shell and coralline fragments and some bivalve and gastropod shells. The bivalve shells and coralline fragments are mainly moderate to well-rounded and abraded. The granule and

pebble lithic fragments are similarly well rounded. The unit has overall high carbonate content (40%) with some well preserved *Posidonia oceanica* (sea grass) leaf fragments. Particle size analysis has revealed a coarse siliciclastic fraction averaging between 0-3 phi. Magnetic susceptibility is uniformly low between 0-5 SI x 10^{-6}. A radiocarbon date on plant material at the top of Unit E (cm in core LT-04) yielded an age of 3860 +/- 120 cal BC.

The coarse-grained character and presence of well-rounded pebbles and coralline fragments in Unit E indicate a high-energy nearshore environment. The top of Unit E corresponds with a distinctive high-amplitude reflector that is traceable as a basin-wide reflector in seismic profiles (Figure 2.7). The interpolated top of Unit E (Figure 2.8) shows several (2-3) linear north-west trending ridges that are interpreted as drowned beach barriers. Assuming the beach sediments were deposited in shallow water (< 1 m), the shoreline position ca. 3800 ka was ~6 metres below present sea level.

Unit E has been identified as a paleo-shoreline rather than a major environmental event due to the lack of any depositional features (i.e. interbedding or fining-upward sequences). The presence of organics and the poor sorting indicates a random depositional process influenced by wave action.

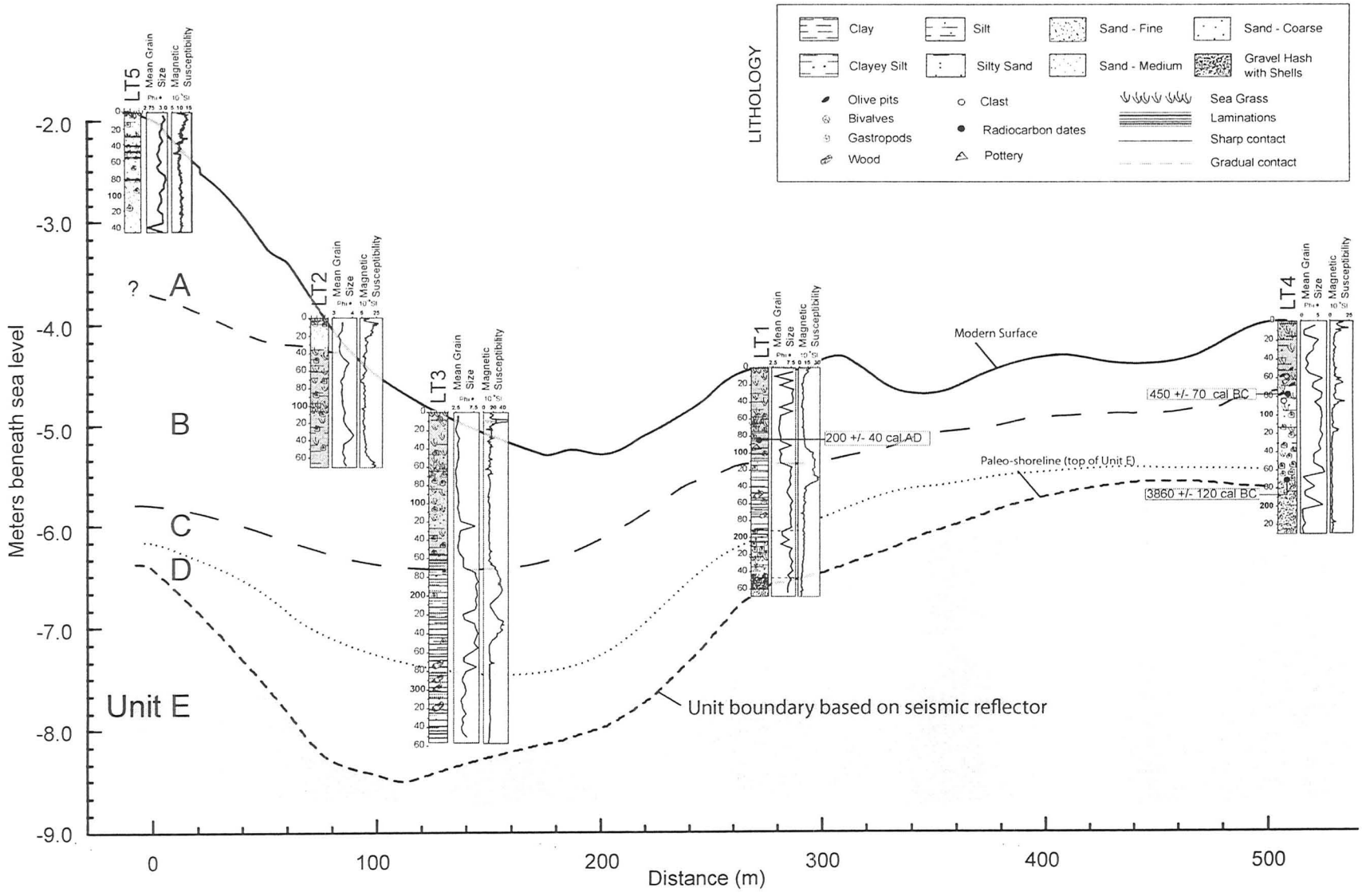

Figure 2.3: N-S cross-section showing core lithologic logs, mean grain size and volume magnetic susceptibility. Five sedimentary units (A-E) were recognized within the Holocene sediment package. The top of Unit E is associated with a distinctive basal reflector in the 24 KHz chirp seismic profiles (Figure 2.7).

Unit D: Wetland silt facies.

Unit D consists of crudely laminated silt lithofacies containing peat and woody reed fragments with a few disseminated shell fragments. The unit overlies Unit E across a conformable transitional contact. The unit reaches a thickness of over 80 cm within a small basin indicated by a depression in the surface of surface of Unit E (Figure 2.3), Grain size fines upward throughout the unit from fine sand to a coarse silt (5 to 7 phi). The carbonate content is much lower than underlying Unit E (loss of shell material, ~ 20%) and organics increase to from 5% to 10%. The volume magnetic susceptibility (κ) is low, between 0 and 15 SI x 10^{-6}.

The laminated silts in Unit D marks a conformable transition from a high-energy beach environment to a low-energy, wetland. As sea-levels rose in the area, the beach system (Unit E) was inundated and a shallow wetland system covered the area. The upwards-fining trend within Unit D indicates an increase in water depth within the area and a shift to lower energy conditions. Laminations and reed fragments are consistent with deposition in a shallow, sheltered wetland environment. The location of this wetland shoreward from Unit E indicates a beach-barrier and back wetland/environment existed sometime after ~3860 BC.

Unit C: Lagoonal silt facies

Unit C is a fine to medium laminated silt lithofacies. The unit shows a continuing fining-upward sequence from Unit D to a medium silt (7.5 Phi) with cm-scale laminations. In LT-04, Unit C contains a large (30 cm) horizon of abundant, well-

preserved olive pits at 47-77 cm depth. In LT-01, pottery fragments are present at 68-70 and 91-92 cm depth. Organic content increases up to 18%, corresponding with a decrease in carbonate content (up to 10-15%). The volume magnetic susceptibility is high (up to 30-40 SI x 10^{-6}), and shows several discreet peaks that correspond with decreasing grain size. Radiocarbon dates obtained on olive pits from LT-04 yielded a date of 450 +/- 70 cal BC at 76-77 cm depth, giving the maximum age of causeway construction.

The presence of laminated sediments and the fining upward trend in Unit C indicates rising water levels and the development of a back-barrier lagoon system. The geometry of the sediment package, thickening within a shallow basin and thinning over the beach ridge (Unit E) is consistent with this interpretation. The presence of olive pits and pottery fragments at the top of the unit indicates human activity around the ancient city of Klazomenai. Variability in magnetic susceptibility in Unit C indicates changes in the flux of terrestrial sediments being delivered to the lagoon. The primary source of magnetic particles is likely titano-magnetite derived by erosion of volcanic highlands. Peaks in magnetic susceptibility indicating phases of erosion may be related to climatic factors or anthropogenic activities such as land clearance (Figure 2.3).

Unit B: Organic-rich silty sand facies

Unit B is a massive silty sand lithofacies with abundant well-preserved plant macrofossils. Dominant organic matter is the remains of *Posidonia oceanica* seagrass. The contact between Units C and B is abrupt with a distinct grain size coarsening from

fine to medium silt (7.5 phi) to a silty sand (1-4 phi). Organics remain steady throughout this unit (up to 10%) and carbonates begin to increase (up to 20%). Magnetic susceptibility shifts to lower values across the boundary, (0 to 5 SI x 10^{-6}). All cores jump to higher (>10 <20) SI values in the top 5 cm of each core (Core 3 jumps to over 70 SI x 10^{-6}). Radiocarbon ages obtained on plant organics at 84-85 cm depth in LT-01 was dated to approximately 2nd c AD.

Unit B records a major shift in depositional environments a few cm above the radiocarbon date of ~450 BC. With calculated deposition rates of ~.3 cm/year, this places the major depositional change at approximately the mid to early 4th c BC. One major even that occurred during that time period was the construction of the Alexander causeway in 334 BC. The causeway accelerated shoreline progradation that had begun after 2800 BC (Goodman, 2006), and is recorded by a shift to coarser grain sizes in Unit B. A similar explanation identifies Unit B as a relict beach barrier 'tail' recording sea-level rise and movement of the barrier system identified by Goodman (2006) inshore. The date of 450 BC underneath this horizon, however, disproves this theory as Goodman's (2006) barrier was in place prior to 2800 BC. The silty substrate of Unit B provided an ideal environment for the growth of extensive *Posidonia Oceanica* meadows in the shallow embayment that formed after causeway construction.

Unit A: Fine sand facies

Unit A consists of fine, well-sorted quartz sand (3-4 Phi) with a few thin (1 cm) horizons of articulated shells. The carbonate and organic content is negligible and the

magnetic susceptibility is moderately high, between 5 to 25 x 10^{-6} SI.

Unit A overlies Unit B across a sharp, unconformable contact. The well-sorted and dominantly sandy composition of Unit A is consistent with deposition in a foreshore or beach environment. The lithofacies records the progradation of recent beach sediments over the older Holocene sequence.

2.5.2 Micropaleontology:

The downcore trends in foram abundances are shown in Figure 2.4. A total of 17 statistically significant, foram genera were identified (Figure 2.5). The most prevalent taxa are the Rodalinids, most notably *Rosalina* sp. (15-30% of total abundance). Cluster analysis yielded three distinct clusters that indicate three major biofacies (Figure 2.6). The biofacies correspond with major depositional phases recognized from the core lithostratigraphy and physical property data (Figure 2.3).

Biofacies 1:

Biofacies 1 is defined by a lowermost cluster (120-210 cm depth; Figure 2.4; 2.6)) that corresponds with depositional environments in Unit E and the transition to Unit D. The biofacies is dominated by *Ammonia, Rosalina, Triloculina, and Quinqueloculina* sp (10-20%). Many tests show signs of abrasion and rounding and fragmented shells are also abundant, consistent with reworking in a shallow, foreshore environment. Most of the genera show a increasing abundance towards the top of Unit E, except the notable decline in *Ammonia*, *Triloculina* and *Haynesina* species. *Bolivina* sp. and *Planorbulina* sp. are in

low abundance (0-0.5%), as both species are typically found in lower energy settings (i.e. seagrass meadows; Murray, 2002) and have a low preservation in high-energy beach or environments (Murray, 2002). The gradual increase in species across the Unit E/Unit D boundary in consistent with the transitional nature of the contact.

Biofacies 2: 2A and 2B

Biofacies 2A corresponds with Unit D (wetland) and is marked by a gradual decrease of the larger species mentioned in Biofacies 1, and an increase in the less populous genera (*Planorbulina* sp., *Spiroloculina* sp.) as waters begin to calm and become more vegetated.

Biofacies 2B corresponds with Unit C (Lagoon) with a major eutrophication signal (*Bolivinids)* increasing up to 3% mirroring a decrease in larger *Quinqueloculina* sp., *Triloculina* sp. and *Miliolinella* sp. that fall from over 35% to less than 10% abundance. A second eutrophication indicator, *Rosalina* sp., also peaks in Biofacies 2A, up to 30%. These two indicator species are also identified in Goodman (2006) as harbour eutrophication indicator species. Peaks in LT-04 correspond with the same time period as Goodman's biofacies, indicating a eutrophication over a larger area that is anthropogenically influenced.

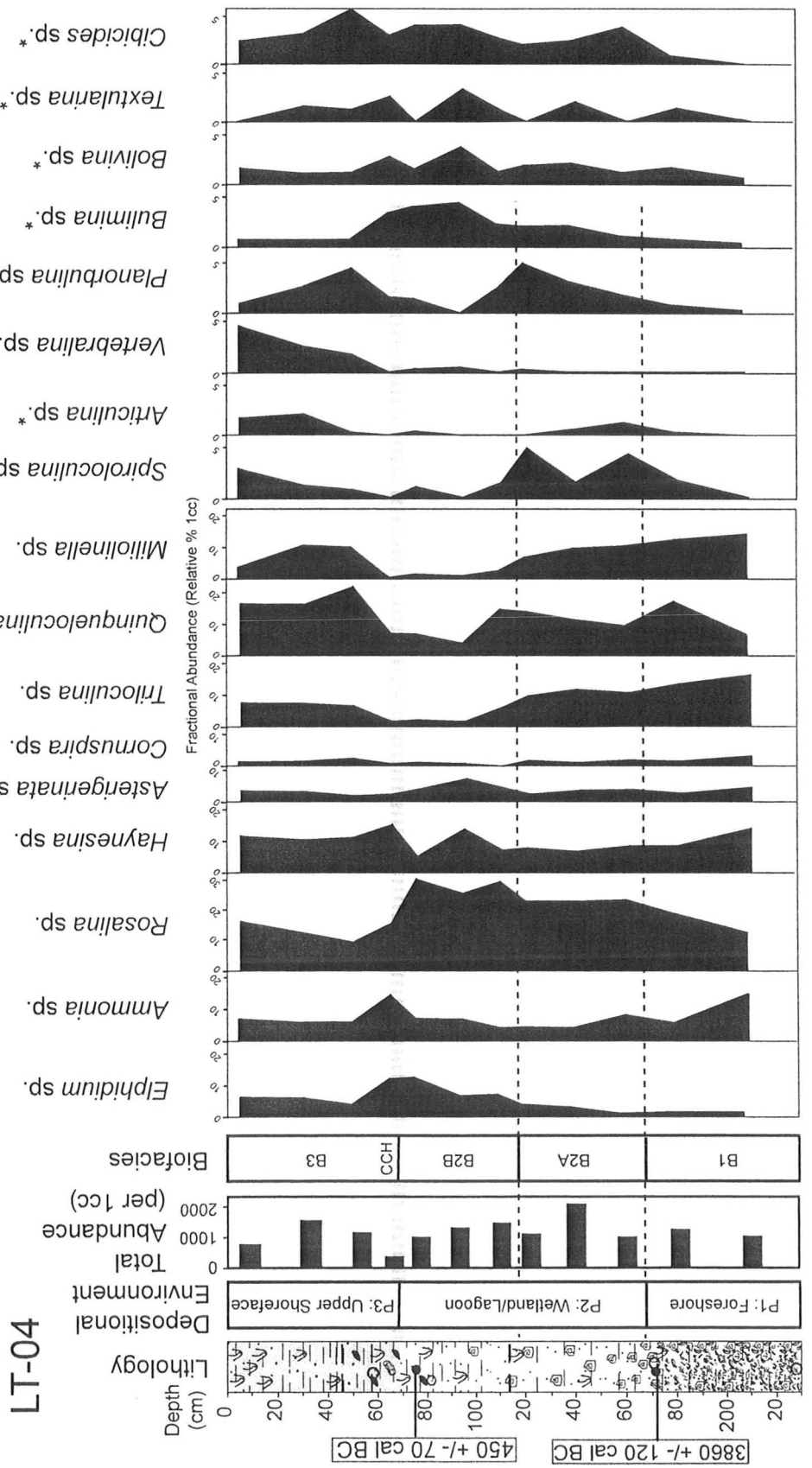

Figure 2.4: Foram percentage abundances for core LT-04 (weighted to 1 cc). Note distinct shift in foram abundances at 75 cm that also coincides with changes in grain-size and magnetic susceptibility associated with the causeway construction horizon (CCH). The shift to higher abundance of Bolivinids and Rodalinids and decrease in other species indicates an increasing eutrophication of the waters around Karantina Island during the Archaic period.

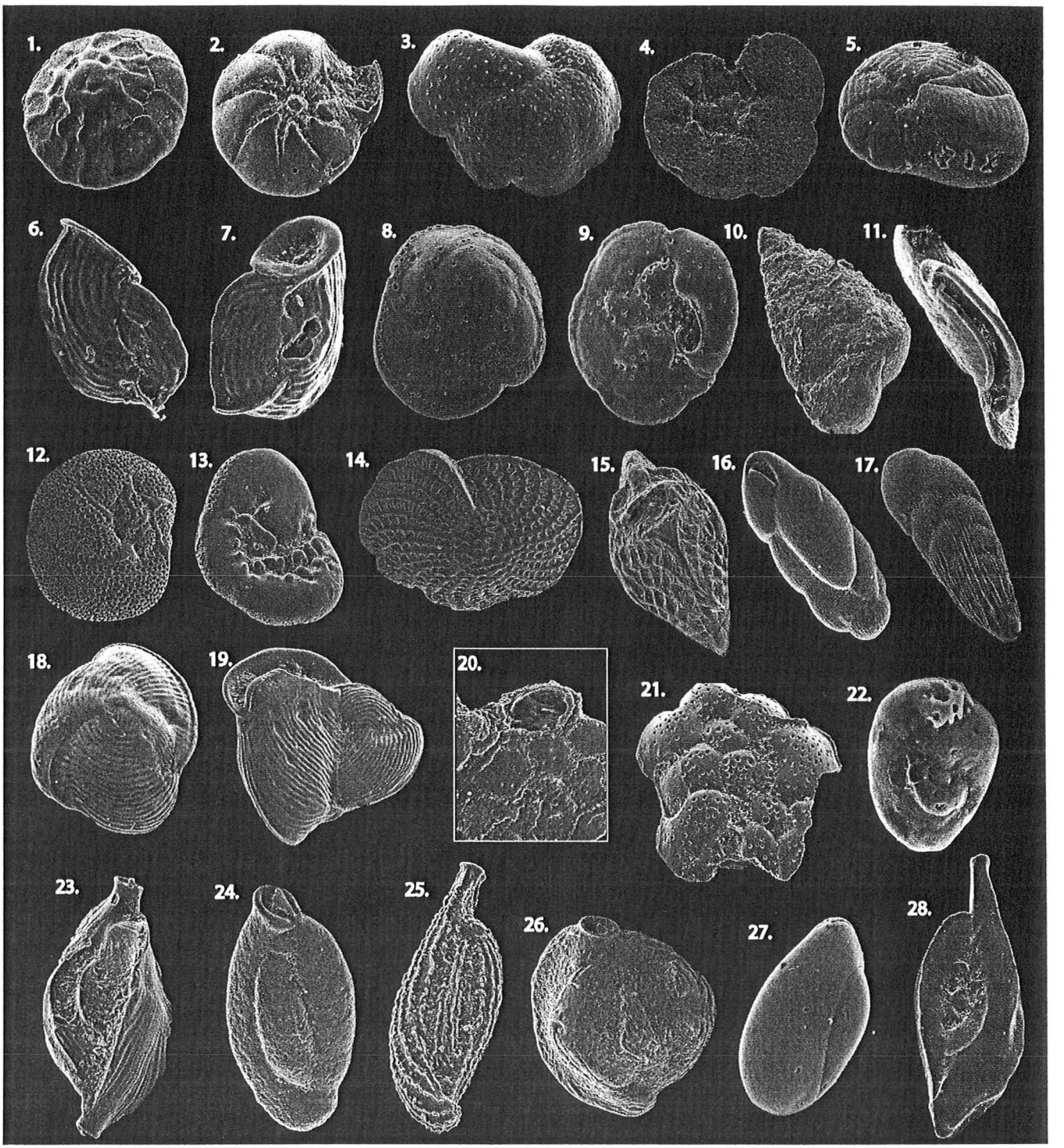

Figure 2.5: Scanning electron microscope (SEM) images of representative forams. **1**. *Ammonia* sp. spiral side (x 106) **2**. *Ammonia* sp.umbilical view (x 263) **3**. *Cibicides* sp. spiral view (x 263) **4**. *Cibicides* sp. umbilical view with aperture (x 252) **5**. *Haynesina* sp. (x 300) **6**. *Articulina* sp. spiral side (x 424) **7**. *Articulina* sp with aperture (x 312) **8**. *Asterigerinata* sp. ventral view (x 263) **9**. *Asterigerinata* sp. umbilical view with aperture (x 263) **10**. *Textularina* sp. (x 106) **11**. *Vertebralina* sp. apertural view on edge (x 156) **12**. *Rosalina* sp. spiral view (x 170) **13**. *Rosalina* sp. umbilical view (x 170) **14**. *Elphidium* sp. spiral view (x 7.15) **15**. *Elphidium* sp. on edge (x 163) **16**. *Bulimina* sp. with aperture (x 388) **17**. *Bolivina* sp. (x 252) **18**. *Vertebralina* sp. spiral view (x 212) **19**. *Vertebralina* sp. apertural view (x 163) **20**. *Planorbulina* sp., apertural view (x 406) **21**. *Planorbulina* sp. ventral view (x 178) **22**. *Miliolinella* sp. (x 655) **23**, **24**, **25**, **26**. *Miliolid* sp. (x 126, 137, 137, 137) **27**. *Triloculina* sp. (x 312) **28**. *Spiroloculina* sp. (x 143).

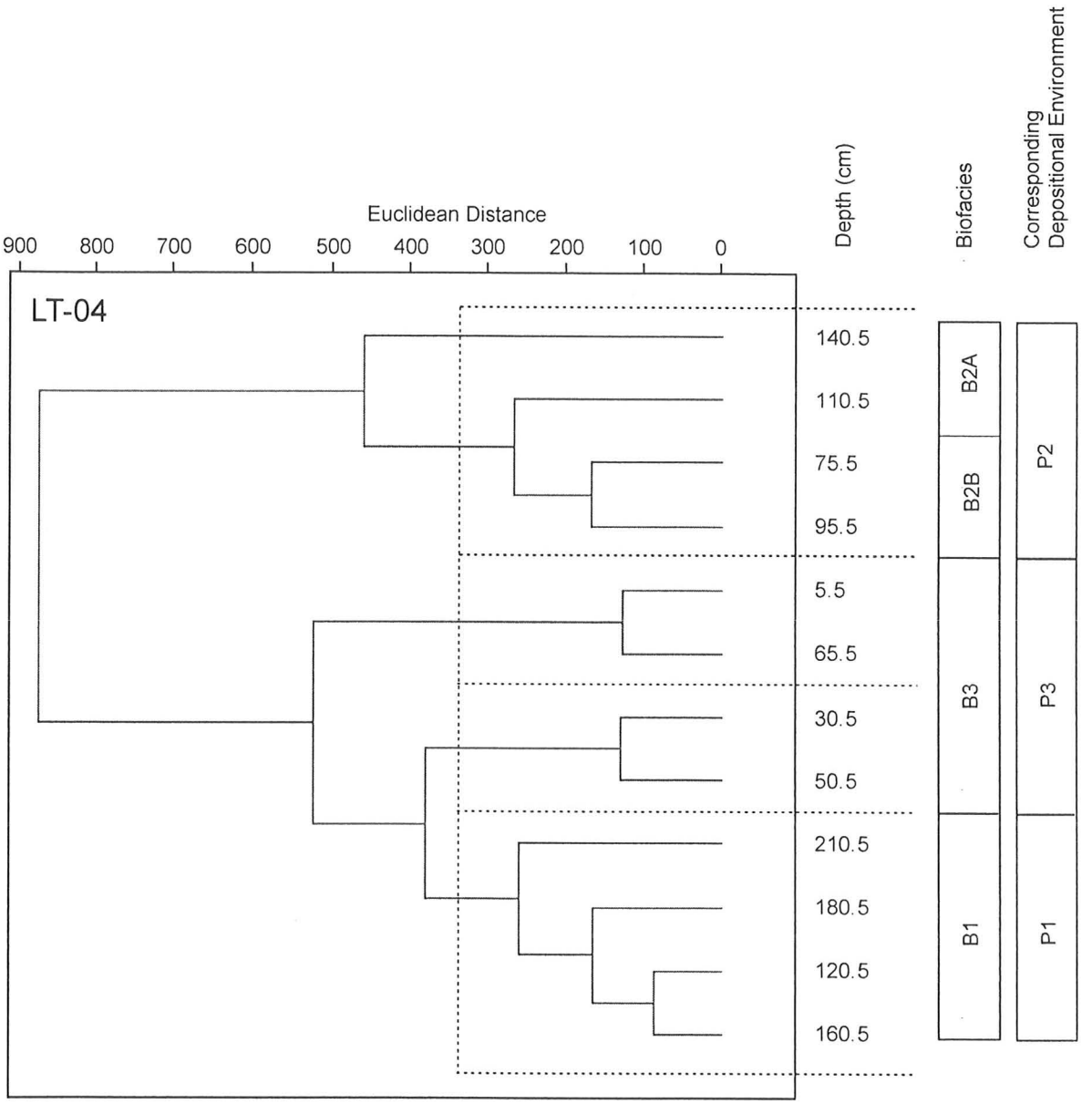

Figure 2.6: Q-mode cluster analysis of foram data using Wards cluster method. Three main biofacies are recognized based on clustering. Biofacies 1/Phase 1: Upper shoreface environment corresponding with Late Neotithic/Early Chalcolithic shoreline, Biofacies 2 (A and B)/ Phase 2: Shallow wetland/lagoonal environment, Biofacies 3/ Phase 3: Shallow marine prograding beach environment.

Biofacies 3:

Biofacies 3 corresponds with the shallow marine environment that was formed after the causeway construction horizon (~334 BC). Many foraminifera abundances revert back to pre- Unit C/ Biofacies 2A abundances. This change is the most visible trend in the foraminiferal data set. *Rosalina* sp. decrease to 10%, *Quinqueloculina* sp. increase from ~7% to over 20%. Many of the less abundant genera (*Vertebralina* sp., *Articulina* sp.) also increase immediately after the causeway construction horizon. These species did not show major abundances lower in the core and first begin to show significant percentages at the top of the core. *Planorbulina* sp. also increase again in Biofacies 3, indicating the onset of the modern *Posidonia Oceanica* meadows.

Major changes in foraminiferal abundances occur at the boundary between Unit D and C, and between C and B, transitioning from a wetland to a lagoon to the post-causeway environment (Figure 2.4). More focused foraminifera work will have to be undertaken in order to determine species-level identification and to discern the more subtle environmental changes, however a preliminary relationship has been established linking foraminiferal changes with lithology. The fact that major trends in foraminifera abundances do not appear to shift toward abundances indicating brackish water, that sea-waters were accessible to the area at all times. This indicates a steady supply of sea-water into the back wetland/lagoon, possibly from a channel or opening to the west (under the causeway structure).

Additionally, using foraminiferal trends, a rise in *Bolivinid* sp. was noted throughout Unit C (lagoonal). Goodman (2006) describes a similar rise in *Bolivinid* sp. during a eutrophic period in harbour construction on the western side of the causeway, located inside the harbour at Liman Tepe (Figure 3.7 – Chapter 3) These trends would indicate that anthropogenic influences had an influence on the entire basin-wide area during the Archaic period. This corresponds with an increase in the civilization's industry and its rise as a leading producer of olive oil products.

2.5.3 Bathymetry and seismic profiling

The digital bathymetry has been combined with the topographic relief to create a digital elevation model (DEM) shown in Figure 2.1. The bathymetry reveals a rugged sea-bed topography with minimal sediment cover to the west of Karantina Island, and a smooth, gradually sloping sea-bed to the east. The western portion of the map shows several submerged features, including relict river channels, shorelines and former coastal promontories. The shoreline locations are indicated by steeper sea-floor gradients occurring at depths of ca. -10 m, -14 m and -16 m beneath relative sea level (m rsl). The bathymetry also clearly shows the location of a previously studied submerged Archaic-age (AH; 6th c. BC) harbour at Liman Tepe and a later (Classical) harbour (CH) structures on the east and west of Karantina Island (Figure 2.1).

The smooth bottom relief to the east of Karantina Island is a result of coastal progradation and infilling of the sea-floor topography by Holocene sediments (Figure 2.3). A N-S linear feature to the east of Karantina Island marks the location of a shallow

trench and pipeline that carries effluents from a the local sewage treatment plant (circa 1992).

Changes in the thickness and geometry of the Holocene package on the east side of Karantina Island were determined from the sub-bottom seismic profiles (Figure 2.7). Chirp profiles were also collected to the west of the island but the seismic penetration was limited here by the presence of thin reflective (sandy) sediments and bedrock outcrops.

To the east of the island, the uppermost sequence of lagoonal mud and marine muddy silt (Units B-D) is represented by a crudely-stratified seismofacies that is draped across a distinctive basal reflector (Unit E; Figure 2.7). The surface relief on top of Unit E and the isochore thickness map of the overlying sediment sequence (Units B-D) are shown in Figure 2.8. Seismic data reveals a series of linear terraces made up of sediment consistent with Unit E at levels similar to bathymetry data on the western side of the causeway (~-10, -14 and -16 m depth). The major feature seen between -6 and -10 m depth has been identified as a drowned beach barrier, and chirp seismic shows a lagoonal lowland shoreward from the feature. A headland can also be seen near Liman Tepe, most likely associated with later shoreline progradation. A small channel structure appears to open to the west of the lagoon (under the causeway structure) but was not traced beyond the modern causeway. The base of Unit E was not resolved due to the limited penetration of the chirp source but other work using a low-frequency boomer seismic indicates Unit E in places directly overlies the Neogene limestone bedrock (Mueller et al., in press).

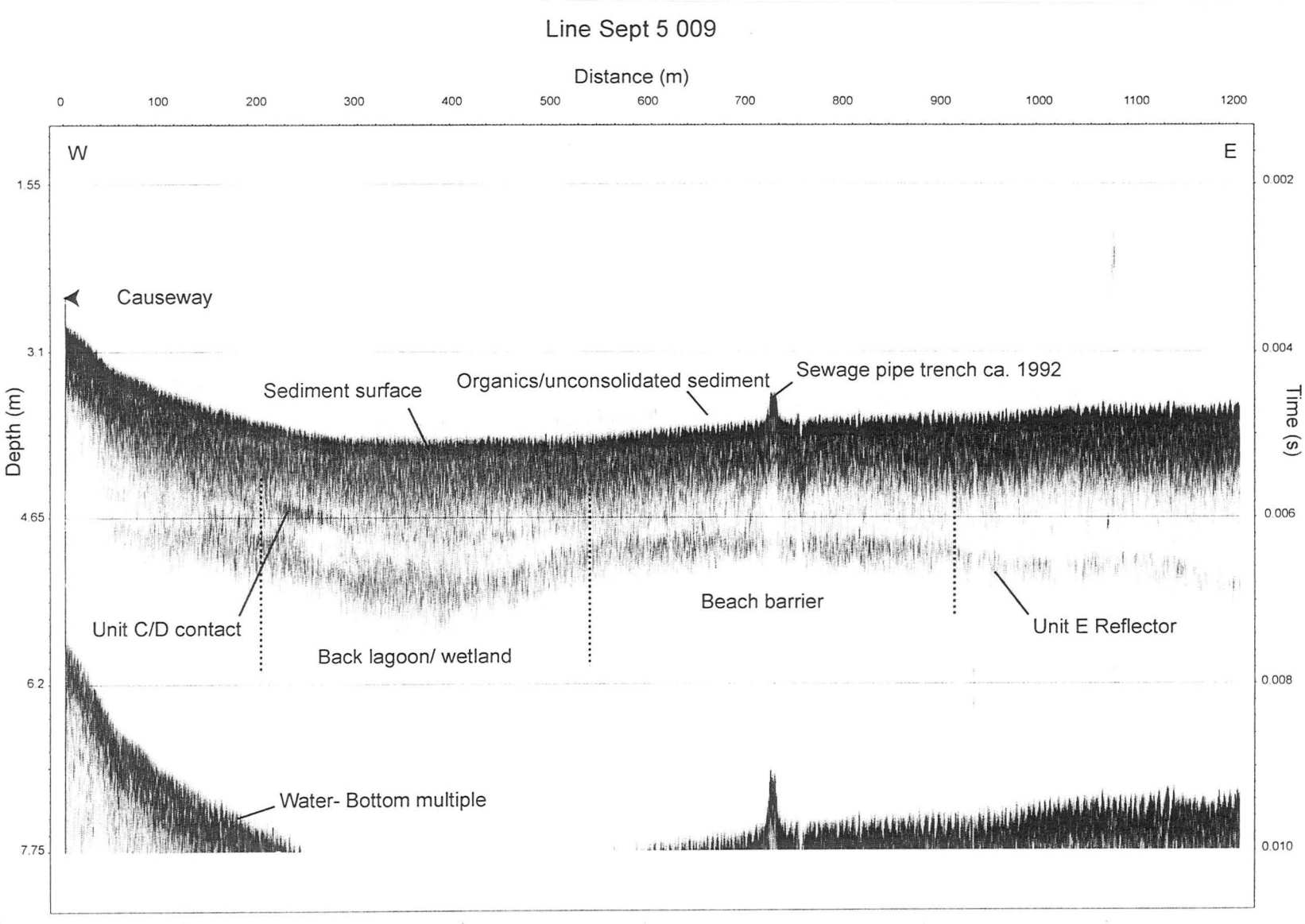

Figure 2.7: Chirp seismic reflection profile, showing thin sequence of lagoonal and shallow marine mud deposits (Units B-D) overlying poorly-sorted, shelly sand facies (Unit E).

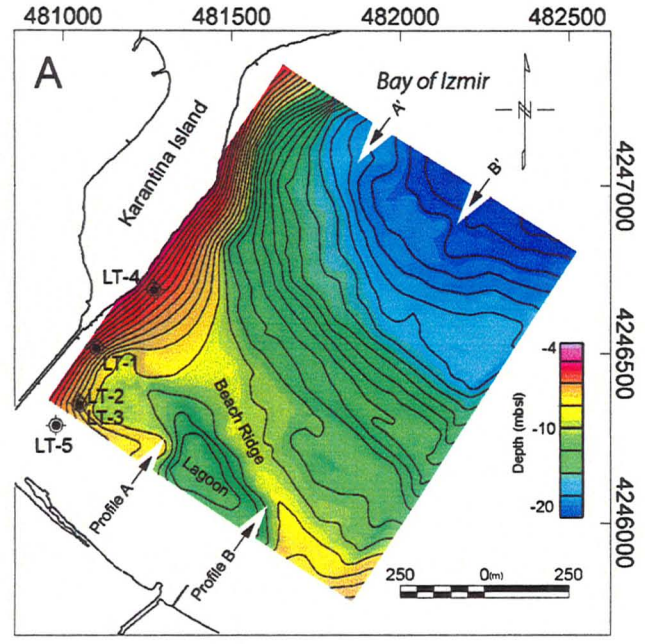

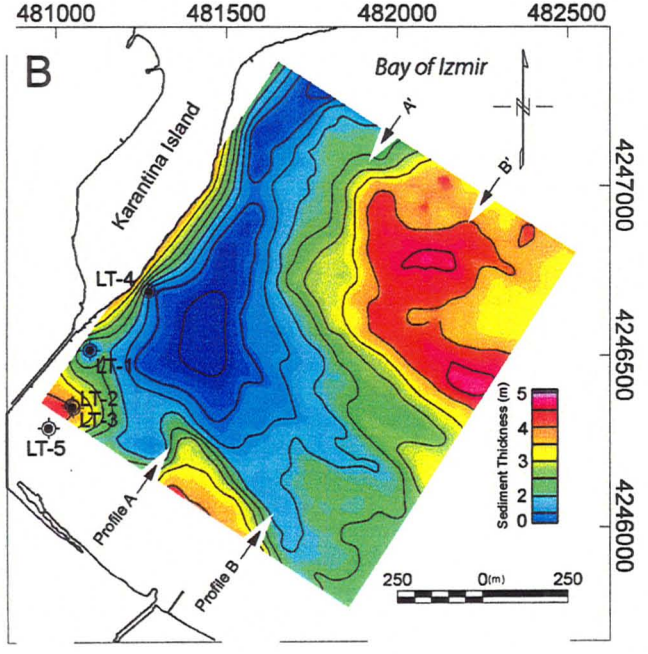

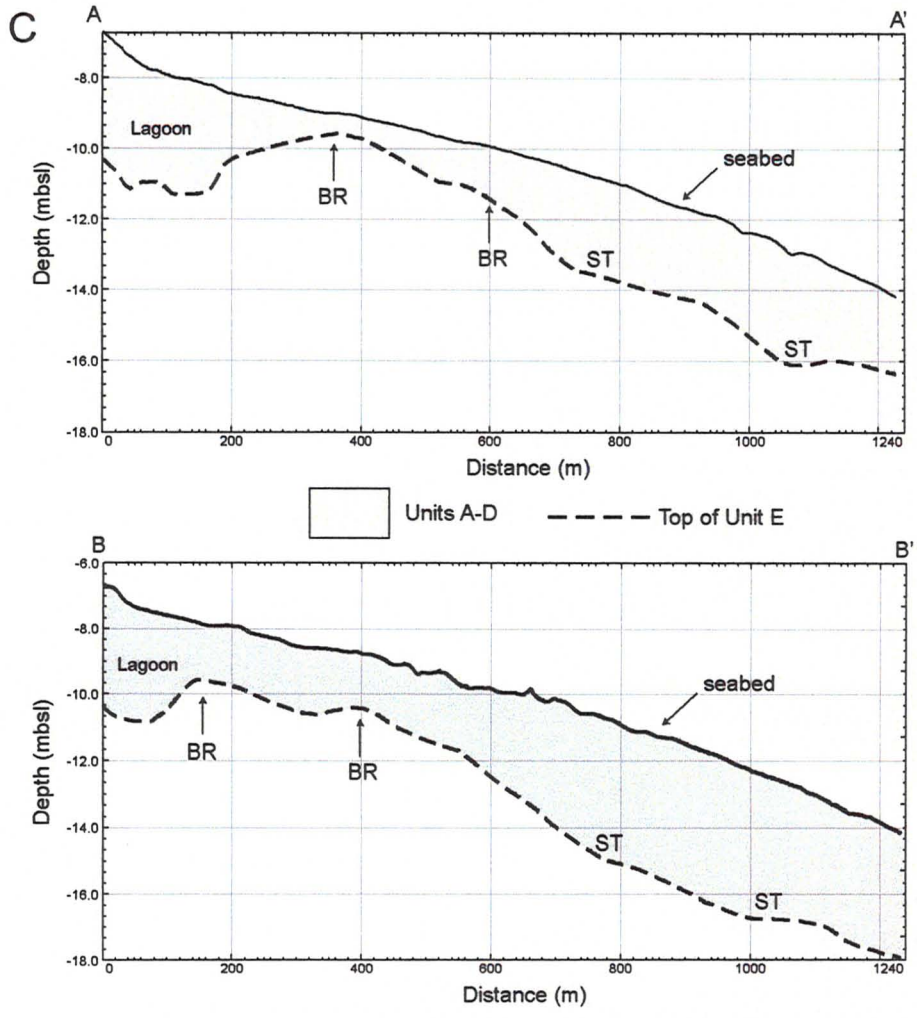

Figure 2.8: **A**. Surface relief on Unit E based on interpolation of basal reflector in chirp seismic data (contour interval 0.5 m). The reflector surface shows a number of north-east trending ridges that are interpreted as buried beach barriers. **B**. Isochore map of sediment infill (Units B-D) showing thickening of mud sequence within back-barrier lagoon (contour interval 1 m). **C**. Beach ridges and shoreline terraces are also recognized in profiles (A-A' and B-B') of the reflector surface. The beach ridges at 9-11 mbsl (meters beneath sea level) and terraces at -14 and -16 m rsl correspond with paleoshoreline features visible in the bathymetry map to the west of Karantina Island (Figure 2.1). BR: Beach Ridge; ST: Shoreline Terrace.

Bathymetric and seismic data reveal Karantina Island was connected to the mainland sometime before 3860 BC. As water-levels rose, the former shoreline became a shallow-marine platform that was a nucleus for shoreline progradation. This platform was taken advantage of by Alexander the Great's troops when building his causeway.

2.6 Discussion

2.6.1 Depositional environments

Sedimentological and geophysical surveys at Liman Tepe have identified several relict shorelines that are associated with a drowned beach barrier/lagoonal system that existed during the late Neolithic age (~3860 BC) (Figures 2.3; 2.8). A previous coastal reconstruction by Goodman et al. (in press) using land-core data found evidence for a higher level barrier/lagoon system dated to ca. 2800 BC (Bronze-Age). This younger barrier is represented on land by a broad, low-level ridge (<1 m above sea level) that lies ~200 m inland from the present shoreline (BR; Figure 2.1). The ridge is backed by a broad depression in the surface topography that marks the location of a former lagoon. The barrier-lagoon facies succession from the land core data is shown in Figure 2.9 for comparison with the lithofacies identified in this study. The high-level barrier identified by Goodman et al. (in press) is characterized by shoaling upward succession, consisting of upper shoreface sands overlain by lagoonal deposits and capped by foreshore sands and terrestrial sediments. The shoaling upwards sequence was interpreted by Goodman et al. (in press) as a prograding shoreface environment, formed during a highstand following the mid-Holocene (ca. 5-6 Ka) deceleration in sea level rise (Lambeck and Bard, 2000).

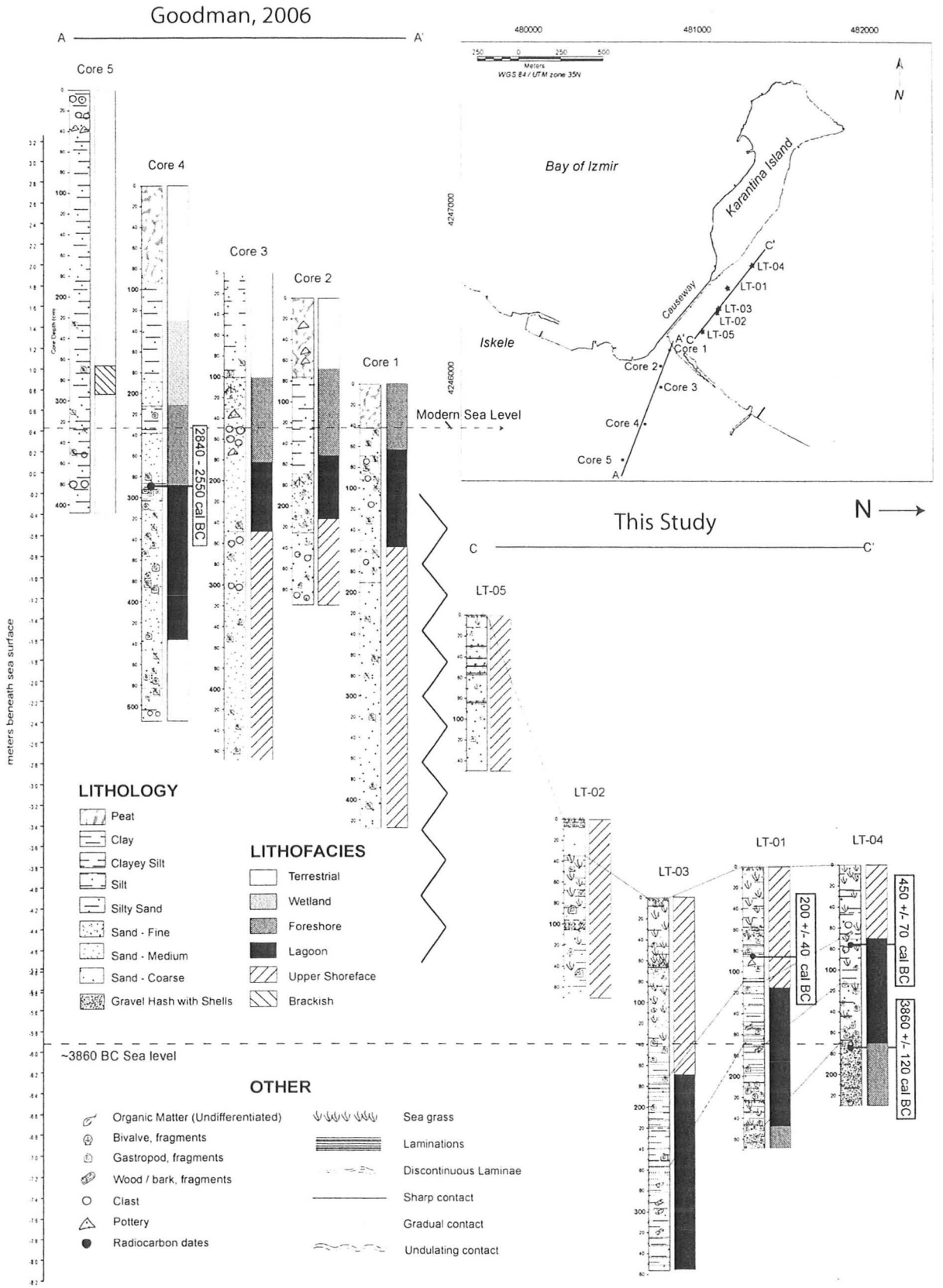

Figure 2.9: North-south cross-section showing stratigraphic relations between trangressive barrier/lagoonal system interpreted in terrestrial core data (from Goodman et al., in press) and barrier/lagoonal system in this study. The barrier complex identified by Goodman et al. (In press) represents a younger (Bronze-age) barrier system formed during a high stand phase. The barrier sediments in cores LT-01 and LT-04 (Unit E) represent a remnant barrier system that existed during Late Neolithic time (8,000-3,500 BC).

As sea levels stabilized close to modern sea level, the sediment supply to the coast began to outstrip the available accommodation space and the coastline prograded rapidly.

The facies succession of the Late Neolithic barrier system identified in this study shows a deepening-upwards succession (Figure 2.3; 2.9). The sequence is comprised of foreshore sediments at the base (Unit E) followed by wetland silty muds (Unit C) and lagoonal muds (Unit D) that clearly indicate increasing water depths. This sequence is capped by foreshore sand and silts (Units A, B). These two uppermost units were not part of the late Neolithic barrier-lagoonal complex and were deposited during later regressive phase following the causeway construction (~4th c BC). The barrier-lagoon deepening upwards succession identified in this study is indicative of a transgressive barrier system that underwent drowning in place as a result of a rapid sea level rise (Rampino and Sanders, 1980; Elliot, 1986).

2.6.2 Paleogeographic Reconstruction

Using geophysical data, the paleoshoreline represented by the foreshore facies (Unit E) can be traced to both the western and eastern sides of the causeway at approximately -6 to -10 m (Figure 2.10). This shoreline was used in a paleogeographic model to re-create the former shoreline for the Late Neolithic/Early Chalcolithic time period around 3860 BC (Figure 2.11A). Seismic data reveals a small lagoon on the eastern side bordered by a beach barrier (Figure 2.8). Relict channels cut through the old shoreline and the lagoon flanked by two small promontories.

According to Lambeck and Bard (2000) water-levels had begun to stabilize 5-6000 years ago, however, a local period of rapid transgression occurred locally between 3860 and 2800 BC, drowning the relict shoreline and preserving its erosional features. A shallow wetland covered land formerly exposed between the mainland and what is now Karantina Island. As water-levels rose, the wetland environment transitioned into a lagoonal and later shallow-marine environment (Figure 2.11 B).

During the Archaic period, major settlement arose in the area as Klazomenai developed into a major olive oil production center and trading port (Figure 2.11 C). Refuse (olive pits, pottery fragments) and higher magnetic susceptibility levels can be identified in Unit C demonstrating increased human activity. During this time period, major harbour constructions on land (Liman Tepe) and later on Karantina Island were built. Sea-levels continue to slowly rise, depositing even finer grains off-shore in the lagoonal environment.

The Archaic period also marks Persian encroachment into the Bay of Izmir and as a result, the re-establishment of Klazomenai onto Karantina Island. After Alexander the Great ordered the construction of a causeway connecting the island to the mainland, long-shore currents were interrupted and rapid progradation of the shoreline accelerated (Figure 2.11 D). Modern-day environments feature a shoreline that has prograded approximately 200 m into the bay since 2800 BC, the thickest sediment deposition occurring proximal to the causeway construction. Turkish officials are planning on removing the current causeway construction in order to encourage re-establishment of long-shore currents and slow beach progradation.

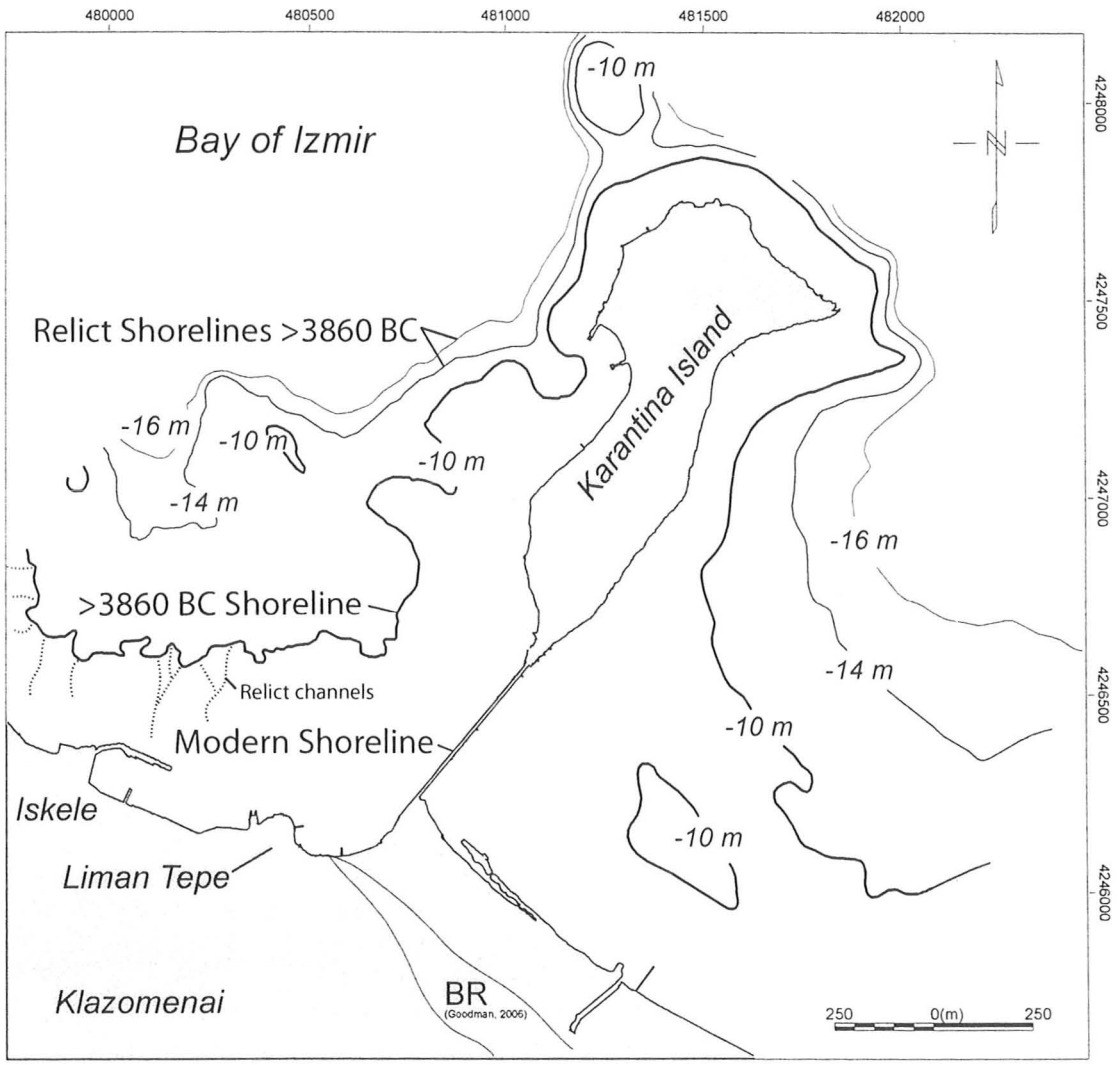

Figure 2.10: Reconstructed position of paleoshorelines position near Liman Tepe. Shorelines lie buried beneath the early Holocene sediment cover to east of Karantina but are also clearly visible in the bathymetry map to the west side of the island, where the marine muds are thinner. The shorelines are identified in bathymetry map by an increase in slope gradient at ca. -10, -14, and -16 m water depth. The -10 m contour (see also Figure 2.8) corresponds with a Unit E 14C date of 3,860 BC and is inferred to be of Late Neolithic/Early Chalcolithic age.

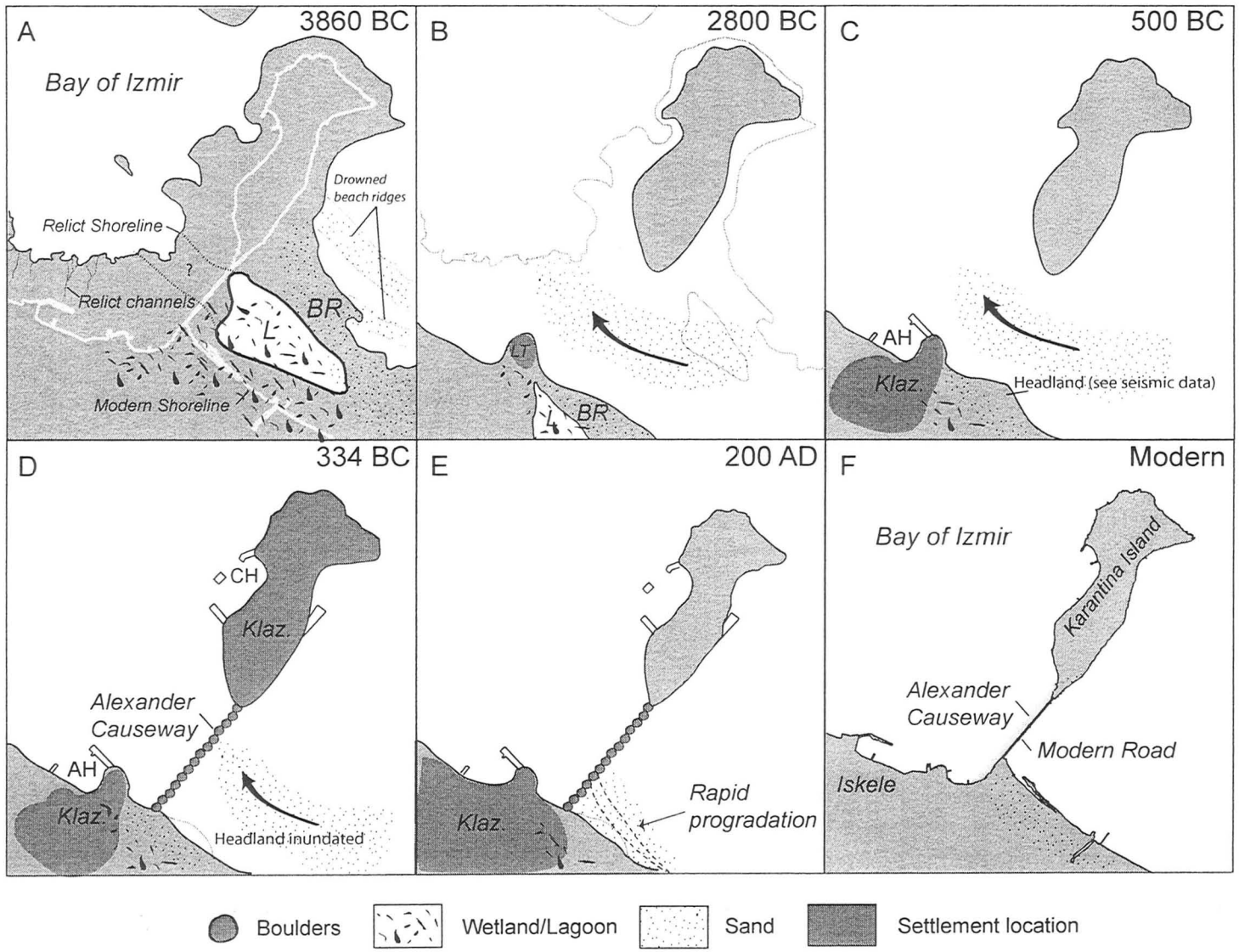

Figure 2.11: Paleogeographic map showing reconstructed shoreline and coastal environments at: **A**. 3860 BC (Late Neolithic/Early Chalcolithic). **B**. 2800 BC (Bronze-age; after Goodman et al., in press). **C**. ca. 500 BC (Archaic). A small headland (shown in seismic data) might have existed and was recorded by progradation documented in Goodman (2006) **D**. 334 BC construction of Alexander's causeway construction phase. Sea-levels continued to rise ~1-1.5 m since construction. **E**. 200 AD (Roman Klazomenai) progradation of the coastline to the east of the causeway. **F**. Modern day coastline showing prograded shoreline, modern beach barrier and lagoon.

2.6.2 Sea-level Reconstruction

Using core and geophysical data from this study as well as sea level indicators from previous work (Goodman, 2006) a local sea-level curve has been constructed to constrain the ages of shorelines identified in this study (Figure 2.12). The global eustatic sea-level curve and hydro-glacio-isostatic curve for the Mediterranean are also shown for comparison (Fleming, 1998; Lambeck, 1995). This study has identified a relict beach environment at – 6 m (ca. 3860 BC) and several older shorelines at -10, -14 and 16 m below present sea level. The reconstructed sea level curve provides a basis for constraining the ages of these older relict features. The local curve shows that sea levels at Liman Tepe prior to 3000 BC were up to 3 to 4 m below the hydro-glacio-eustatic sea level curve of Lambeck (1995). The difference in the local versus modeled curve can be attributed to rapid tectonic subsidence within the Bay of Izmir. The local sea level curve also shows that the mid-Holocene sea level deceleration did not occur until after 2800 BC, about 1000 years after the inflection indicated by Lambeck's modeled curve. The curve, when back-extrapolated, indicates that the older relict shorelines (-10 to -16 m) are likely 6-8000 years old. Further sea level indicators and radiocarbon dates are needed to constrain the ages of these older shorelines. The preliminary estimates obtained in this study, however, show that they are of likely Neolithic age and warrant investigation for prehistoric sites.

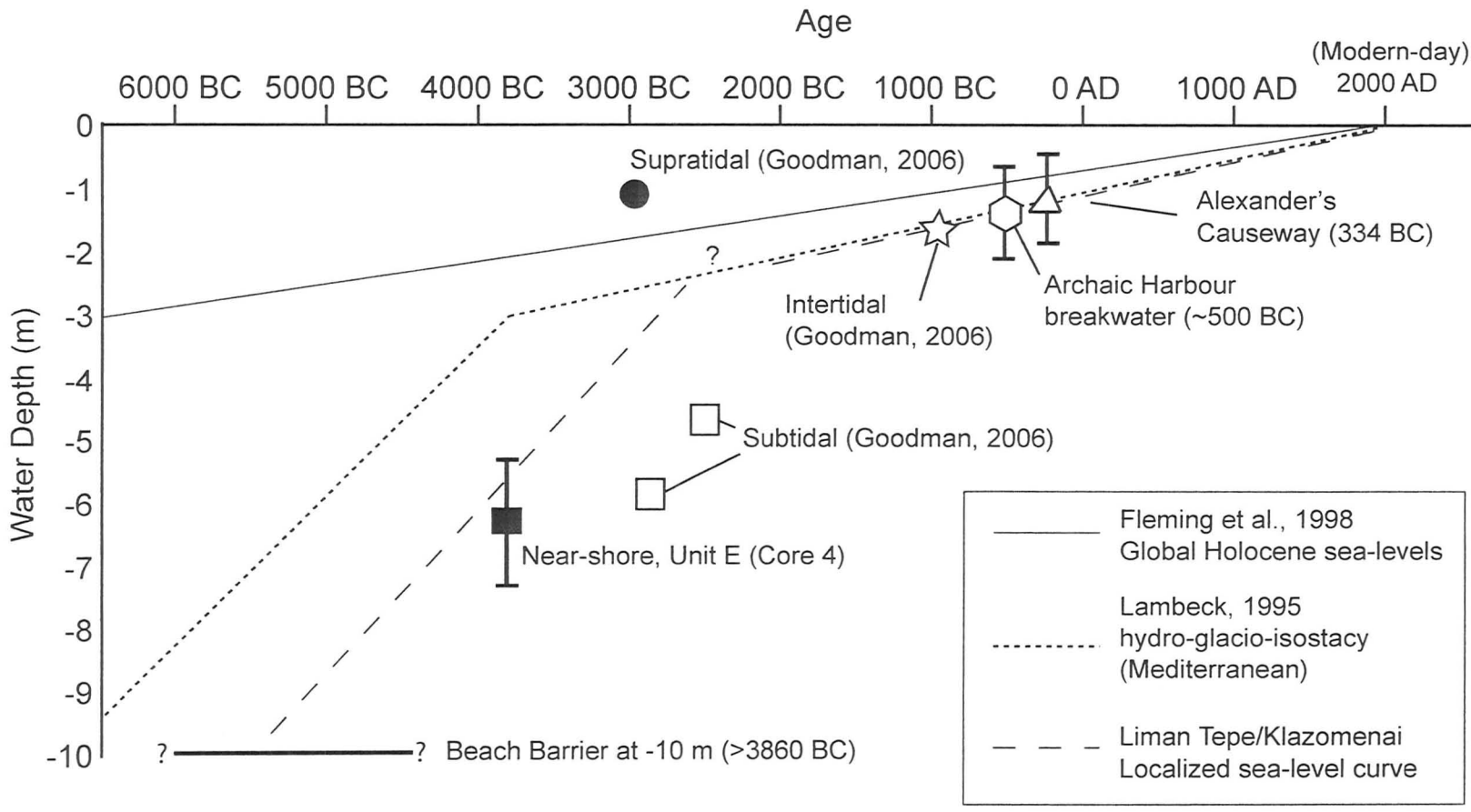

Figure 2.12: Sea-level curves as specified by Lambeck, 1995 and Flemming et al., 1998. Local variations at Liman Tepe from Goodman (in press) and this study have been used to create a local sea-level curve at Liman Tepe. Tidal variations range between 20 and 30 cm.

2.7 Conclusion:

Liman Tepe has experienced sea-level rise of approximately 10 m since 3860 BC, slowing to only a ~1.5 m rise since Archaic harbour construction (~500 BC). By compiling sea level indicators, a local sea-level curve has been estimated showing that sea levels during the Neolithic and Bronze Age were considerably lower (ca. 3-4 metres) than predicted by models (Lambeck, 1995; Lambeck and Bard, 2000; Fleming et al., 1998; Goodman, 2006) (Figure 2.12). The mapped locations of the submerged shoreline and age constraints provide a basis for further archaeological exploration at Liman Tepe for prehistoric settlements. This study also demonstrates the advantages of integrating geophysical and sedimentological analysis in order to achieve a more complete understanding of the paleogeography of submerged pre-historic shorelines.

2.8 References

Bailey, G. (2004) The wider significance of submerged archaeological sites and their relevance to world prehistory. *In* N.C. Fleming (ed.) Submerged prehistoric archaeology of the North Sea. Council for British Archaeology: York, p. 3-10.

Beierle, B.D., Lamoureux, S.F., Cockburn, J.M.H., and Spooner, I. (2002) A new method for visualizing sediment particle size distribution. Journal of Paleolimnology, 27: 279-283.

Boyce, J.I., Krezoski, G.M., Erkanal, H. and Saholgu, V. (In review) Shallow water mapping of a submerged Archaic-age harbour at Liman Tepe, Turkey using data-fused magnetic and side-scan sonar data. Journal of Archaeological Sciences.

Brinkman, R. (1972) Mesozoic Troughs and Crustal Structure in Anatolia. Geological Society of America Bulletin, 83: 819-826.

Cimerman, F., and Langer, M. (1991) Mediterranean Foraminifera. Slovenian Academy of Sciences and Arts: Ljubljana, 118 p., 93 plates.

Clark, C. (2004) Sediment magnetic record of post-colonial environmental change in Frenchman's Bay, Lake Ontario. Unpublished Master's thesis, McMaster University, Canada.

Conley, D.J. and Schelske, C.L. (2001) Biogenic Silica. *In* J.P. Smol, H.J.B. Birks and W.M. Last. Tracking Environmental Change Using Lake Sediments: Volume 3: Terrestrial, Algal and Siliceous Indicators. Kluwer Academic Publishers: Dortrecht. P.281-293.

Davis, J. (2002) Statistics and Data Analysis in Geology. John Wiley and Sons: New York, 638 p.

Duman, M., Avci, M., Duman, S., Demirkurt, E., and Duzbastilar, M. (2004) Surficial sediment distribution and net sediment transport pattern in Izmir Bay, western Turkey. Continental Shelf Research, 24: 965-981.

Elliott, T. (1986) Clastic Shorelines. *In* Reading, H.G., (ed) Sedimentary environments and facies. Blackwell Scientific Publications: Oxford, p. 143-177.

Erinc, S. (1978) Changes in the Physical Environment in Turkey since the Last Glacial. *In* W.C. Brice (ed.) The Environmental History of the Near and Middle East. Academic Press, London. p. 87-110.

Erkanal, H., (2008) Liman Tepe: New Light on Prehistoric Aegean Cultures. *in* Erkanal, H., Hauptmann, H., Sahoglu, V., Tuncel, R. (eds) The Aegean in the Neolithic, Chalcolithic and the Early Bronze Age. Ankara University Press, Ankara. P. 179-190.

Fleming, K., Johnston, P., Zwartz, D., Yokoyama, Y., Lambeck, K., and Chappell, J. (1998) Refining the eustatic sea-level curve since the Last Glacial Maximum using far- and intermediate-field sites. Earth and Planetary Science Letters, 183: 327-342.

Goodman, B.N., (2006) The paleogeography of Liman Tepe, Turkey: A multi-proxy geoarcheological study, unpublished Ph.D. thesis, McMaster University, Canada.

Goodman, B.N., Reinhardt, E.G., Dey, H., Boyce, J.I., Schwarcz, H., Sahoglu, V., Erkanal, H., and Artzy, M. (In Press) Evidence for Holocene marine transgression and shoreline progradation due to barrier development in Iskele, Bay of Izmir, Turkey: Journal of Coastal Research.

Hammer, O., Harper, D., and Ryan, P. (2001) Past: Paleontological statistics software package for education and data analysis. Paleontologia Electronica, vol. 9.

Kraft, J.C., Aschenbrenner, S. E., and Rapp, G. (1977) Paleogeographic Reconstruction of Coastal Aegean Archaeological Sites. Science, 195:4282 p. 941-947.

Lambeck, K., (1995) Late Pleistocene and Holocene sea-level change in Greece and south-western Turkey: a separation of eustatic, isostatic and tectonic contributions. Geophysics Journal International, 122: 1022-1044.

Lambeck, K., and Bard, E. (2000) Sea-level change along the French Mediterranean coast for the past 30 000 years. Earth and Planetary Science Letters, 175: 203-222.

Marriner, N., Morhange, C., and Doumet-Serhal, C. (2006) Geoarchaeology of Sidon's ancient harbours, Phoenicia. Journal of Archaeological Science, 33: 1514-1535.

Mueller, C., Woelz, S., Ersoy, Y., Boyce, J.I., Jokisch, T., Wendt, G. and Rabbel, W. (In Press) Ultra high-resolution marine 2D-3D seismic investigation of the Liman Tepe/Karantina Island archaeological Site (Urla, Turkey): Journal of Applied Geophysics.

Murray, J. (2006) Ecology and Applications of Benthic Foraminifera. Cambridge University Press: New York, 438 p.

Ocakoglu, N., Demirbag, E., and Kuscu, I. (2005) Neotectonic structures in Izmir Gulf and surrounding regions (western Turkey): Evidences of strike-slip faulting with compression in the Aegean extensional regime. Marine Geology, 219: 155-171.

Pausanius, (2nd c BC) Guide to Greece, tr. by Peter Levi (1984) London: Penguin Books Inc. Vol 1. 587 p.

Rampino, M.R., and Sanders, J.E. (1980) Holocene transgression in south-central Long Island, New York. Journal of Sedimentary Petrology, 50: 1063-1080.

Rivieros, N. V., Babalola, A.O., Boudreau, R., Patterson, R. T., Roe H. M., and Doherty, C. (2007) Modern distribution of salt marsh foraminifera and thecamoebians in the Seymour-Belize Inlet Complex, British Columbia, Canada. Marine Geology, 242: 39-63.

Sahoglu, V. (2005) The Anatolian Trade Network and the Izmir region during the Early Bronze Age. Oxford J. Archaeology: 24, 339-361.

Sayin, E. (2003) Physical Features of the Izmir Bay. Continental Shelf Research, 23: 957-970.

Sonnenburg, E.P. and Boyce, J.I. (2008) Data-fused digital bathymetry and side-scan sonar as a base for archaeological inventory of submerged landscapes in the Rideau Canal, Ontario, Canada. Geoarchaeology, 23: 654-674.

Stiros, S.C., Laborel, J., Laborel-Deguen, F., Papageorgiou, S., Evin, J., and Pirazzoli, P.A. (2000) Seismic coastal uplift in a region of subsidence: Holocene raised shorelines of Samos Island, Aegean Sea, Greece. Marine Geology, 170: 41-58.

van Hengstum, P., Reinhardt, E., Boyce, J., and Clark, C. (2007) Changing sedimentation patterns due to historical land-use change in Frenchman's Bay, Pickering, Canada: evidence from high-resolution textural analysis. Journal of Paleolimnology, 37: 603-618.

Chapter 3: COASTAL SEDIMENT RECORD OF THE CONSTRUCTION OF ALEXANDER THE GREAT'S CAUSEWAY AT KLAZOMENAI, TURKEY

G.M. Krezoski, J.I. Boyce and E.G. Reinhardt

School of Geography and Earth Sciences, McMaster University, Ontario, Canada

V. Sahoglu and H. Erkanal

Dept. of Humanities, Ankara University, Turkey

For Submission to Journal of Archaeological Sciences

3.1 Abstract

In 334 BC, Alexander the Great ordered the construction of a 400 m long causeway connecting the port city of Klazomenai (modern-day Karantina Island, western Turkey) with the Ionian mainland to defend the island against Persian attack. The causeway construction interrupted the natural long-shore currents, creating a sheltered basin on the eastern (leeward) side of the causeway. A detailed multi-proxy study was conducted on five marine sediment cores to document changes in the coastal environments resulting from the causeway construction and to verify the early 4th c. BC age of the structure.

Three distinct depositional phases were recognized based on core lithofacies, particle-size, magnetic properties, trace metals and foram abundances. The pre-causeway environment is recorded by a lowermost sequence of coarse-grained pebbly sand with abundant shell fragments deposited in a high-energy foreshore environment (Phase 1). Plant material in the Phase 1 beach sediments yielded a ^{14}C age of 3860 ± 120 cal BC. The beach sediments are transitional above to a laminated silt facies deposited in a back-barrier lagoon that developed during a phase of Holocene coastal transgression (Phase 2).

The onset of causeway construction (Phase 3) is identified by a shift to coarser mean grain size within an uppermost organic-rich silty mud layer containing abundant *Posidonia Oceanica* sea grass fragments. The transition is associated with the appearance of pottery fragments, masonry and abundant olive pits which yielded a ^{14}C date of 450 ± 70 cal BC, giving a maximum age for the causeway. The transition to the post-causeway environment is also clearly recognizable in changes in foram abundances, trace metals

and sediment magnetic susceptibility. The causeway construction dramatically altered the coastal sediment budget, contributing to accelerated sedimentation and rapid progradation of the coastline to the east of the barrier.

3.2 Introduction:

During his campaign against the Persians (ca. 334-331 BC), Alexander the Great laid siege to a number of well-fortified cities including the coastal settlements at Miletus, Halicarnassus and Tyre (Pausanius, 2nd c. BC; Quintus Curtius Rufus, 1st c. AD) (Figure 3.1A). The siege of Tyre was one of Alexander's most difficult conquests as the ancient city was located on a small island one kilometre off the Phoenician coast. The Tyrians also possessed a superior naval fleet, which discouraged a direct Macedonian attack by sea (Nir, 1996). In order to conquer Tyre, Alexander ordered the construction of a causeway connecting the island with the mainland. The project was a major undertaking, considering the required length of the causeway (> 1 km) and the prevailing strong winds and heavy sea conditions on the Phoenician coast (Nir, 1996). After approximately six months and several failed attempts, the causeway was completed and Alexander's forces gained Tyre's walls, sacking the city in 332 BC (Pausanius, 2nd C. BC; Quintus Curtius Rufus, 1st c. AD).

Geological and geoarchaeological investigations at Tyre have documented the impact of the causeway construction on the coastline and have established that the structure was built on top a pre-existing natural isthmus (Nir, 1996; Marriner et al., 2007; Stafford, 2007). Marriner et al. (2007) interpreted the isthmus as a submerged proto-

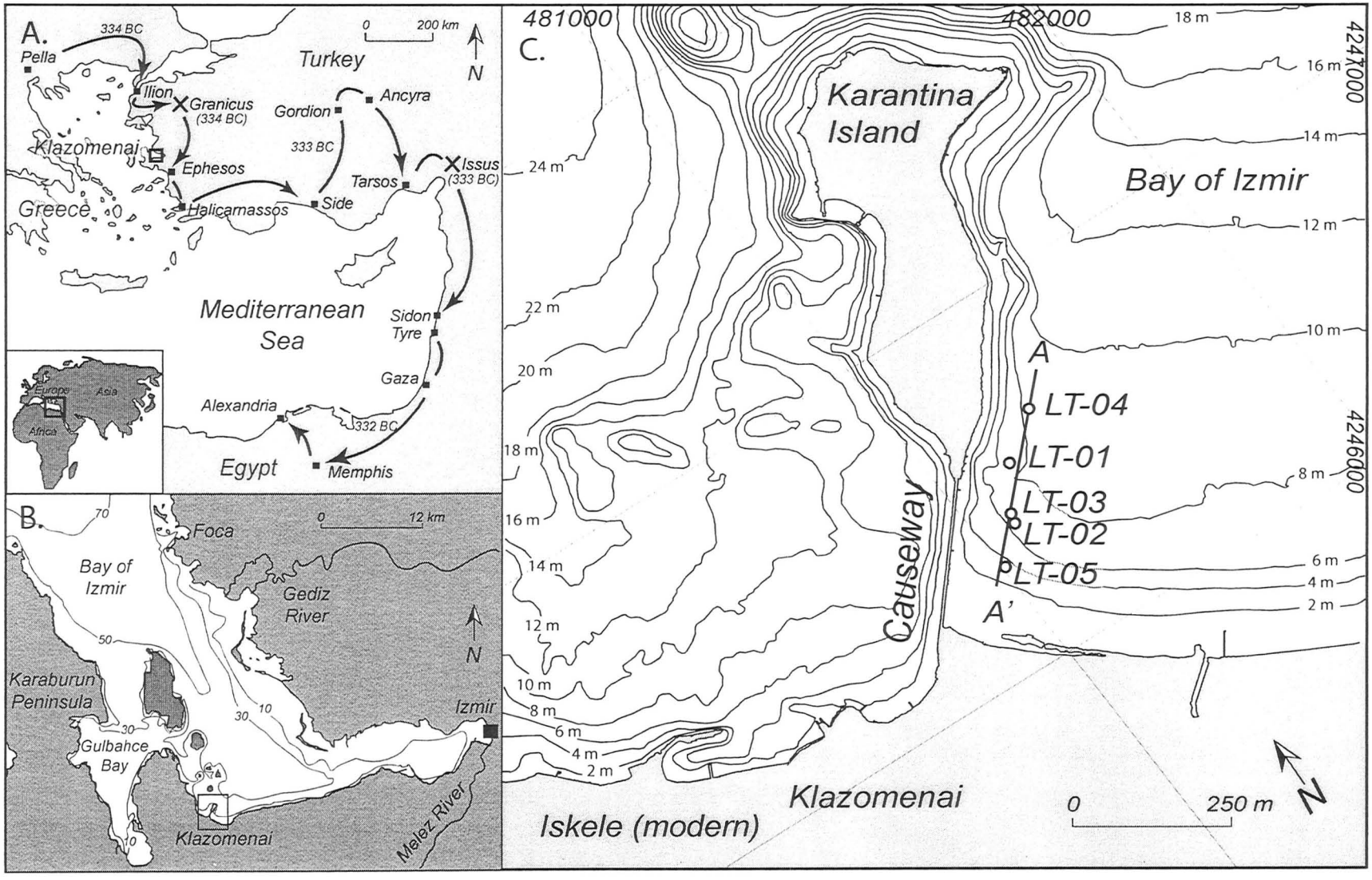

Figure 3.1: **A**. Map of Alexander the Great's campaigns, 334-331 BC. The causeway at Klazomenai was constructed shortly after the battle of the Granicus in 334 BC. **B**. Location of study area within the Bay of Izmir. **C**. Study area showing location of cores and generalized bathymetry (contour interval 2 m).

tombolo (sand spit) extending from a promontory on the mainland to the eastern side of the island. Considering the lower sea levels (ca. 1.5 m) during the early Classical period (Nir, 1996) the proto-tombolo would have provided an ideal foundation for the construction of a mole. According to historical sources, the mole structure was built out from the headland with rubble from the ruins of mainland Tyre and shored up with timber (Quintus Curtius Rufus, 1st c. AD). The structure acted essentially in the same manner as a coastal pier, blocking the natural long-shore transport along the coast and leading to rapid growth of a broad wave-dominated tombolo that now joins the old city with the modern shoreline (Nir, 1996; Marriner et al., 2007). Nir (1996) estimated that on the order of 10 million m^3 of sand accumulated within the tombolo since 332 BC. Following his success at Tyre, Alexander commissioned the construction of another causeway in Alexandria's harbour to link the mainland with Pharos Island (the Heptastadion; Millet and Goiran, 2007).

The causeways at Tyre and Alexandria were impressive feats of coastal engineering that significantly altered the natural coastal environments (Nir, 1996; Stanley and Bernasconi, 2006; Marriner at al., 2007; Millet and Goiran, 2007). These structures were not unique in antiquity, however, as they were proto-typed on an earlier causeway commissioned by Alexander in 334 BC to defend the port city of Klazomenai, in western Ionia (Figure 3.1C) against Persian attack. At that time the city centre of Klazomenai was located on a small island lying ~500 m off the Ionian mainland (modern day Karantina Island; Figure 3.1C). In order to secure the island against a naval invasion, Alexander ordered his general Parmenion to build a causeway connecting it with the mainland to

allow the Macedonian army rapid access to the city (Figure 3.1C) (Green, 1991). The details of the causeway construction at Klazomenai are not known, as the only descriptions of the structure in antiquity were written by historians centuries after it was built (ex. Pausanius, 2nd c. BC; Pliny the Elder, 1st c BC). The causeway underwent several phases of renovation and rebuilding during the Hellenistic and Roman periods. The ruins of the Roman causeways are visible close to modern sea level ca. 10 m to the west of the modern causeway bridge (Figure 3.2). The remains of the original earthen-work causeway are obscured by these later constructions but its general form is indicated by a broad rubble platform that is visible in bathymetry images to the east of the modern road (Figure 3.2).

The causeway at Klazomenai is important not only as example of coastal engineering in antiquity (e.g. Nir, 1996; Marriner et al., 2007) but also as an valuable archive of the long-term impacts of engineering structures on coastal processes. The sheltered basin created on the east side of the causeway following its construction provided favorable conditions for the accumulation of a continuous record of the post-causeway sediments. In this paper we examine the coastal sediment record of the causeway construction and alteration of coastal environments at Klazomenai using multi-proxy analysis of marine sediment cores. The results show that causeway barrier produced an abrupt change in the coastal currents and sedimentation patterns in the Bay of Izmir as recorded by distinctive shifts in lithology, particle size, foram abundances and a range of other sediment physical properties. ^{14}C dates on organics from the pre- and

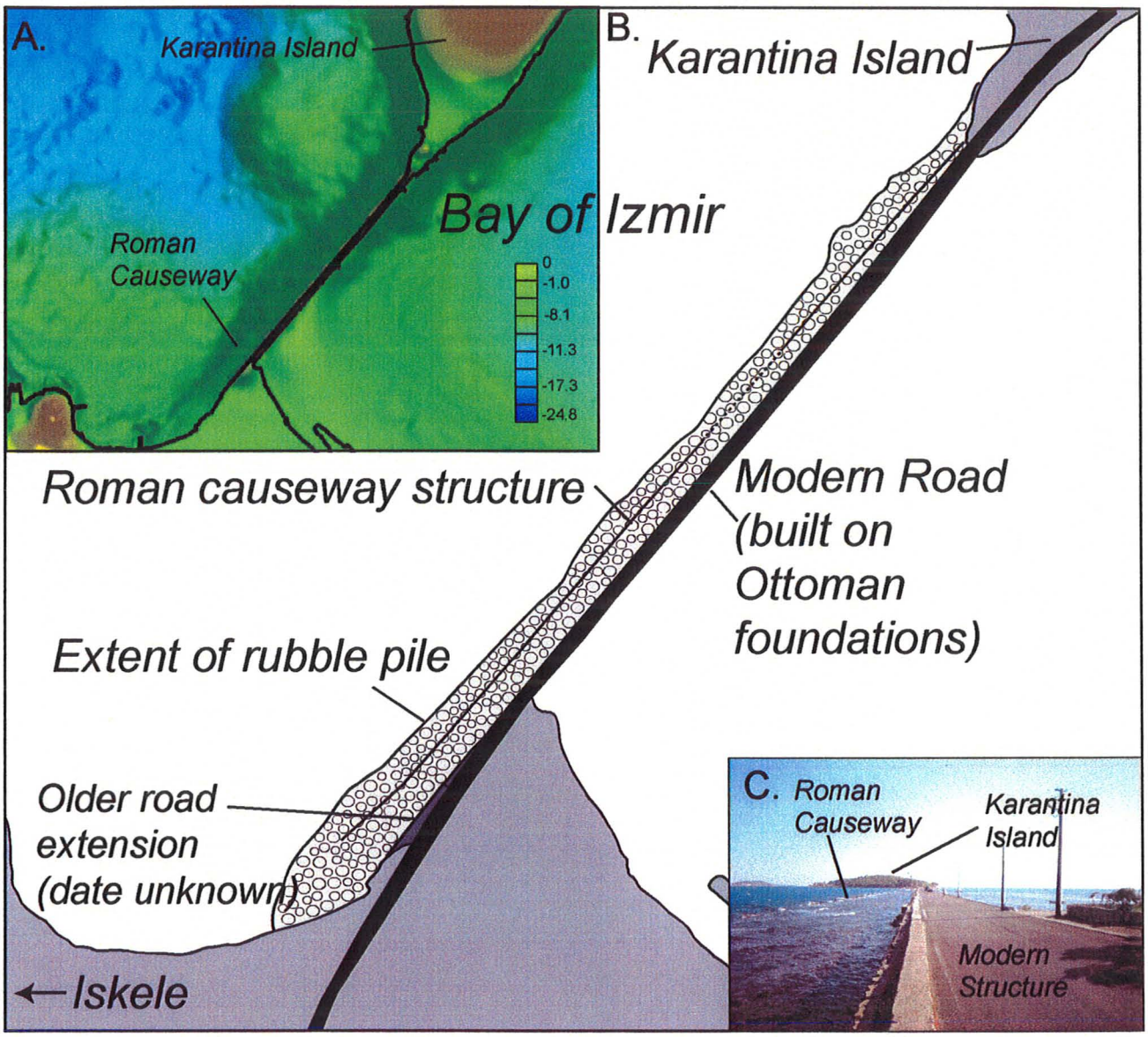

Figure 3.2: **A**. Portion of bathymetry map showing broad submerged platform, paralleling the modern causeway. **B**. The original earth-work causeway constructed by Alexander underwent successive phases of reconstruction during Hellenistic and Roman periods. The remains of the Roman phase are present close to water level about 10 metres west of the modern causeway. **C**. The modern causeway is of Ottoman construction.

post-causeway constrain the age of the causeway to within the 4th c. BC, verifying the descriptions by historical sources.

The long-term record of the coastal impacts documented at Klazomenai provides baseline data for evaluating future coastal developments in the Bay of Izmir. These future developments include plans by the local municipal governments to construct a new elevated causeway bridge on pylons in an attempt to re-establish longshore flow and nourishment of beaches on the west side of the causeway. Our results provide a basis for evaluating the potential environmental consequences of these planned engineering interventions.

3.3 Study Area

The ancient port city of Klazomenai is located near the modern town of Iskele on the southern shore of the Bay of Izmir, approximately 40 km east Izmir in western Turkey (Figure 3.1B). The area is of archaeological importance, as it contains a number of long-occupied coastal archaeological sites. The small coastal promontory to the east of modern Iskele harbour was the site of an important prehistoric coastal settlement known as Liman Tepe (Figure 3.1). Liman Tepe was first occupied in the Late Neolithic/Early Chalcolithic period and during the Early Bronze Age (EBA) became an important port city with well-fortified walls and monumental architecture (Erkanal, 2008; Sahoglu, 2008). The EBA city figured prominently in the trade and trans-shipment of goods between central Anatolia and the western Aegean (the Anatolian Trade Network; Sahoglu, 2005).

The city of Klazomenai was founded on top of the Bronze-age settlement in the 9th c. BC by Ionian settlers from the Greek mainland and later became one of the 12 cities of the Ionian League (the Dodecapolis; Herodotus, 5th c BC). The city, a contemporary of the famous Troy, was located initially on the mainland but was moved to Karantina Island sometime during the early 6th c. BC during the Ionian Revolt against the Persians (Ersoy, 1993). Later in Classical and Roman times the city became and important shipping port and olive producing centre.

The study area lies within the tectonically active Aegean extensional province in western Turkey. The Bay of Izmir is a major fault-bounded graben structure that is associated with active seismicity and tectonic subsidence. The bedrock within the region consists of Neogene volcanics (predominantly rhyolites, andesites) and sedimentary rocks (Ocakoglu et al., 2005). Tertiary limestones form the local bedrock within the study area and are draped by a variable thickness of unconsolidated late Quaternary and Holocene sediments. On the west side of the causeway, the bottom sediments are thin or absent, and bedrock is partially exposed (Boyce et al., in review). The main sediment input to the Bay is from the Gediz River approximately 30-40 km north-east of the study site (Duman et al., 2004). On the southern shore of the Bay, sediments are derived from erosion of the coastal highlands and delivered to the coast by seasonal wadi flow (Duman et al., 2004).

3.4 Methods

A total of six cores were extracted from the east and west side of the causeway in water depths of 1-4 m using a percussion corer operated from a Zodiac inflatable boat.

The coring system employed a 50 kg slide hammer to drive the 6 m long aluminum tubes (60 mm dia.) up to 3.8 m into the seabed sediment. The sediment-filled core tubes were extracted using airbag lift systems deployed by SCUBA divers. The cores were drained, cut into 1 m sections, shipped, and placed in cold storage (4-6 degrees C) until processed.

The split cores were sampled at 5 cm intervals for grain size analysis and loss on ignition (LOI) measurements. LOI was conducted on 2 gram samples according to the methods outlined by Heiri et al. (2001). Grain size analysis was performed on 5 cm^3 samples using a Beckmann LS 230 Coulter Counter with three repeat runs for each sample. The full grain size distribution curve was recorded for each sample and summary statistics (average mean, mode, and standard deviation) calculated and plotted versus depth. To facilitate interpretation the particle size abundances were gridded and plotted as a colour surface plot of depth, grain diameter (ϕ) and percentage abundance (Beierle et al., 2002; van Hengstum et al., 2007).

Volume magnetic susceptibility (κ) was measured at 5 mm intervals on split cores using a Bartington MS2E probe. Air measurements were taken every 5-7 measurements to monitor instrumental drift and corrections were interpolated and applied to the data set.

Micropaleontological analyses (foraminifera) were completed on a single core (LT-04) to aid in interpretation of environmental conditions. Twelve samples of ca. 5 cm^3 were taken between 10 and 30 cm spacing. Samples were sieved using a 500 μm and 63 μm sieve and then dried. Forams were picked and identified according to Cimerman and Langer (1991). Samples were recorded, calculated to 1 cc abundances and plotted for

relative percent. Further analysis, including diversity indices and cluster analysis, are included in Krezoski et al., (Chapter 2).

Trace metal analyses have been used in widely in studies of soils from terrestrial archaeological sites to determine occupation histories and metal use but have rarely been used in marine archaeological contexts. In this study, the down-core abundances of selected trace metals in marine were determined using mass spectrometry for comparison with other environmental indicators. Digested samples were prepared following the EPA 3050B guidelines (1998) for environmentally available metals and measured on a Micromass ICP-MS at the University of Wisconsin, Milwaukee. All trace metal data were corrected for mean enrichment factors (EF) using Aluminum and plotted versus depth (Tylmann, 2007). Six metals associated with historical human usage were measured including Copper (Cu), Lead (Pb), Tin (Sn), Arsenic (As), Antimony (Sb), Nickel (Ni), and Iron (Fe).

Three radiocarbon dates were obtained on organic materials from cores to constrain the timing of causeway construction. Olive pits were taken from 76-77 cm depth in LT-04, and bulk organic samples were taken from 171-172 cm in LT-04, and 84-85 cm and 99-101 cm depth in LT-01. AMS ^{14}C dates were performed by Beta Analytic in Florida, USA and calibrated to calendrical ages.

3.5 Results

3.5.1 Core Lithostratigraphy and Depositional environments

Five distinctive lithostratigraphic units (A-E; Figure 3.3) were recognized in cores based on sedimentary facies characteristics, grain size and down-core shifts in foraminifera abundances. The correlated core lithostratigraphy is shown in a N-S cross-section in Figure 3.3. The correlation of sedimentary units was also aided by chirp sub-bottom seismic reflection profiles acquired as part of a detailed coastal reconstruction conducted by Krezoski et al., (Chapter 2). The units were grouped and three main depositional phases were identified.

Phase 1: Pre- causeway high-energy beach environment

The earliest phase of deposition is represented in cores by a coarse-grained pebbly sand shell hash (Unit E; Figure 3.3; 3.4; 3.5). The unit contains abundant abraded coralline fragments, some well-preserved organic matter and abraded bivalve and gastropod shells. The hash has a mean grain size of 0-3 ϕ and overall low magnetic susceptibility (0-5 SI x 10^{-6}) and high carbonate content (up to 30%).

The coarse-grained character and presence of abraded shell and coralline fragments are indicative of deposition in a high-energy foreshore (beach) environment. Organic matter from the top of Unit E has been dated to 3860 +/- 120 cal. BC placing it within the Late Neolithic/Early Chalcolithic. Paleogeographic reconstruction of the coastline by Krezoski et al. (Chapter 2) has identified Unit E as a paleoshoreline that existed at ca. 6-10 m below present sea levels.

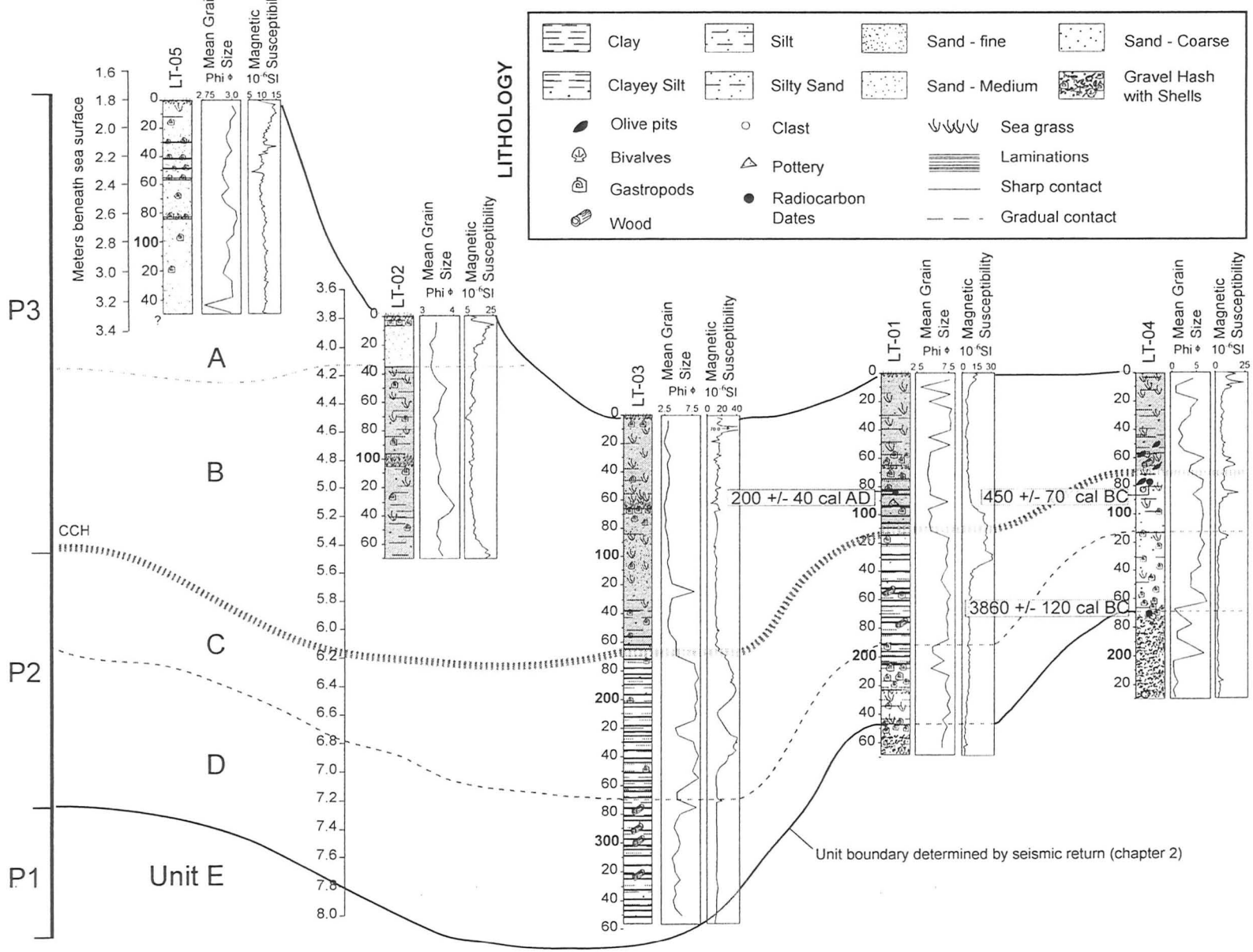

Figure 3.3: North-south cross-section (location shown in Figure 1) showing core lithostratigraphy and downcore changes in, mean grain size and magnetic susceptibility. Three main phases of deposition are recognized. P1: Pre- causeway high-energy beach environment; P2: Pre-causeway wetland/lagoonal environment; P3: Post-causeway sheltered embayment. CCH: Causeway Construction Horizon

Phase 2: Pre-causeway wetland/lagoonal environment

Phase 2 is recorded by a fining-upwards sequence of laminated silts and organic-rich muds (Units C, D) that were deposited in a coastal wetland and back-barrier lagoonal environment. The facies show a marked shift to finer grain sizes and a reduction in carbonate content (10-20%) (Figures 3.3; 3.4; 3.5). Unit D contains peat and reed fragments and is transitional to more organic-rich and fine-grained laminated silt of Unit C. The magnetic susceptibility is overall low throughout the sequence with several correlatable higher peaks towards the top of Unit C. The peaks in susceptibility indicate an increased influx of magnetic minerals into the lagoon, possibly as a result land clearance with the growth of Klazomenai (see Discussion). At a depth of 80-95 cm in Unit C a distinct zone of cultural materials, including pottery fragments and well-preserved olive pits is noted in cores LT-01 and LT-04 (Figure 3.3; 3.4; 3.5). AMS ^{14}C dates obtained on olive pits from the top of Unit C (76-77 cm LT-04) yielded an age of 450 BC +/- 70 cal BC.

Phase 2 indicates a period of rising sea-levels and a transition from near-shore beach environments to lower-energy shallow lagoonal environments. Krezoski et al. (Chapter 2) have interpreted the Phase 2 sediment sequence as a transgressive barrier system that formed during rapid Holocene transgression after ca. 3800 BC. The reed fragments and peat materials in Unit C record coastal wetlands that were inundated by rising sea levels after ~3800 BC.

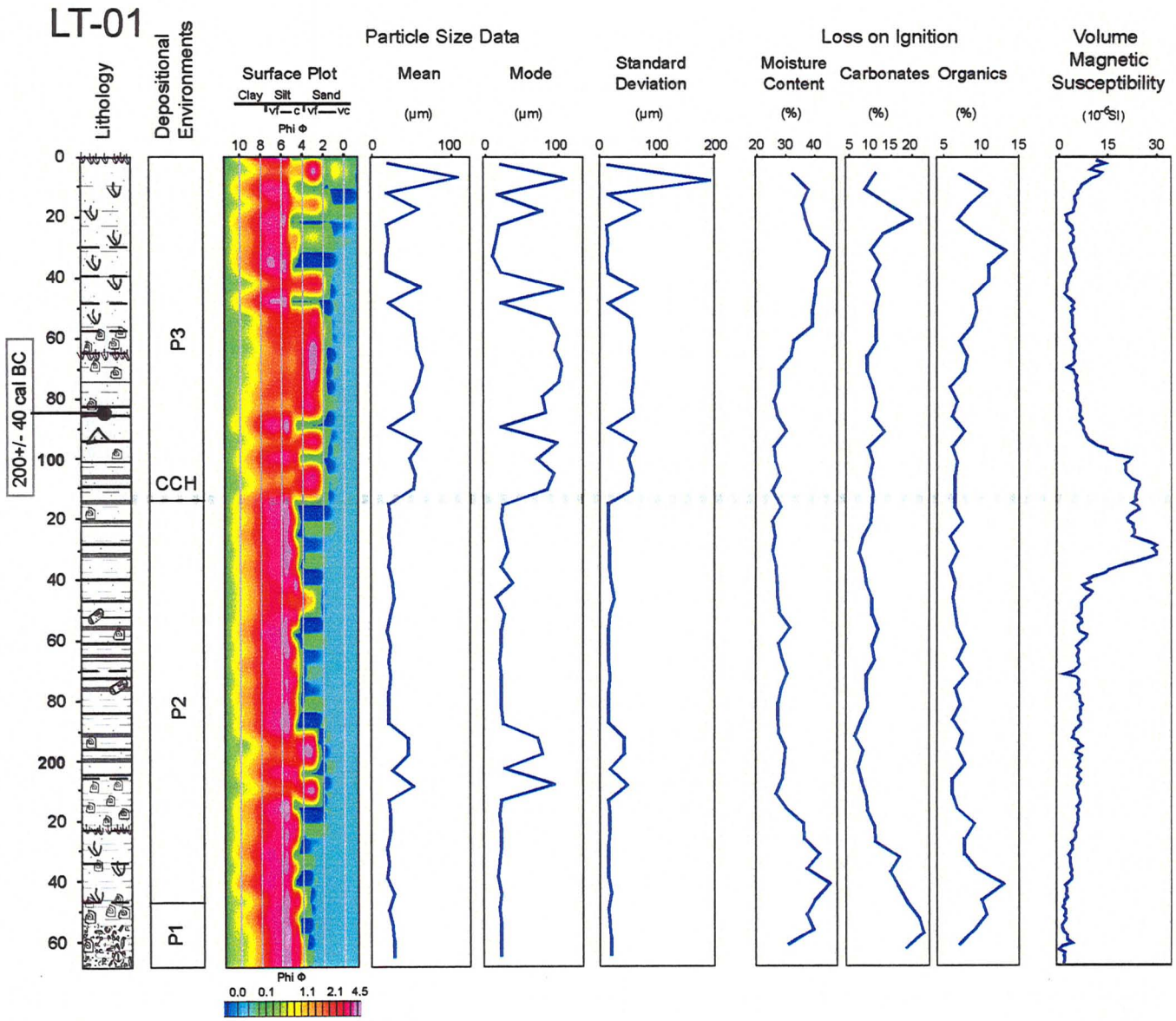

Figure 3.4: Particle size and physical property data for core LT-01. The causeway construction horizon (CCH) is identified at 115 cm by an abrupt shift to coarser grain size.

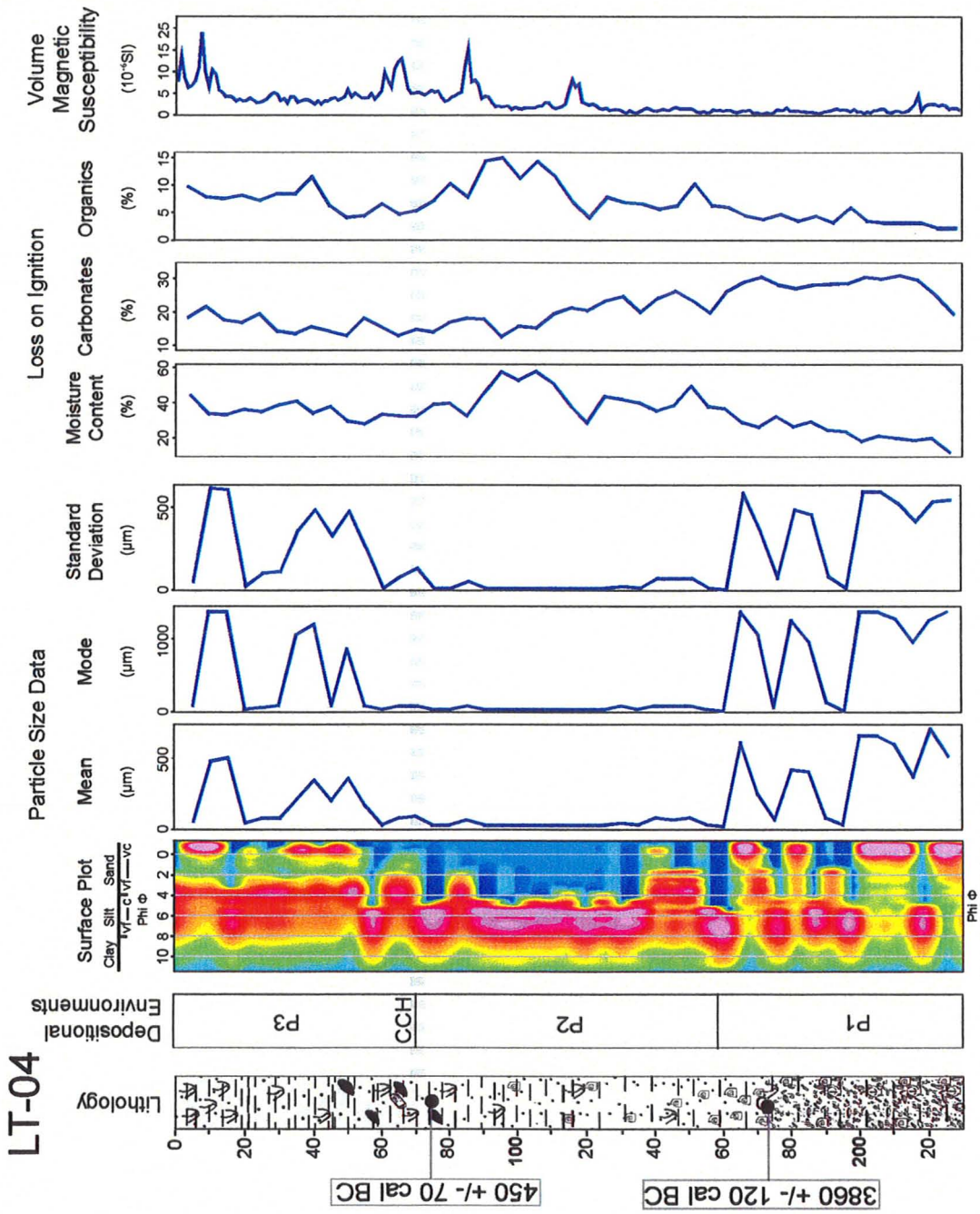

Figure 3.5: Particle size and physical property data for core LT-4. The causeway construction horizon (CCH) is indicated at ~70 cm by an abrupt shift to coarser grain size. A 14C date obtained on olive pits at 76-77 cm depth yielded an age of 450 +/- 70 cal BC, confirming the 4th c. age for the causeway.

Phase 3: Post-causeway sheltered embayment

Phase 3 is identified by a distinct shift to coarser grain sizes (from 0 to 4 ϕ) at the contact between Units B and C (ca. 115 cm in core LT-1 and 70 cm depth core LT-04) (Figures 3.3; 3.4; 3.5). Unit B consists of crudely-laminated to massive sandy silt with abundant *Posidonia Oceanica* fragments in the upper part of the unit. The organic content correspondingly shows an increase to over 15%. The magnetic susceptibility is low throughout the unit and shows a gradual increase in the upper 10-15 cm of the core. A ^{14}C date taken at 84-85 cm in core LT-1 yielded a Late Roman age of ~ 200 - 300AD. The linear sedimentation rate using both ^{14}C ages is consistent between cores LT-01 and LT-04 at 0.3 $mmyr^{-1}$.

The phase 3 sequence is capped closest to shore by a well-sorted fine sand (Unit A) with no organics and thin shell horizons. Unit A is interpreted as a beach deposit formed by shoreline progradation (Figure 3.3).

The Unit C - Unit B transition marks the change from shallow-marine environment to a low energy coastal embayment formed by the closure of the coastline following shoreline progradation that was accelerated by causeway construction. The causeway interrupted the dominant west-east long-shore current creating eddy current on the east side of the island and the trapping of sediment. In the shallow nutrient-rich low-energy environment, *Posidonia oceanica* meadows began to thrive. The onset of causeway construction is constrained by the radiocarbon date of 450 BC +/- 70 cal BC obtained from Unit C just below the boundary.

3.5.2 Micropaleontology:

Foraminifera have been employed in a number of previous studies to reconstruct water depths, salinity and paleoenvironmental conditions at coastal archaeological sites (Scott et al., 2001). In this study, shifts in the abundance of two foram genera (Rodalinids and Miliolinids) were examined and compared with the depositional phases identified by sediment physical properties (Figure 3.6).

Rodalinid species show a marked increase in abundance just prior to the onset of causeway construction and decrease rapidly above the boundary. *Elphidium* sp. in particular show a clear peak in abundance corresponding with the boundary (Figure 3.6). *Miliolid* sp. are dominant in the Phase 1 sediments and show a rapid decline to < 10% in Unit C, just prior to the interpreted causeway construction horizon. The abundance of *Miliolid* sp. rebounds to more than 20% above the causeway horizon. Bolivinid species show a marked inverse trend, increasing in abundance to ca. 10% within the same horizon.

An increase in the abundance of Bolivinids and Miliolinids was also identified in Late Archaic harbour sediments from Klazomenai by Goodman (2006). Figure 3.7 shows the foram abundances from this study and Goodman (2006) for comparison. The increase in these two genera was interpreted by Goodman (2006) as an indicator of increasing anoxia and eutrophication of the harbour basin. The cause of the eutrophia is not known but may have resulted from an increased loading of nutrients and organic matter to the harbour. This in turn would have led to anoxic bottom water conditions that are favoured

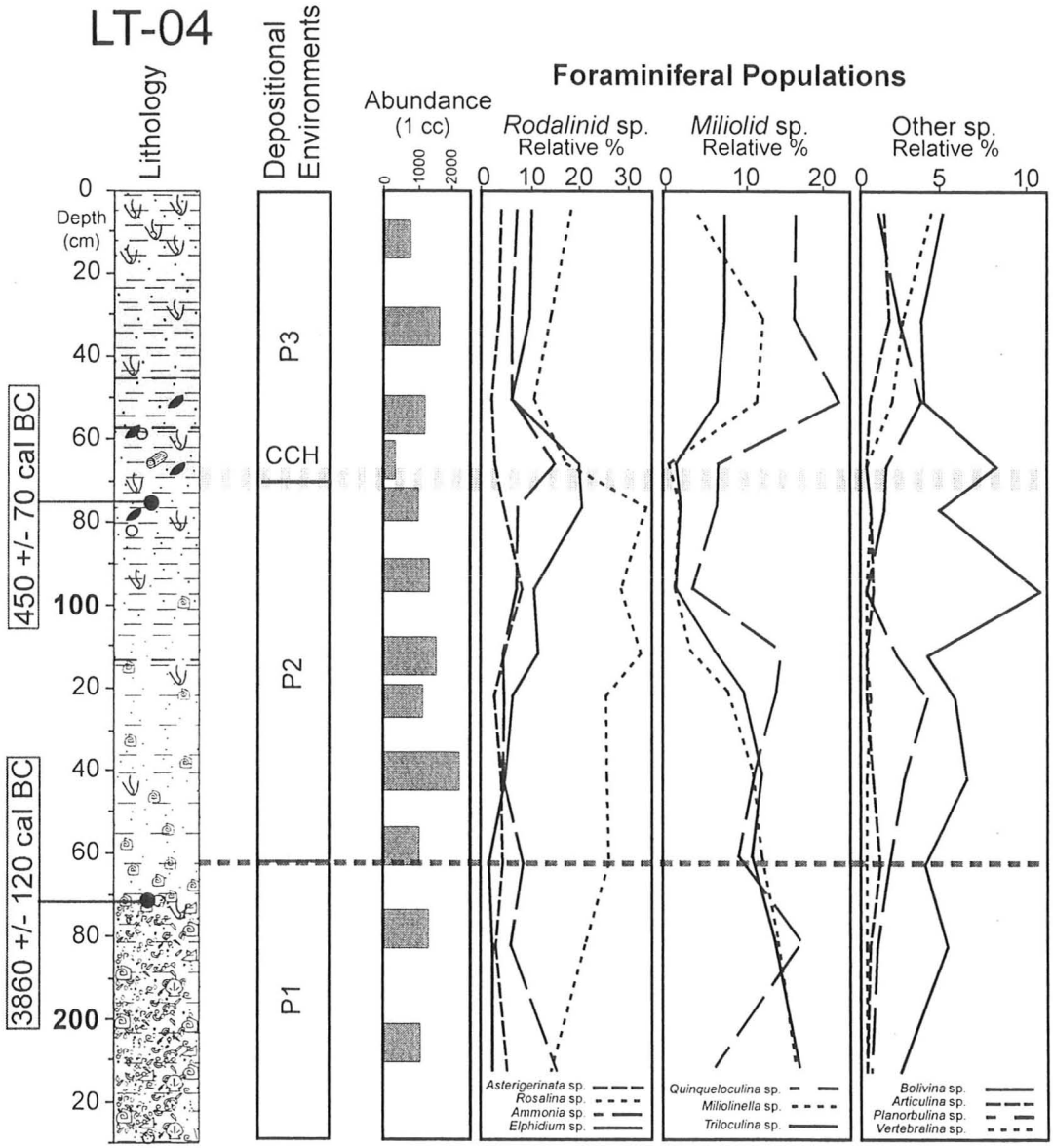

Figure 3.6: Downcore changes in foram abundance in core LT-04. Causeway boundary is associated with major shifts in the abundance of Bolivinids, Rodalinids and Miliolinids.

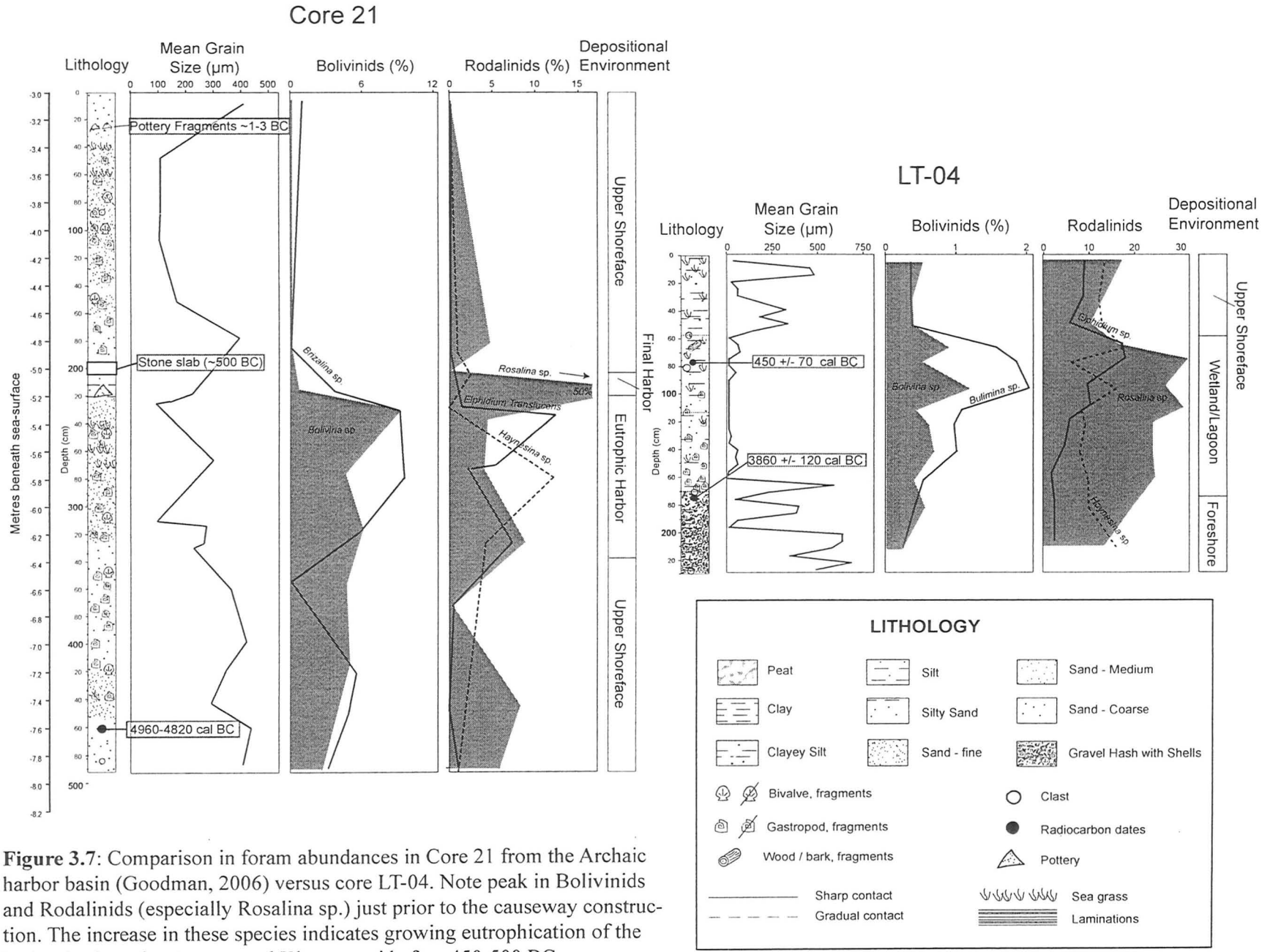

Figure 3.7: Comparison in foram abundances in Core 21 from the Archaic harbor basin (Goodman, 2006) versus core LT-04. Note peak in Bolivinids and Rodalinids (especially Rosalina sp.) just prior to the causeway construction. The increase in these species indicates growing eutrophication of the harbor basin and waters around Klazomenai before 450-500 BC.

by Bolivinid sp. (Goodman, 2006). It is noted that a sharp decrease in these foraminifera genera occurs in both data sets after ca. 500-450 BC, corresponding with a period of harbour construction and renewed activity in the Late Archaic period at Klazomenai (Figure 3.7).

3.5.3 Trace Metals:

Trace metal ratios for LT-01 and LT-04 corrected for enrichment factors are shown in Figure 3.8. Trace metal ratios are low; however ratios higher than 1 typically indicate enrichment caused by either anthropogenic sources or increased weathering rates in the area indicating a change in metal flux (Ngriau, 1996; Tylmann, 2007). Copper (Cu), lead (Pb) and tin (Sn) show higher ratios at the base of the core corresponding with Neolithic/Chalcolithic ages, then demonstrate a downward trend toward the causeway horizon. A small spike occurs in the top 10 cm of the core most likely correlating with a modern-day pipe releasing raw sewage into the embayment.

Overall trace metal analysis at this site does not reveal abundant information for historical pollution levels. Trends that are identified could correspond with ancient land clearance or climate change that would correspond with increased erosional rates during the Neolithic time period. The small increase at the top of the core samples indicates modern-day pollution, possibly related to a sewage pipe installed circa 1992 on the eastern side of the causeway.

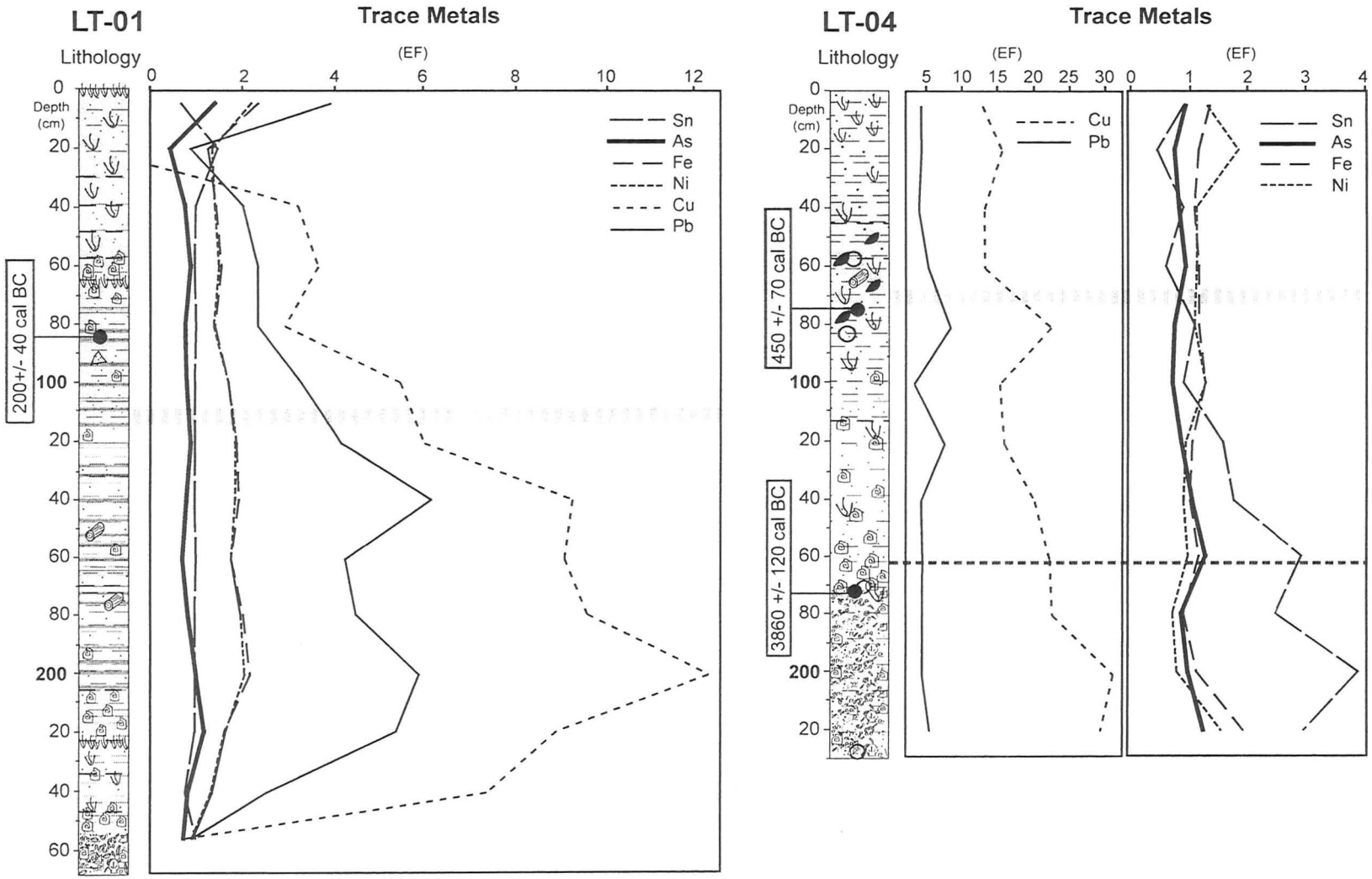

Figure 3.8: Downcore changes in trace metal abundance for cores LT-01 and LT-04.

3.6 Discussion

3.6.1. Impacts on Coastal Environments

The generalized modern day circulation patterns in the Bay of Izmir are shown in Figure 3.9. The movement of surface water masses is dependent on wind direction and salinity gradients generated by inflow from the Gediz River (Sayin et al., 2003). On the south shore of the bay the dominant wind direction is from the N-NW and generates strong longshore currents traveling south and eastward from the northern tip of the Urla peninsula towards Iskele. A weaker, but significant component of westerly alongshore transport also occurs due to a clockwise circulation of surface water in the central Bay of Izmir. As a result, a large volume of sediment released from the Gediz River is transported southeast towards Izmir and then westward along the southern shore of the bay.

The construction of the causeway in 334 BC effectively shut-down the west to east longshore transport between Karantina Island and the mainland, and created an eddy circulation pattern in the lee side of the island trapping sediment arriving from both directions. This in turn accelerated shoreline accretion, creating small beach ridges that prograded into the sheltered embayment. A sediment drape also covered the floor of the embayment, obscuring former topographic features.

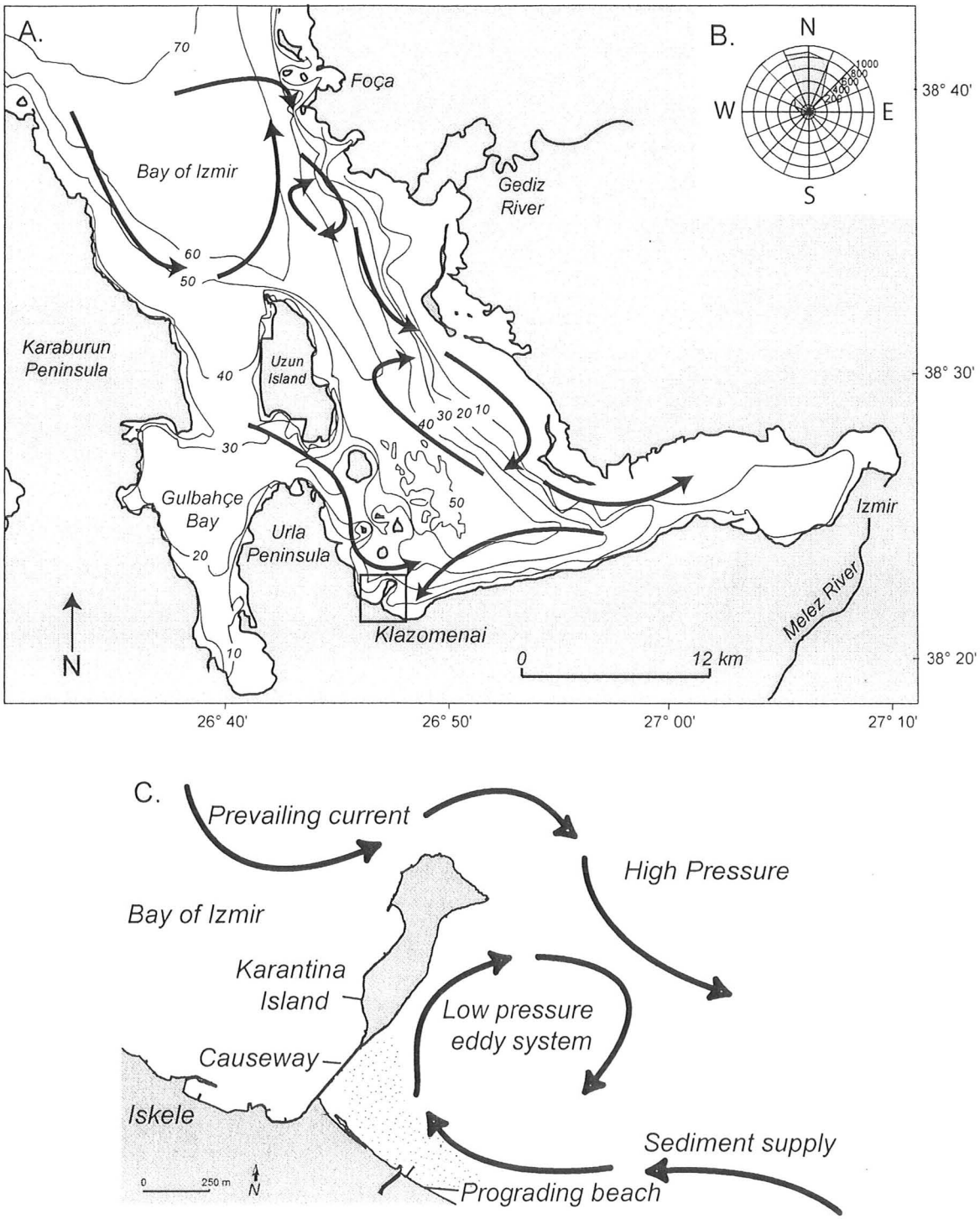

Figure 3.9: **A**. Major water circulation patterns and longshore sediment transport directions in the Bay of Izmir. **B.** Dominant wind direction is from the north-northwest, resulting in a dominant northwest-southeast longshore flow on the south side of the Bay (from Sayin, 2003). **C**. Construction of causeway in 334 BC shut-down west-east longshore transport. Sedimentation is dominated by progradation of the coastline and sediment supply from the east.

3.6.2 Archaeological Significance

The new data presented in this paper confirms the 4th c. BC date for the causeway construction and provides important insights into configuration of the coastline at the time of its construction. Changes in the paleogeography of the coastline at Klazomenai from Late Neolithic times to present are shown in Figure 3.10. The coastal reconstruction is based in part on detailed coring and geophysical investigations conducted by Krezoski et al. (Chapter 2) and shoreline reconstructions for the Bronze-age phase by Goodman et al. (in press). During the Late Neolithic (Phase 1) sea levels were more than 6-10 m below present and the island was connected to the mainland by broad system of beach barriers with an extensive back-barrier lagoons and wetlands (Figure 3.10A). As sea levels continued to rise during the late Holocene transgression (Phase 2) the barrier system was drowned in place and Karantina Island was separated from the mainland. By the Early Bronze-age (2800 BC) the sea level rise had slowed and a high-level prograding beach barrier and lagoon were established during a relative high-stand close to the modern sea level (Figure 3.10B). By the Late Archaic period (500 BC) a harbour had been constructed from the headland at Liman Tepe and the shoreline had prograded basinward as a headland identified in seismic data (Chapter 2).

In depositional Phase 3 at the time of causeway construction (334 BC), the island and mainland were separated by shallow shoreface environment (Figure 3.10D). The water depth on the shoreface is not known but was likely less than 1-2 m in order for Alexander's engineers to construct the causeway platform out to the island. The construction of the barrier interrupted the west-east longshore flow, creating a sheltered

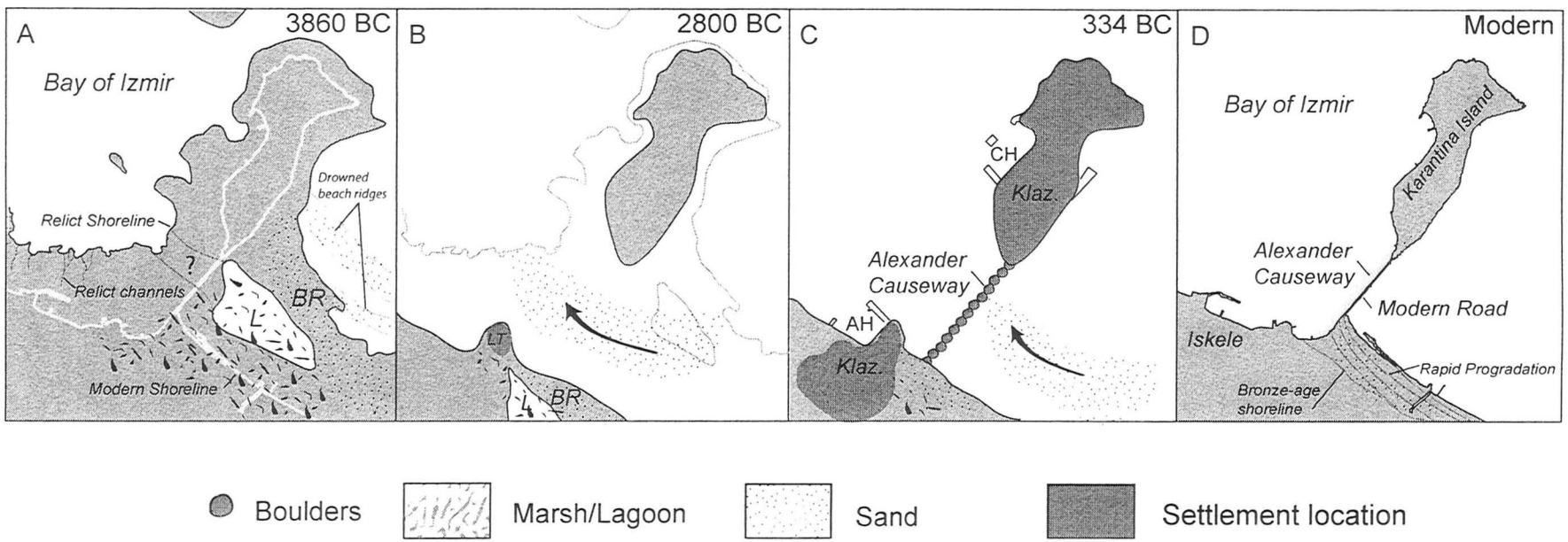

Figure 3.10: Paleogeographic reconstruction of the shoreline position and coastal environments at: **A**. Late Neolithic/Early Chalcolithic (ca. 3800 BC) (after Krezoski et al., Chapter 2). **B**. Early Bronze-age phase (after Goodman et al., in prep). **C**. At time of causeway construction (334 BC). **D**. Modern coastline; shoreline position has prograded more than 200 m since 4th c. BC. BR: Beach Ridge, L: Wetland/Lagoon, LT: Liman Tepe, Klaz.: Klazomenai, AH: Archaic harbour, CH: Cassical harbour.

embayment on the east side of the island and accelerating the progradation of the shoreline and trapping of sediments on the eastern side(Phase 3, Figure 3.10C; D). Though progradation had occurred prior to 334 BC, the causeway has been attributed to being the major sediment trap due to there being no deposition on the western side of the causeway. The construction of the causeway froze sediment supply to the west, and therefore a record of the original pre-causeway shoreline exists near Liman Tepe. The beach barrier identified by Goodman (2006) is close to the modern-day shoreline near Liman Tepe (<50 m). By examining the original shoreline prior to causeway construction, it can be seen that the causeway became a major sediment trap, causing the shoreline to prograde more than 200 m into the Bay of Izmir from the 2800 BC shoreline (Figure 3.10D).

3.7 Conclusion:

Geological analysis has begun to play a larger part of archaeological excavations, providing much-needed context in order to determine where and why sites exist. Cities such as Troy, a major part of the Mediterranean historical record, have often been geomorphologically altered over the past millennia by river-delta progradation or inundation by coastlines (Kraft, 1980; 2003). Often a complete archaeological record, or even the actual site cannot be found without the background landscape information. By understanding land usage, harbour locations, and how the landscape has changed since original construction, it is possible to understand the original settlement logistics and even find new site locations.

Overall by combining many studies into one in order to examine all aspects of depositional environments, anthropogenic alterations could be identified. Radiocarbon dates have also proven useful in the quest to constrain causeway ages. Future archaeological projects should incorporate geological methods in order to understand the entire environmental background of a study area.

3.8 References:

Beierle, B.D., Lamoureux, S.F., Cockburn, J.M.H., and Spooner, I. (2002) A new method for visualizing sediment particle size distribution. Journal of Paleolimnology, 27: 279-283.

Boyce, J.I., Krezoski, G.M., Erkanal, H. and Saholgu, V. (In review) Shallow water mapping of a submerged Archaic-age harbour at Liman Tepe, Turkey using data-fused magnetic and side-scan sonar data. Journal of Archaeological Sciences.

Cimerman, F., and Langer, M. (1991) Mediterranean Foraminifera. Slovenian Academy of Sciences and Arts: Ljubljana, 118 p., 93 plates.

Duman, M., Avci, M., Duman, S., Demirkurt, E., and Duzbastilar, M. (2004) Surficial sediment distribution and net sediment transport pattern in Izmir Bay, western Turkey. Continental Shelf Research, 24: 965-981.

EPA guideline 3050B (1998) Acid digestion of sediments, sludges and soils. *In* Test Methods for Evaluating Solid Waster: Physical/Chemical Methods, EPA SW-846, Third Ed., Vol 1, Section A, Chapter 3 (Inorganic Analytes), p.3050B-1-3050B-12, U.S. Environmental Protection Agency, Office of Solid Waste and Emergency Response, Washington D.C. Available at: http://www.epa.gov/epaoswer/hazwaste/test/pdfs/3050b.pdf.

Erkanal, H., (2008) Liman Tepe: New Light on Prehistoric Aegean Cultures. *in* Erkanal, H., Hauptmann, H., Sahoglu, V., Tuncel, R. (eds) The Aegean in the Neolithic, Chalcolithic and the Early Bronze Age. Ankara University Press, Ankara. P. 179-190.

Ersoy, Y. (1993) Klazomenai: The Archaic Settlement. Unpublished PhD thesis, Bryn Mawr College. 700 p.

Goodman, B.N., (2006) The paleogeography of Liman Tepe, Turkey: A multi-proxy geoarcheological study, unpublished Ph.D. thesis, McMaster University, Canada.

Goodman, B.N., Reinhardt, E.G., Dey, H., Boyce, J.I., Schwarcz, H., Sahoglu, V., Erkanal, H., and Artzy, M. (In Press) Evidence for Holocene marine transgression and shoreline progradation due to barrier development in Iskele, Bay of Izmir, Turkey: Journal of Coastal Research.

Green, P. (1991) Alexander of Macedon, 356-323 B.C.: A Historical Biography. University of California Press: California. 617 p.

Heiri, O., Lotter, A., and Lemcke, G. (2001) Loss on ignition as a method for estimating organic and carbonate content in sediments: reproducibility and comparability of results. Journal of Paleolimnology, 25: 101-110.

Herodotus (5th c. BC) The Histories. tr. by A de Selincourt (1996) Penguin Books: New York. 622 p.

Kraft, J., Kayan, I., and Erol, O. (1980) Geomorphic Reconstructions in the Environs of Ancient Troy. Science, 209: 776-782.

Kraft, J., Rapp, G., Kayan, I., and Luce, J. (2003) Harbor areas at ancient Troy: Sedimentology and geomorphology complement Homer's *Iliad*. Geology, 31: 163-166.

Marriner, N., Morhange, C., and Muele, S. (2007) Holocene morphogenesis of Alexander the Great's isthmus at Tyre in Lebanon. PNAS, 104: 9218-9223

Millet, B., and Goiran, J-P. (2007) Impacts of Alexandria's Heptastadion on coastal hydro-sedimentary dynamics during the Hellenistic period: a numerical modeling approach. The International Journal of Nautical Archaeology, 36.1: 167-176.

Murray, J. (2006) Ecology and Applications of Benthic Foraminifera. Cambridge University Press: New York, 438 p.

Nir, Y. (1996) The City of Tyre, Lebanon and its Semi-Artificial Tombolo. Geoarchaeology: An International Journal, 11(3), 235-250.

Nriagu, J. (1996) A history of global metal pollution. Science, 272: 223-224.

Ocakoglu, N., Demirbag, E., and Kuscu, I. (2005) Neotectonic structures in Izmir Gulf and surrounding regions (western Turkey): Evidences of strike-slip faulting with compression in the Aegean extensional regime. Marine Geology, 219: 155-171.

Pausanius, (2nd c BC) Guide to Greece, tr. by Peter Levi (1984) London: Penguin Books Inc. Vol 1. 587 p.

Pliny the Elder, (1st c. AD) Natural History. Harvard University Press: Cambridge Mass. 10 volumes.

Quintus Curtius Rufus (1st c. AD) The History of Alexander. Tr. by Heckel, W., and Yardley, J. (1984) Penguin Books: New York. 332 p.

Sahoglu, V. (2005) The Anatolian Trade Network and the Izmir region during the Early Bronze Age. Oxford Journal of Archaeology, 24: 339-361.

Sahoglu, V. (2008) Liman Tepe and Bakla Tepe: New Evidence for the relations between the Izmir region, the Cyclades and the Greek mainland during the late fourth and third Millennia BC. *in* Erkanal, H., Hauptmann, H., Sahoglu, V., Tuncel, R. (eds) The Aegean in the Neolithic, Chalcolithic and the Early Bronze Age. Ankara University Press, Ankara, p. 483-501.

Sayin, E. (2003) Physical Features of the Izmir Bay. Continental Shelf Research, 23: 957-970.

Scott, D. B., Medioli, F. S., and Schafer, C. T. (2001) Monitoring Coastal Environments using Foraminifer and Thecamoebian Indicators. Cambridge University Press: New York. 177 p.

Stanley, J-D., and Bernasconi, M. (2006) Holocene Depositional Patterns and Evolution in Alexandria's Eastern Harbor, Egypt. Journal of Coastal Research, 22: 283-297.

Tylmann, W., Golebiewski, R., Wozniak, P., and Czarnecka, K. (2007) Heavy metals in sediments as evidence for recent pollution and quasi-estuarine processes: an example from Lake Druzno, Poland. Environmental Geology, 53: 35-46.

van Hengstum, P., Reinhardt, E., Boyce, J., and Clark, C. (2007) Changing sedimentation patterns due to historical land-use change in Frenchman's Bay, Pickering, Canada: evidence from high-resolution textural analysis. Journal of Paleolimnology, 37: 603-618.

Chapter 4: Research Summary and Conclusion

4.1 Summary of Research Results

This thesis has investigated the marine sediment record of changing coastal environments at Liman Tepe/Klazomenai. In Chapter 2, core data were combined with detailed bathymetry and seismic reflection profiles to identify a series of submerged relict shorelines at depths of -10 m rsl and were correlated with pebbly beach sands of Unit E and dates to ca. 3800 BC. The shoreline appears to record a phase of decelerating sea level rise at the end of the Holocene transgression. The contoured upper surface of Unit E reveals that Karantina Island was attached to the mainland via a beach barrier during the mid-Holocene.

In order to determine a chronology for shoreline development, sea level indicators from previous work (Goodman, 2006) were compiled with the new data to produce a relative sea level curve for Liman Tepe (Figure 2.12). This curve shows that the relative sea levels were -6 to -10 metres lower during the Mid- to Late Neolithic (5000-3800 BC). These estimates are more than 2-3 metres below the modeled hydro-glacio-isostatic curve developed for the Mediterranean by Lambeck (1995) and Lambeck and Bard (2000) (Figure 2.12), indicating the importance of local tectonic effects in the Bay of Izmir. The shoreline maps and reconstructed paleogeography of the coastline (Figure 2.11) provide a useful framework for predicting the potential locations of Neolithic settlements on the prehistoric coast

In Chapter 3 the sedimentology of core data was examined in detailed to identify a record of coastal changes stemming from the construction of the Alexander causeway at

Klazomenai. The causeway construction horizon (CCH; Figure 3.3) was identified by distinctive shift in lithology particle size, and foram abundances. 14C dates obtained on organics from just below this transition confirm the 4th c. BC age for the structure as recorded in historical writings. This causeway created a sheltered embayment, trapping sediment and accelerating progradation of beach sediments. The study has shown that high-resolution particle-size analysis was the most sensitive discriminator of these environmental changes. Micropaleontological analysis also revealed subtle environmental changes, showing a major genera shift beneath the causeway horizon that is interpreted as a shift to more eutrophic conditions. Lithology and loss on ignition were important for determining major organic and carbonate horizons, and magnetic susceptibility for identifying phase of increased magnetic mineral loadings, possibly indicating changes in land use around Klazomenai.

4.2 Depositional Environments

This thesis has documented a change in relative sea level on the western Anatolian coastline of more than 10 metres since the Late Neolithic (Figure 2.12). This sea level change has resulted in significant changes in the coastal depositional environments and configuration of shorelines. The lithostratigraphic sequence revealed by coring fits well the 'drowned-in-place' transgressive barrier model forwarded by Rampino et al. (1980). The sequence of depositional environments is shown in a conceptual model in Figure 4.1. The relict shorelines identified in the bathymetry and core data (Figure 2.10) were formed during a mid-Holocene phase of relatively rapid sea

level rise. The presence of several discrete shoreline terraces seems to indicate several periods of shoreline stabilization, followed by deceleration of sea level rise around 3800 BC and the formation of an extensive beach-barrier complex (Figure 4.1 A). The fining-upwards sequence of lagoonal muds overlying foreshore sands, records the shoreward expansion of the back-barrier lagoon as a result of transgression. By 2800 BC, the shoreline had transgressed several hundred metres inland of the present shoreline, and a new, higher-level beach barrier complex was established during a high-stand phase. This last phase of transgression must have been rapid, possibly associated with co-seismic subsidence, as the relict wadi channels on the 3800 BC shoreline were preserved. By about 2800 BC sea level rise had slowed to modern rates and a high-stand systems tract obtained (Goodman, 2006; Goodman et al., in press). The coastline began to build rapidly into the basin through the growth of small barriers and the progradation of shoreface as indicated by the coarsening upwards sequence of shoreface sediment over lagoonal deposited identified in land cores (Goodman, 2006). The progradation of the coast was greatly accelerated during the early Hellenistic Period (334 BC; Figure 4.1 D), when the causeway created a sheltered embayment, trapping the sediment delivered by long-shore transport from east. Since that time the shoreline position has regressed more than 200 metres into the Bay of Izmir, as recorded by the presence of modern sandy beach facies (Unit A; Figure 2.3) over an older lagoonal sequence. The shoreline regression continues on the modern day coastline (Figure 4.1D) which consists of welded beach barrier ridges

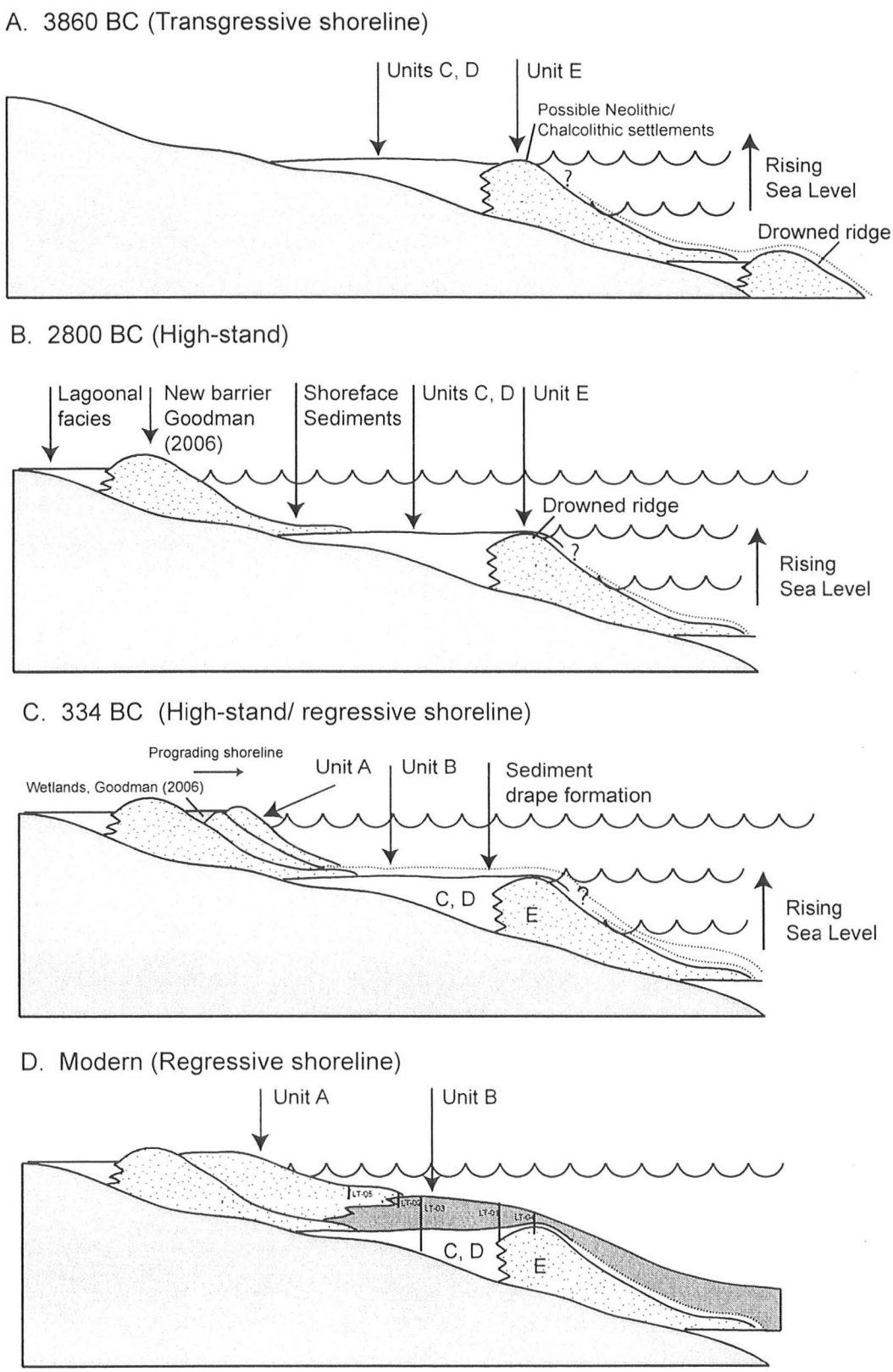

Figure 4.1. Conceptual model showing changes in depositional environments at Liman Tepe/Klazomenai (3860 BC to present). **A**. Pre-historic (3860 BC) beach ridge with a back-barrier lagoonal environment formed during mid-Holocene transgression (after Reinson, 1992). **B**. As water levels rose rapidly, the barrier was drowned in-place and a higher-level barrier established shoreward during a high-stand phase (2800 BC) (Goodman, 2006). **C**. Causeway construction (334 BC) accelerated beach progradation. **D**. Continued progradation of modern beach (Unit A) over mid-Holocene lagoonal sediments. Approximate core locations from this study are shown.

with intervening shallow lagoons (Figure 4.1 C). The process will be altered significantly when the existing causeway is removed and longshore transport is established along the coast to the south of Karantina Island.

4.3 Limitations

One major limitation on the resolution that was achieved in this thesis is the core sampling interval. For a number of properties (trace metal, micropaleontology) a coarse sampling interval was necessary in order to complete the study in time. Trace metal analyses were conducted on 44 samples from 4 separate cores. Higher-resolution core sampling (e.g. at 10 cm intervals) would have provided a more detailed record of trends in trace metals. Trace metals are expensive to run, however, and require a large time commitment for digestion. Similarly for micropaleontology, a higher-resolution data set with identification down to the species level would have provided the ability to identify subtle changes depositional environments and environmental conditions. Though these limitations apply to this specific project, the potential to still complete these analyses exists for future work.

A second limitation to the project was its location in Turkey. Often data (geologic maps, geology of the area) was obtained through second-hand information. Articles from the field area in Turkish had to be translated or completely overlooked due to translation issues. The distance for collecting additional samples proved insurmountable due to high operating and transportation costs. Also, due to the remote location, supplies (vibra-corer) were not available and more rudimentary methods had to be applied. In turn, these

methods might have limited the author from collecting cores deeper than Unit E in order to determine sub-unit E sedimentation.

4.4 Broader implications

The results have broader implications for understanding the archaeological record at Liman Tepe/Klazomenai and future impacts of coastal developments in the Bay of Izmir. This project examined the utility of combining multiple data-sets in order to create a complete model of site morphogenesis at Liman Tepe/Klazomenai over the past 6,000 years. Using this information, the IRERP project currently excavating Bronze-age sites at Liman Tepe can trace the Neolithic shoreline to determine where ancient settlements might have once existed. This data-set has proven valuable in order to determine likely locations of archaeological sites in a previously inaccessible area.

In addition, the Turkish government is eager to begin new plans to alter near-shore sedimentation at the causeway location by replacing the structure with a bridge supported by pylons. This bridge will re-instigate normal coastal sedimentation. This study provides the information on the environment of deposition, in another two-thousand years a second study can determine how this new construction has positively (or negatively) affected shoreline processes.

4.5 Future work

The potential for future work on this project is high, possibly providing the opportunity for further thesis work by additional undergraduate or graduate students.

Micropaleontology has proved relative easy and cheap to determine depositional environments. Preliminary interpretations have been carried out in this thesis, however a high-resolution micropaleontology survey on (abundant) remaining core samples would provide further insight into the subtle environmental changes of this anthropogenically rich area. Also, a more detailed look at trace metals would determine if trends seen in the data-sets are real or simply a result of processing or natural erosive processes.

A second study can also examine land-sites nearby surrounding the area, creating an even larger regional paleo-geographic reconstruction and applying this data to the work done by Sahoglu (2005) on evidence for the regional trade network.

References Cited:

Abraham, J. (1998) Spatial Distribution of major and trace elements in shallow reservoir sediments: an example from Lake Waco, Texas. Environmental Geology, 36: 349-363.

Aksu, A. E., Piper, D. J. W., and Konuk, T. (1987) Late Quaternary tectonic and sedimentary history of outer Izmir and Candarli Bays, western Turkey: Marine Geology, v. 76, p. 89–104.

Aksu, A.E., Yasar, D. and Uslu, O. (1998) Assessment of Marine Pollution in Izmir Bay: Heavy Metal and Organic Compound Concentration in Surficial Sediments. Turkish Journal of Engineering and Environmental Science, p. 387-415.

Aksu, A. E., Yasar, D., and Uslu, O. (1998) Assessment of Marine Pollution in Izmir Bay: Heavy Metal and Organic Compound Concentrations in Surficial Sediments. Turkish Journal of Engineering and Environmental Sciences. 22: 387-416.

Arrian (2nd c. AD) The campaigns of Alexander (Anabasis Alexandri). Tr. by A. de Selincourt, Penguin Books: Baltimore, MD. 430 p.

Bartington Instruments (2004) Bartington Instruments Magnetic Susceptibility Systems.

Beierle, B.D., Lamoureux, S.F., Cockburn, J.M.H., and Spooner, I. (2002) A new method for visualizing sediment particle size distribution. Journal of Paleolimnology, 27: 279-283.

Bell T. and Renouf, M.A.P. (2003) Prehistoric Cultures, Reconstructed Coasts: Maritime Archaic Indian Site Distribution in Newfoundland. World Archaeology, 35(3): 350-370

Bergman, I., Passe, T., Olofsson, A., Zackrisson, O., Hornberg, G., Hellberg, E. and Bohlin, E. (2003) Isostatic land uplift and Mesolithic landscapes: lake-tilting, a key to the discovery of Mesolithic sites in the interior of Northern Sweden. Journal of Archaeologica Science 30: 1451-1458.

Bizsel, N. and Uslu, O. (2000) Phosphate, nitrogen and iron enrichment in the polluted Izmir Bay, Aegean Sea. Marine Environmental Research, 49: 101-122.

Blott, S.J., and Pye, K. (2006) Particle size distribution analysis of sand-sized particles by laser diffraction: an experimental investigation of instrument sensitivity and the effects of particle shape. Sedimentology, 53: 671-685.

Boyce, J.I., Krezoski, G.M., Saholgu, V. and Erkanal, H. (In review) Shallow-water mapping of a submerged Bronze/Archaic-age harbour at Liman Tepe, Turkey using data-fused magnetic and side-scan sonar data. Journal of Archaeological Sciences.

Boyce, J.I., Reinhardt, E.G., Raban, A. and Pozza, M.R. (2004) Marine magnetic survey of a submerged Roman harbour, Caesarea Maritima, Israel. International Journal of Nautical Archaeology, 33: 122-136.

Boyd M. (2007) Early postglacial history of the southeastern Assiniboine Delta, glacial Lake Agassiz basin. Journal of Paleolimnology 37: 313-329.

Bozkurt E. and Sozbilir, H. (2004) Tectonic Evolution of the Gediz graben: field evidence for an episodic, two-stage extension in Western Turkey. Geological Magazine, 141: 63-79.

Brinkman, R. (1976) Geology of Turkey. Elsevier Scientific Publishing Co.: New York 158 p.

Chapman H.P. (2006) Landscape Archaeology and GIS. Tempus Publishing, Ltd.: Gloucestershire, 191 p.

Cimerman, F., and Langer, M. (1991) Mediterranean Foraminifera. Slovenian Academy of Sciences and Arts: Ljubljana, 118 p., 93 plates.

Clark, C. (2004) Sediment magnetic record of post-colonial environmental change in Frenchman's Bay, Lake Ontario. Unpublished Master's thesis, McMaster University, Canada.

Conley, D.J. and Schelske, C.L. (2001) Biogenic Silica. *In* J.P. Smol, H.J.B. Birks and W.M. Last. Tracking Environmental Change Using Lake Sediments: Volume 3: Terrestrial, Algal and Siliceous Indicators. Kluwer Academic Publishers: Dortrecht. P.281-293.

Conolly J. and Lake M. (2006) Geographical information systems in archaeology. Cambridge University Press: Cambridge, 338 pp.

Davis, J. (2002) Statistics and Data Analysis in Geology. John Wiley and Sons: New York, 638 p.

Duman, M., Avci, M., Duman, S., Demirkurt, E., and Duzbastilar, M. (2004) Surficial sediment distribution and net sediment transport pattern in Izmir Bay, western Turkey. Continental Shelf Research, 24: 965-981.

EPA guideline 3050B (1998) Acid digestion of sediments, sludges and soils. *In* Test Methods for Evaluating Solid Waster: Physical/Chemical Methods, EPA SW-846, Third Ed., Vol 1, Section A, Chapter 3 (Inorganic Analytes), p.3050B-1-3050B-12, U.S. Environmental Protection Agency, Office of Solid Waste and Emergency Response, Washington D.C. Available at: http://www.epa.gov/epaoswer/hazwaste/test/pdfs/3050b.pdf.

Erinc, S. (1978) Changes in the Physical Environment in Turkey since the Last Glacial. *In* W.C. Brice (ed.) The Environmental History of the Near and Middle East. Academic Press, London. p. 87-110.

Faught, M. (2002-2004) Submerged Paleoindian and Archaic Sites of the Big Bend, Florida. Journal of Field Archaeology, 29: 273-290.

Fedje, D.W. and Christensen, T. (1999) Modeling Paleoshorelines and Locating Early Holocene Coastal Sites in Haida Gwaii. American Antiquity 64: 635-652.

Firth A. (2004) Prehistory in the North Sea: questions for development-led archaeology. *In* N. C. Flemming (ed.), Submarine prehistoric archaeology of the North Sea. English Heritage/Council for British Archaeology: York. p. 89-94.

Fishbein, E. and Patterson, R.T. (1993) "Error-Weighted Maximum Likelihood (EWML): A new statistically based method to cluster quantitative micropaleontological data. Journal of Paleontology, 67: 475-486.

Flatman, J. and Blue, L. (1998) Maritime Archaeology in Britain and Northern Ireland, 1997-1998. International Journal of Nautical Archaeology, 28(2):174-199.

Flatman, J., Staniforth, M., Nutley, D., and Shefi, D. (2005) Submerged Cultural Landscapes. Cultural Landscapes Symposium, Adelaide, Australia.

Fleming, K., Johnston, P., Zwartz, D., Yokohama, R., Lambeck, K., and Chappell, J. (1998) Refining the eustatic sea level curve since the Last Glacial Maximum using far and intermediate field sites. Earth and Planetary Science Letters, 163: 327-342.

Flemming, N.C. (1978) Holocene eustatic changes and coastal tectonics in the northeast Mediterranean: Implications for models of crustal consumption, Phil. Trans. R. Soc. London, 289: 405-458.

Flemming, N.C., Ed. (2004) Submarine Prehistoric Archaeology of the North Sea. Council for British Archaeology Research Report: London. 141 p.

Goodman, B.N., (2006) The paleogeography of Liman Tepe, Turkey: A multi-proxy

geoarcheological study, unpublished Ph.D. thesis, McMaster University, Canada.

Goodman, B.N., Reinhardt, E.G., Dey, H., Boyce, J.I., Schwarcz, H., Sahoglu, V., Erkanal, H., and Artzy, M. (In Press) Evidence for Holocene marine transgression and shoreline progradation due to barrier development in Iskele, Bay of Izmir, Turkey: Journal of Coastal Research.

Green, P. (1991) Alexander of Macedon, 356-323 B.C.: A Historical Biography. University of California Press: California. 617 p.

Grøn O. and Skaarup J. 2004. Submerged Stone Age coastal zones in Denmark investigation strategies and results. *In* N. C. Flemming (ed.), Submarine prehistoric archaeology in the North Sea. English Heritage/Council for British Archaeology: York, p. 53-56.

Hakyemez, H., Erkal, T., and Goktas, F. (1999) Late Quaternary evolution of the Gediz and Buyuk Menderes grabens, Western Anatolia, Turkey. Quaternary Science Reviews, 18: 549-554.

Hammer, O., Harper, D., and Ryan, P. (2001) Past: Paleontological statistics software package for education and data analysis. Paleontologia Electronica, vol. 9.

Heiri, O., Lotter, A., and Lemcke, G. (2001) Loss on ignition as a method for estimating organic and carbonate content in sediments: reproducibility and comparability of results. Journal of Paleolimnology, 25: 101-110.

Herodotus (5th c. BC) The Histories. tr. by A de Selincourt (1996) Penguin Books: New York. 622 p.

Hughes-Clarke, J.E. (2004) Seafloor characterization using a keel-mounted sidescan: compensation for radiometric and geometric distortion. Canadian Hydrographic Conference, Ottawa, ON.

Ivanov, V., Kubryakov, A. and Shapiro, N. (1998) Thermohaline structure and dynamics of waters in the Izmir Bay. Physical Oceanography 9: 273-296.

Jones, E.J.W. (1999) Marine Geophysics. John Wiley and Sone: West Sussex, 466 p.

Karrow, P.F., Appleyard, E.C. and Endres, A.L. (2007) Geological and Geophysical evidence for pre-Nipissing (>5,000 years BP) transgression infilled valleys in the Lake Huron basin, Ontario. Journal of Paleolimnology 37: 419-434.

Kemp, A.L.W., Thomas, R.L., Dell, C. I., and Jaquet, J-M. (1976) Cultural Impact on the Geochemistry of Sediments in Lake Erie. Journal of the Fisheries Research Board of Canada, Vol. 33, 3: 440-462.

Kraft, J.C., Rapp, G., and Aschenbrenner, S. (1975) Late Holocene Paleogeography of the Coastal Plain of the Gulf of Messina, Greece, and its Relationship to Archaeological Settings and Coastal Change. Geological Society of America, 86: 1191-1208.

Kraft, J.C., Aschenbrenner, S. E., and Rapp, G. (1977) Paleogeographic Reconstruction of Coastal Aegean Archaeological Sites. Science, 195:4282 p. 941-947.

Kraft, J., Kayan, I., and Erol, O. (1980) Geomorphic Reconstructions in the Environs of Ancient Troy. Science, 209: 776-782.

Kraft, J., Rapp, G., Kayan, I., and Luce, J. (2003) Harbor areas at ancient Troy: Sedimentology and geomorphology complement Homer's *Iliad.* Geology, 31: 163-166.

Kucuksezgin, F., Kontas, A., Altay, O., Uluturhan, E., and Darilmaz, E. (2006) Assessment of marine pollution in Izmir Bay: Nutrient, heavy metal and total hydrocarbon concentrations. Environmental International, 32: 41-51.

Lambeck, K., (1995) Late Pleistocene and Holocene sea-level change in Greece and south-western Turkey: a separation of eustatic, isostatic and tectonic contributions. Geophysics Journal International, 122: 1022-1044.

Lambeck, K. (1996) Sea-level change and shore-line evolution in Aegean Greece since Upper Paleolithic time. Antiquity, 70:588-613.

Lambeck, K., and Bard, E. (2000) Sea-level change along the French Mediterranean coast for the past 30 000 years. Earth and Planetary Science Letters, 175: 203-222.

Lambeck K. and Chappell, J. (2001) Sea-level change through the Last Glacial Cycle. Science, 292:679-686.

Lambeck, K and Purcell, A. (2005) Sea-level change in the Mediterranean Sea since the LGM: model predictions for tectonically stable areas. Quaternary Science Reviews, 24(18-19): 1969-1988.

Manning, S.W. (1995) The Absolute Chronology of the Aegean Early Bronze Age: Archaeology, Radiocarbon and History (Vol. 1) Sheffield Academic Press: Sheffield, 370 p.

Marriner, N., and Morhange, C. (2007) Geoscience of ancient Mediterranean harbours. Earth-Science Reviews, 80:137-194.

Marriner, N., Morhange, C., and Doumet-Serhal, C. (2006) Geoarchaeology of Sidon's ancient harbours, Phoenicia. Journal of Archaeological Science, 33: 1514-1535.

Marriner, N., Morhange, C., Boudagher-Fadel, M., Bourcier, M., and Carbonel, P. (2005) Geoarchaeology of Tyre's ancient northern harbour, Phoenicia. Journal of Archaeological Science, 32: 1302-1327.

Matthews, M.D., (1991) The effect of pretreatment on size analysis. *In* J.P.M. Syvitski (ed) Principles, Methods and Applications of Particle Size Analysis. Cambridge University Press: New York. p. 34-42.

Millet, B., and Goiran, J-P. (2007) Impacts of Alexandria's Heptastadion on coastal hydro-sedimentary dynamics during the Hellenistic period: a numerical modeling approach. The International Journal of Nautical Archaeology, 36.1: 167-176.

Momber, G. 2004. The inundated landscapes of the Western Solent. *In* N. C. Flemming (ed.), Submarine prehistoric archaeology of the North Sea Council for British Archaeology: York, p. 37-42.

Morhange, C., Blanc, F., Schmitt-Mercury, S., Bourcier, M., Carbonel, P., Oberlin, C., Prone, A., Vivent, D., and Hesnard, A. (2003) Stratigraphy of the late-Holocene Deposits of the ancient harbour of Marseilles, southern France. The Holocene, 13: 593-604.

Mourtzas, N.D. (1988) Holocene vertical movements and changes of sea-level in the Hellenic arc, In: Marinos P and Koukis G (Eds), The engineering geology of ancient works, monuments arid historical sites, Vol 4, Balkema pp 2247-2262.

Murray, M.R. (2002) Is laser particle size determination possible for carbonate-rich lake sediments? Journal of Paleolimnology, 27(2): 173-183.

Murray, J. (2006) Ecology and Applications of Benthic Foraminifera. Cambridge University Press: New York, 438 p.

Ocakoglu, N., Demirbag, E., and Kuscu, I. (2005) Neotectonic structures in Izmir Gulf and surrounding regions (western Turkey): Evidences of strike-slip faulting with compression in the Aegean extensional regime. Marine Geology, 219: 155-171.

Pausanius, (2nd c BC) Guide to Greece, tr. by Peter Levi (1984) London: Penguin Books Inc. Vol 1. 587 p.

Pirazzoli, P.A. (1991) World atlas of Holocene sea-level changes. Elsevier, p 58

Pliny the Elder, (1st c. AD) Natural History. Harvard University Press: Cambridge Mass. 10 volumes.

Quinn, R., Cooper, A.G., and Williams, B. (2000) Marine geophysical investigation of the inshore coastal waters of Northern Ireland. The International Journal of Nautical Archaeology, 29(2): 294-298.

Quintus Curtius Rufus (1st c. AD) The History of Alexander. Tr. by Heckel, W., and Yardley, J. (1984) Penguin Books: New York. 332 p.

Rampino, M.R., and Sanders, J.E. (1980) Holocene transgression in south-central Long Island, New York. Journal of Sedimentary Petrology, 50: 1063-1080.

Reinhardt, E., Patterson, R. T., Blenkinsop, J., and Raban, A. (1998) Paleoenvironmental evolution of the inner basin of the ancient harbor at Caesarea Maritima, Israel; foraminiferal and Sr isotopic evidence. Revue Paleobiologie Geneve, 17: 1-21.

Reinhardt, E. and Raban, A. (1999) Destruction of Herod the Great's harbor at Caesarea Maritima, Israel – Geoarchaeological evidence. Geology, 27: 811-814.

Reinhardt, E.G., Boyce, J.I. and Yakovenko. A. (2006a) The Bova Marina Archaeological Project – underwater survey of the San Pasquale River Valley, Calabria, Italy. Geological Society of America Annual Meeting, October 22-25, 2006, Philadelphia, Pennsylvania, Abstracts with Programs, Vol. 38, No. 7, p. 149.

Reinhardt, E.G., Goodman, B.N., Boyce, J.I., Lopez, G., van Hengstum, P.J., Rink, W.J., Mart, Y., Raban, A. (2006b) The tsunami of 13th December A.D. 115 and the destruction of Herod the Great's harbor at Caesarea Maritima, Israel. Geology, 34, 1061-1064.

Reinhardt, E.G. and Raban, A. (in press) Site Formation and Stratigraphic Development of the Ancient Harbour at Caesarea Maritima. Israel. *In* Caesarea Papers III, K. Holum and A. Raban (eds.) Journal of Roman Archaeology Supplementary Series, University of Michigan Press, Ann Arbor.

Renfrew, A.C. (1972) The Emergence of Civilisation: The Cyclades and the Aegean in the Third Millennium BC. Metheun: London.

Rivieros, N. V., Babalola, A.O., Boudreau, R., Patterson, R. T., Roe H. M., and Doherty, C. (2007) Modern distribution of salt marsh foraminifera and thecamoebians in the Seymour-Belize Inlet Complex, British Columbia, Canada. Marine Geology, 242: 39-63.

Sahoglu, V. (2002) Early Bronze Age Pottery from Liman Tepe and its significance in the Archaeology in the Aegean. Ph.D. Thesis, Ankara University, Turkey.

Sahoglu, V. (2005) The Anatolian Trade Network and the Izmir region during the Early Bronze Age. Oxford J. Archaeology: 24, 339-361.

Sahoglu, V. (2008) Liman Tepe and Bakla Tepe: New Evidence for the relations between the Izmir region, the Cyclades and the Greek mainland during the late fourth and third Millennia BC. *in* Erkanal, H., Hauptmann, H., Sahoglu, V., Tuncel, R. (eds) The Aegean in the Neolithic, Chalcolithic and the Early Bronze Age. Ankara University Press, Ankara, p. 483-501.

Sayin, E. (2003) Physical Features of the Izmir Bay. Continental Shelf Research, 23: 957-970.

Schwamborn, G., Rachold, V., and Grigoriev, M.N. (2002) Late Quaternary sedimentation history of the Lena Delta. Quaternary International, 89: 119-134.

Scott, D. B., Medioli, F. S., and Schafer, C. T. (2001) Monitoring Coastal Environments using Foraminifer and Thecamoebian Indicators. Cambridge University Press: New York. 177 p.

Sonnenburg, E. (2006) Paleoenvironmental reconstruction of submerged landscapes in Colonel By Lake, Ontario using geoarchaeological and geophysical techniques. Unpublished Masters thesis, McMaster University, Canada.

Sonnenburg, E.P. and Boyce, J.I. (2008) Data-fused digital bathymetry and side-scan sonar as a base for archaeological inventory of submerged landscapes in the Rideau Canal, Ontario, Canada. Geoarchaeology, 23: 654-674.

Stanley, J-D., and Bernasconi, M. (2006) Holocene Depositional Patterns and Evolution in Alexandria's Eastern Harbor, Egypt. Journal of Coastal Research, 22: 283-297.

Stanley, J-D., Carlson, R., van Beek, G., Jorstad, T. And Landau, E. (2007) Alexandria, Egypt, before Alexander the Great: A multidisciplinary approach yields rich discoveries. GSA Today, 17: 4-10.

Stiros, S.C., Pirazzoli, P., Rothaus, R., Papageorgiou, S., Laborel, J., Arnold, M. (1996) On the Date of Construction of Lechaion, Western Harbor of Ancient Corinth, Greece. Geoarchaeology: An International Journal, 11(3): 251-263.

Turkiye Jeoloji Haritasi (Geological Map of Turkey) (1964) Izmir. Institute of Mineral Research and Exploration – Ankara.

Tylmann, W., Golebiewski, R., Wozniak, P., and Czarnecka, K. (2007) Heavy metals in sediments as evidence for recent pollution and quasi-estuarine processes: an example from Lake Druzno, Poland. Environmental Geology, 53: 35-46.

van Andel, T.H. & Shackleton, J.C., 1982. Late Paleolithic and Mesolithic coastlines of Greece and the Aegean, J. Field Archaeology, 9: 445-454.

van Andel, T.H. and Lianos, N. (1983) Prehistoric and historic shorelines of the Southern Argolid Peninsula: A sub bottom profiler study. The International Journal of Nautical Archaeology and Underwater Exploration 12(4): 303-324.

van Hengstum, P., Reinhardt, E., Boyce, J., and Clark, C. (2007) Changing sedimentation patterns due to historical land-use change in Frenchman's Bay, Pickering, Canada: evidence from high-resolution textural analysis. Journal of Paleolimnology, 37: 603-618.

van Metre, P., and Callendar, E. (1997) Water-quality trends in White Rock Creek Basin from 1912-1994 identified using sediment cores from White Rock Lake reservoir, Dallas, Texas. Journal of Paleolimnology, 17: 239-249.

Veron, A., Goiran, J-P., Morhange, C., Marriner, N. and Empereur, J. (2006) Pollutant lead reveals the pre-Hellenistic occupation and ancient growth of Alexandria, Egypt. Geophysical Research Letters, 33: L06409.

Warren, P.M. and Hankey, V. (1989) Aegean Bronze Age Chronology. Bristol Classical Press: Bristol.

Appendix A: Methods

1.7 Methods

1.7.1 Sediment coring extraction

Locations for coring were chosen based upon proximity to the causeway feature, as well as assumption of the best sediment records within the basin. Five cores were taken along the eastern edge of the causeway (Figure 1.3) ranging in length from just over one meter to 3.6 meters (Appendix B). A sixth core was taken on the western side of the causeway in order to compare long-shore current facies to the eastern side. This core was not included in the final papers due to a lack of time for interpretation (Appendix B). A percussion corer was used to obtain core samples using a slide hammer to insert 20 foot aluminum irrigation tubes off the back of a zodiac (Figure A.1.A; Figure A.2.A, B, D). Core catchers were installed in the ends of the tubes to stop sediment escape upon extraction. Extension rods were attached to the top of a collar to obtain a maximum amount of sediment (Figure A.1.B). Upon completion, SCUBA divers removed the rods, placed a plastic cap on the top of the core to create suction, and attached air bags to a collar on the core (Figure A.1.C). The air bags were then filled with oxygen from a secondary SCUBA tank, and the core floated to the top (Figure A.1.1.D; Figure A.1.C). Divers capped the bottom of the core prior to removal from the water in order to keep sediment in the tube.

On land, caps were removed from the top of the tube and measurements taken to determine compaction (~ between .5 and 1 m). Sponges were inserted, water allowed to drain, then cores were cut, labeled and shipped to the McMaster Micropaleontology Laboratory for cold storage (~6 degrees C).

Cores were split and lithologic aspects logged prior to sampling. One half of the core was left in cold storage as an archive. Visual sediment changes were correlated within the cores and digitized. Cores were sampled at pre-determined intervals for loss on ignition, grain size analysis, trace metals, volume magnetic susceptibility and micropaleontological analysis (Figure A.3). Core LT-04 was identified as having a more complex sedimentary record and was analyzed in more detail for micropaleontology and trace metals.

1.7.2 Loss on Ignition (LOI)

Loss on ignition (LOI) measures the percent of organic and carbonate contents in the sample by calculating the amount lost in a regime of high-level heating. Following Heiri and others (2001), approximately 2 cm^3 of sediment from a 5 cm interval were placed in crucibles in an oven and dried for a minimum of 24 hours. Samples were then placed in desiccators to cool for eight hours and weighed to determine moisture lost. Samples were baked at a temperature of 550 degrees Celsius for four hours, cooled and weighed for loss of organic matter. Samples were baked again at 950 degrees Celsius for 2 hours, cooled and weighed for loss of carbonates. Weights were then calculated into

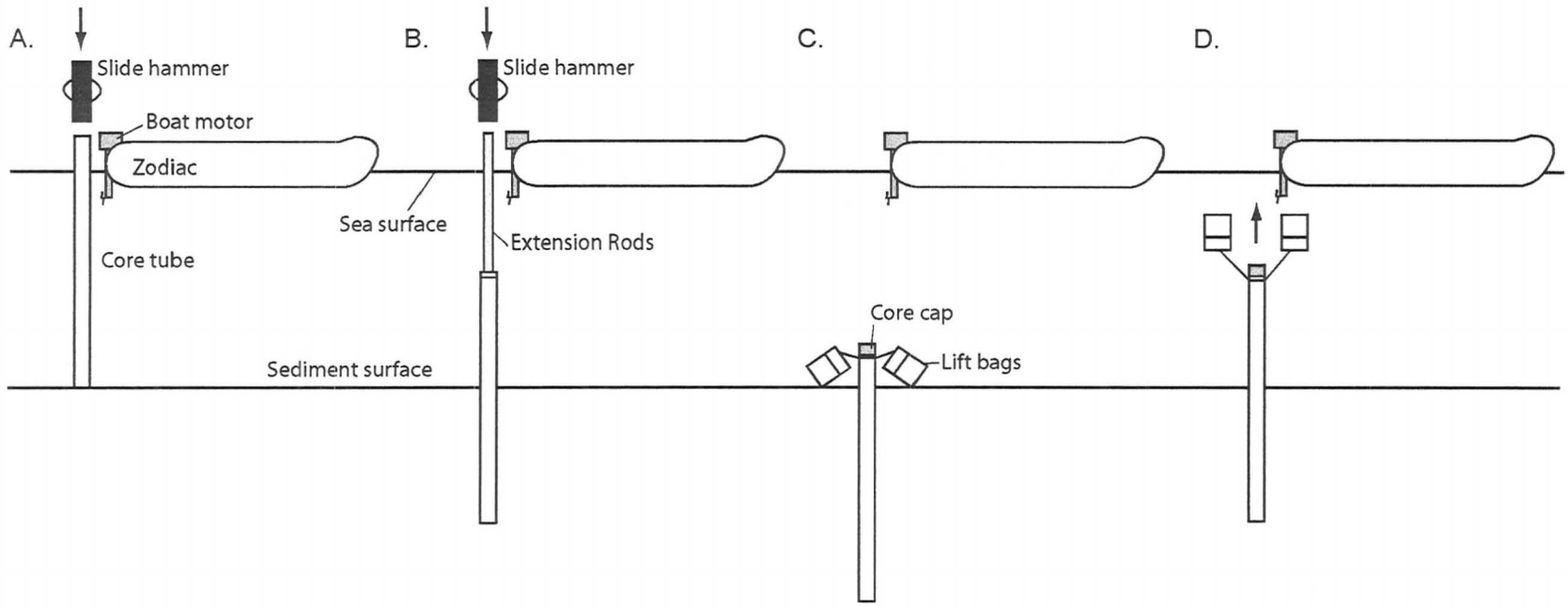

Figure A.1: Percussion coring and core retrieval methods. **A**. Aluminum core tube driven into marine sediment with 30 kg slide hammer. **B**. Extension rods attached to collar to extend the tube underwater. **C**. Extension rods removed, tube capped and float bags attached. **D**. Float bags inflated and core base capped prior to removal from water.

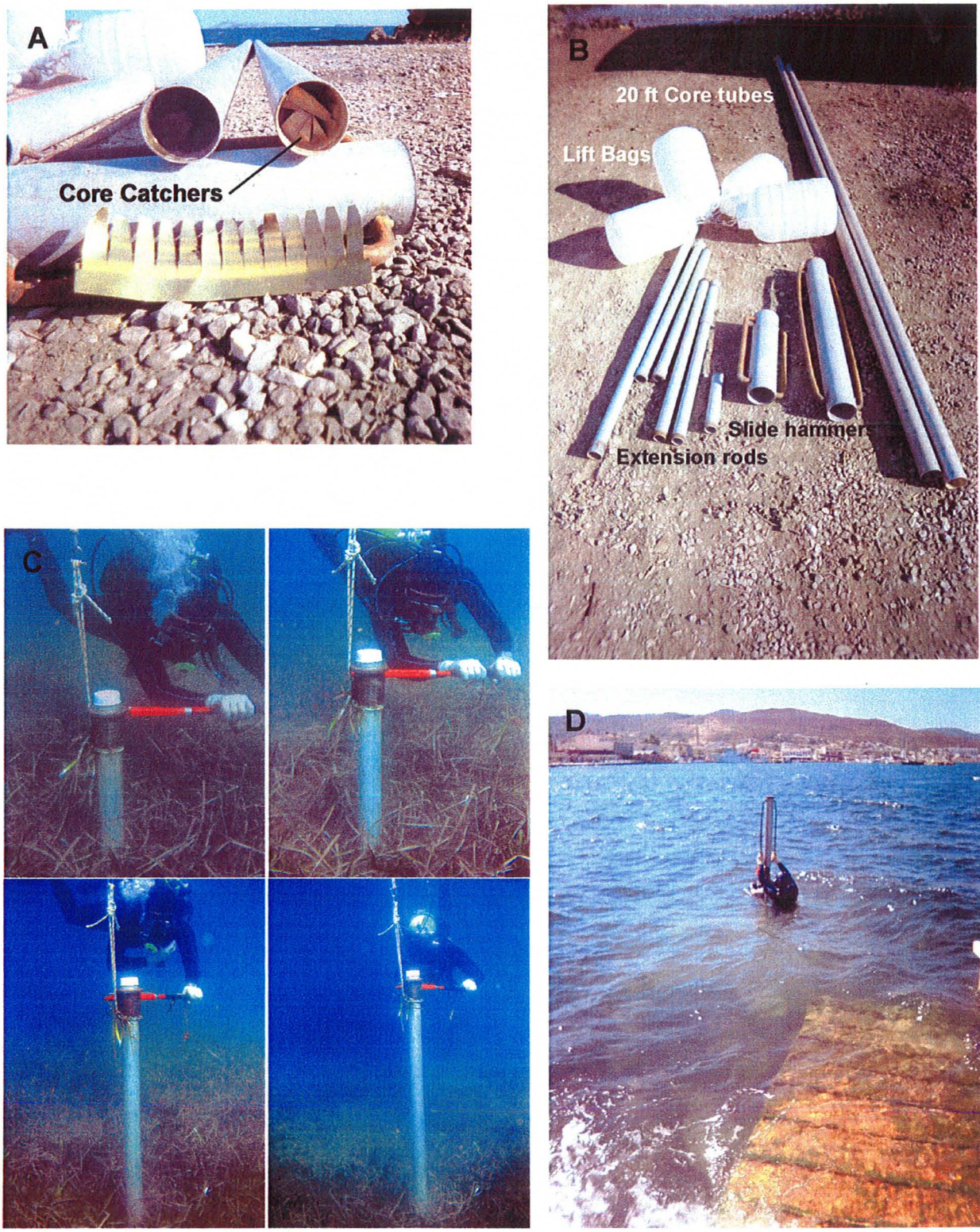

Figure A.2: **A**. Brass core catchers installed in irrigation tubes. **B**. Core tubes and coring components. **C**. Core extraction using lift bags. Note lush Posidonia Oceanica meadows along the sea-floor. **D**. Gravity coring in shallow water.

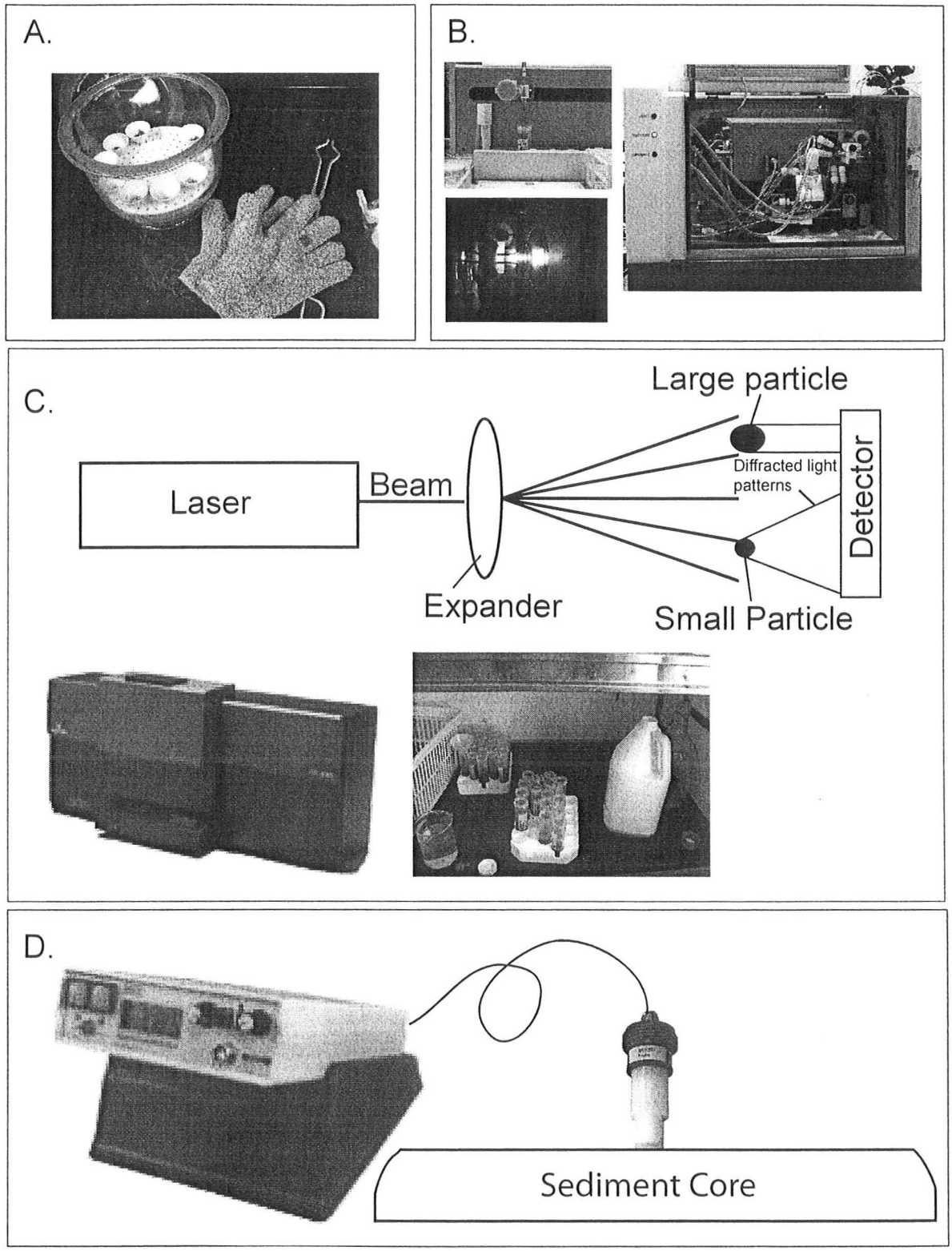

Figure A.3: **A.** LOI sample preparation. **B.** Micromass ICP-MS, University of Wisconsin, Milwaukee **C.** Operation of Coulter laser diffraction counter (after Last, 2001). Pictured are a Beckman LS230 Coulter Counter console and sample vials ready for digestion. **D.** Bartington MS2-F volume magnetic susceptibility meter demonstrating placement of the probe for measurements on the back of archived core samples.

percentages of organic matter and carbonates within the original sample and plotted in Microsoft Excel.

Studies have shown that ovens used for LOI contain convection currents that concentrate heat in the middle of the oven, causing skewed heating rates (Heiri et al, 2001). Because of this, samples were kept at the same size (~ 2 g) and placed slightly away from furnace edges in order to avoid differences in heating. Samples were also randomly moved to different locations each time they were placed in the furnace in order to eliminate any skewed results.

1.7.3 Grain Size Analysis

Grain size analysis was completed to determine source changes for sedimentation within the basin. By determining changes in grain size populations, sedimentation rates and sources can be identified (Schwamborn et al., 2002; Clark, 2004). In this study, five cm^3 of sample taken every 5 cm down-core were placed in 50 mL tubes for digestion according to van Hengstum et al. (2007). Care was taken to avoid the edges of the core tube when sampling in order to avoid any sediment contamination. Samples were treated with a 10% hydrochloric acid (HCl) solution to remove carbonates. Samples were then treated with a 40% hydrogen peroxide (H_2O_2) solution to remove any organics (Matthews, 1991). Samples were centrifuged after each chemical treatment and leftover chemicals decanted. Samples were then heated in a warm bath (85 degrees Celsius) with a 1% sodium carbonate solution (Na_2CO_3) for one hour in order to eliminate biogenic silica (diatoms) (Conley and Schelske, 2001). Samples were then mixed to promote

homogeneity, treated with 1% Calgon to deter sediment clumping, and run through a Beckmann LS 230 Coulter Counter for analysis using the Fraunhofer optical model (Murray, 2002; van Hengstum et al., 2007). Digestion of samples has been shown beneficial when measuring for particle size, as carbonates, organics and diatoms can all skew results (Matthews, 1991; Conley and Schelske, 2001).

Results were plotted to a Wentworth Phi scale in OASIS Montaj Geosoft software using a minimum curvature grid in order to create a colored surface plot diagram (van Hengstum, 2007; Beierle et al., 2002). Further statistics (standard deviation, skewness, mean, median and mode) were recorded and calculated in Microsoft Excel and plotted depth-wise. Though particle size analyzers are quick and efficient, some problems have been recorded with fine (clay) particle measurements in past studies. Because the results demonstrated in Chapter 2 and appendices demonstrate diverse multi-modal populations, it is believed that the differences in particle size are correctly represented (Murray, 2002; Blott and Pye, 2006).

1.7.4 Magnetic Susceptibility

Magnetic susceptibility refers to the ease sediment becomes magnetized when introduced into a magnetic field and is measured with the magnetic field (H) divided by magnetization (κ) per unit volume (M) ($M = \kappa * H$). Measurement of the downcore change in magnetic susceptibility has been used in a number of previous studies to determine the onset soil erosion impacts, the onset of land clearance and deforestation, burning histories and to map environmental pollutants (Clark, 2004).

In order to determine magnetic susceptibility levels, a Bartington Magnetic Susceptibility Meter was used with an MS2F probe (2×10^{-6} SI at 0.1 range – Bartington, 2004). Archived cores were allowed to warm to room temperature, turned over, removed from their core tubes, and the back ~2 cm of sediment removed in order to ensure a lack of metal contamination. Cores were covered with plastic wrap to avoid sediment contamination of the sensor and readings taken every 5 mm, with an air measurement every five to seven measurements prior to re-zeroing the instrument. Results were plotted in Oasis Montaj, corrected for instrument drift and linear susceptibility correlated to core logs.

1.7.5 Trace Metals

Trace metals in the environment allow scientists to discern anthropogenically created pollution levels. Many studies have been carried out on modern-day pollution in near-shore marine settings. The use of trace metal analysis on historic sites has increased over the past decade. Véron et al. (2006) has used lead trace metal and isotope analysis to determine that there was a settlement at the location of Alexandria prior to Alexander's arrival in 332 BC. More recently, trace metal analyses have been completed on surface sediments within the Bay of Izmir as a way to assess pollution levels (Bizsel and Uslu, 2000; Kucuksezgin et al., 2006).

For this study, samples were taken from four sediment cores. LT-04 samples were taken at 20 cm intervals in order to gain a more in-depth look at the 4 lithofacies characteristics. For the rest of the cores, sample sizes varied (Appendix A; Figure 3.8 – Chapter 3).

Metals were digested according to the Environmental Protection Agency 3050B guidelines for trace metal analysis on an Inductively Coupled Mass Spectrometer (ICP-MS). Samples (~2 cc) were placed in crucibles to dry over a 24 hour period. Samples were weighed, and then ground into a fine silt. Samples were re-weighed to determine sediment lost, then placed in Erlenmeyer flasks for digestion. Concentrated ICP-MS grade HNO3 (70%) was diluted to 30% and 10 mL of 1:1 mixture were added to samples. Samples were placed on hot plates for 15 minutes where temperatures ranged from 40-50 degrees C. An additional 5 mL of concentrated HNO3 was added to flasks and heated for 30 minutes until reactions ceased and white fumes observed. Flasks 29-44 required an additional 5 mL of concentrated HNO3.

Samples evaporated overnight to approximately 5 mL, and 10 to 20 mL of 30% H2O2 (2:3 ratio) was added to the samples. Samples 6 through 20 were incorrectly calculated and thus received 15% more H2O2 than other samples. (Note: After samples were run on the Mass Spectrometer, it was found that the trace metals in the high grade H2O2 were negligible for altering sample percentages.) All samples were evaporated to 5 mL and diluted to 100 mL with Distilled Water. Control samples were made without the sediment and extra chemicals were set aside for control analysis.

Samples were run on a Micromass ICP-MS at the University of Wisconsin – Milwaukee. Samples were diluted to a 1:1 dilution for most trace metals. An additional dilution was created of 1:300 for metals that had high concentrations, like Iron (Fe). Samples were tested for As, Fe, Ni, Cd, Cu, Sn, Al, and Pb. Samples were recorded and digitized in Microsoft Excel. The control sample made previously was also run and

concentrations found in the original chemicals were subtracted from metal concentrations.

Many studies have shown that obtaining metal concentrations in parts per million are effective; however there is a certain natural abundance that must be taken into consideration. One way to account for natural metals in the environment is to normalize sample concentrations using Aluminum (commonly called the Mean Enrichment Factor or EF) (Kemp et al., 1976; van Metre and Callendar, 1997). Aluminum is found abundantly in the environment, however humankind did not find a way to extract and use it until the 20th century. Using normalization of to Al also compensates for grain size and mineralogy because aluminum is found in alumino-silicates (typically fine-grained clays) that carry most of the trace metal populations (Abraham, 1998; Tylmann, 2007). By using the equation below it is possible to determine a ratio of anthropogenically placed metals in the environment:

$$EF= (Cx/CAl)s/(Cx/CAl)$$

Where the enrichment factor = the concentration of element (x) over the concentration of Aluminum in the sample divided by the concentration of element (x) over the concentration of Aluminum in unpolluted sediments. A ratio of 1 or more indicates an imbalance and therefore most probably a different source has entered the picture. A ratio of 1 or less indicates natural environments (Tylmann et al., 2007).

In this case, the natural ratio sample was chosen from the base of LT-06. Core 6 is on the western side of the causeway in an area of low deposition. The base, which is almost 3 m under the sediment surface, is most likely free of influence from humankind.

The other ratios from stratigraphically higher samples were compared to the natural state and pollution levels were determined.

1.7.6 Micropaleontology

Foraminifera are single-celled protests (testate rhizopods) that live in all types of salt-water environments. Their calcareous 'test' is preserved in the fossil record and provides an ideal history of local environmental change. Foraminifera are abundant in oceans and seas, and therefore are relatively cheap and efficient to sample, with small sample sizes providing statistically significant numbers. Because the life-span of foraminifera is short, they reproduce quickly and en masse, thus adapting quickly to their environment. The record of these adaptations has been compiled throughout the world, and a comprehensive understanding of these creatures and their environments has aided in many environmental reconstructions (Scott et al., 2001). Geoarchaeologically, Reinhardt et al. (1998) have used foraminifera and their stable isotopes to reconstruct how the ancient harbor at Casearea Maritima off the Israeli coast was destroyed, as well as re-constructing the climatic environment of the living organisms using the isotopes.

A survey of benthic foraminifera in Core LT-04 was completed at approximately 20-30 cm intervals in order to determine large-scale trends within the core. Core 4 was chosen due to the presence of all four historical units and the need to gain further support for the depositional environments.

Samples were chosen from intervals previously analyzed. In some cases, the required 5 cc sample aliquot was not available. In this case, the smaller sample size was

taken then calculated up to 5 cc. Samples were sieved using a 500 um and 63 um sieve, dried, then picked to a statistically significant 300 count or over. Samples were identified using Cimerman and Langer (1991), then plotted in Microsoft Excel for relative abundance.

Individual foraminifera were taken to the McMaster Brockhouse Institute for Materials Research and photographed on a Philips 515 Scanning Electron Microscope. Statistically significant populations were determined according to Rivieros et al. (2007) with the equation: Sxi = 1.96*squarrt(Fi*((1-Fi)/Ni)) where Fi= fractional abundance and Ni = total amount of specimens counted in the sample. Samples were divided to the smallest aliquot (1 cc) and relative abundance placed in Paleontological (PAST) software package to determine diversity indices and cluster analysis (Hammer et al., 2001). The cluster analysis used Q-mode clustering (looking at the relationship between groups to determine if there are patterns) and Ward's method of sorting (using dissimilarity to group clusters using changes in sums of squares) (Davis, 2002). These methods are typically used for micropaleontological work and have proven successful in the past (Fishbein and Patterson, 1993; Reinhardt et al, 2005; Sonnenburg, 2006). Shannon Diversity Index (SDI) was also determined in order to estimate species diversity to determine the richness of the species community (Patterson et al., 2002). Though samples were only counted to the genera level, definite trends were discerned and the term 'biofacies' assigned to major areas between population shifts and were correlated to depositional environments.

1.7.7 Geochronology

Four radiocarbon dates were taken from cores LT-01 and 04. These cores, showing the most complete pre-causeway sediment record, were determined to be prime candidates for sampling in order to discern the causeway horizon (Appendix C). Two samples were taken from LT-04 at 76-77 cm and 171-172 cm. The first sample was taken at the base of an approximately 40 cm thick horizon of olive pits. Klazomenai was known for its olive oil production and thus the olive pits give a spectacular constraint to the beginnings of this industry in the area. The second sample was organics taken from the top of a pebble and shell hash horizon towards the base of the core.

Two more samples were taken from 84-85 cm and 99-101 cm in core LT-01. These samples were bulk organics (rinsed from the sediment) and plant organics (*Posidonia* sp.) respectively. Samples were sent to Beta Analytic and treated using AMS dating (Appendix C).

1.7.8 Bathymetry

Bathymetry data provides a digital model of sea-bed topography. A survey of the area surrounding Liman Tepe/ Karantina Island was conducted using a Knudsen 320 BP single-beam echosounder with a 200 kHz transducer attached to the Zodiac boat (see Boyce et al., in review for set-up). Lines were recorded at 50-75 m spacings in both north-south and east-west transects. Positions were recorded using a Trimble Ag132 Differential Global Positioning System (DGPS) with accuracy to less than 1 m. Data was

processed according to Boyce et al. (in review) and digitized using Oasis Montaj Geosoft software using a minimum curvature grid.

1.7.10 Chirp sub-bottom seismic profiling

Seismic data was acquired on the eastern side of the causeway in order to determine what features existed prior to sediment in-filling after 334 BC. Data was acquired with a Knudsen 24 kHz transducer at 75 m spacings. Data were processed according to Boyce et al. (in review) and analyzed for major return horizons.

Appendix B:
Additional Multi-proxy information for Cores LT-01, LT-02, LT-03, LT-04, LT-05 and LT-06 (not included in analysis)

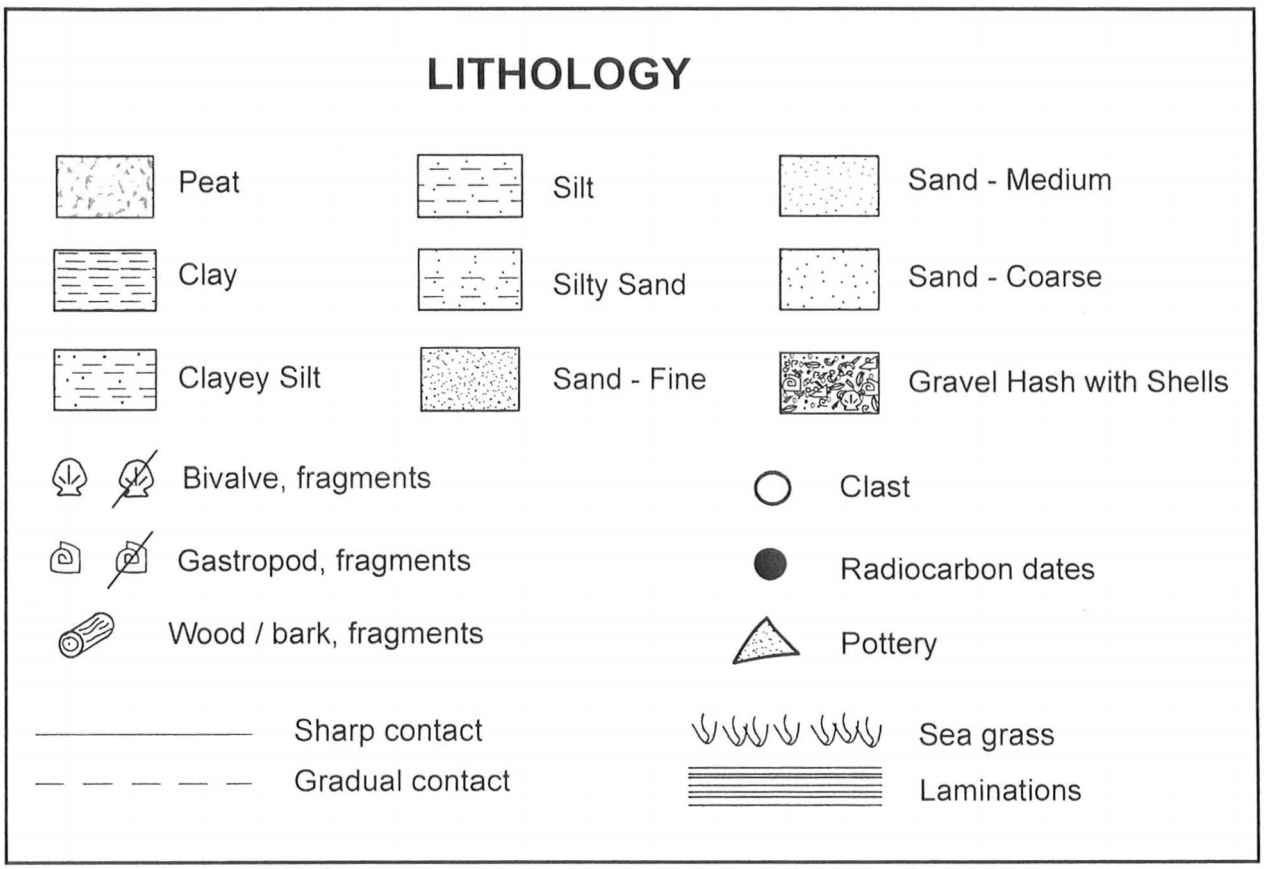

Figure B.1: Lithologic descriptors for core logs

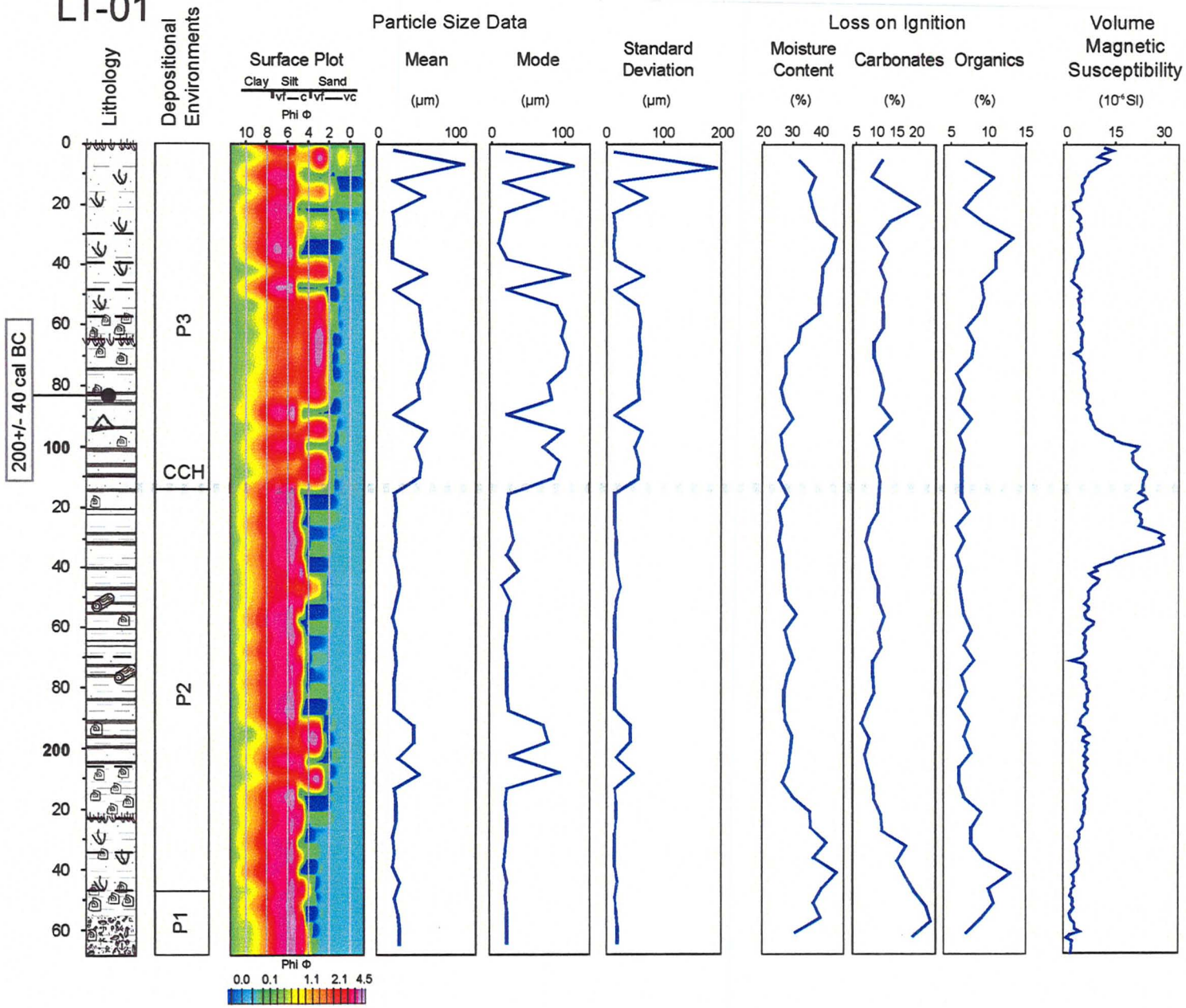

Figure B.2: Particle size and physical property data for core LT-01. The causeway construction horizon (CCH) is identified at 115 cm by an abrupt shift to coarser grain size.

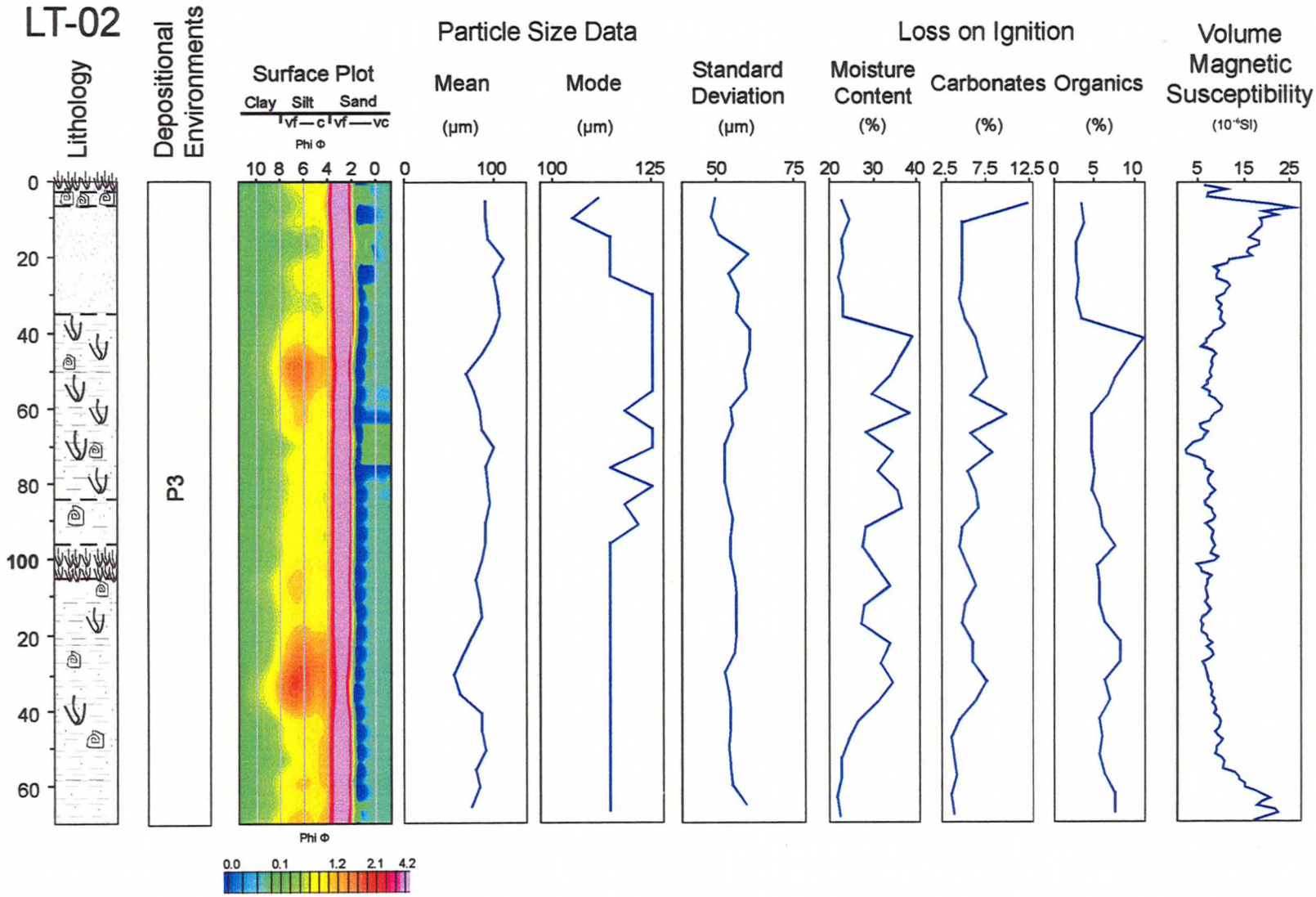

Figure B.3: Particle size and physical property data for core LT-02. P3: Post-causeway (334 BC) deposition.

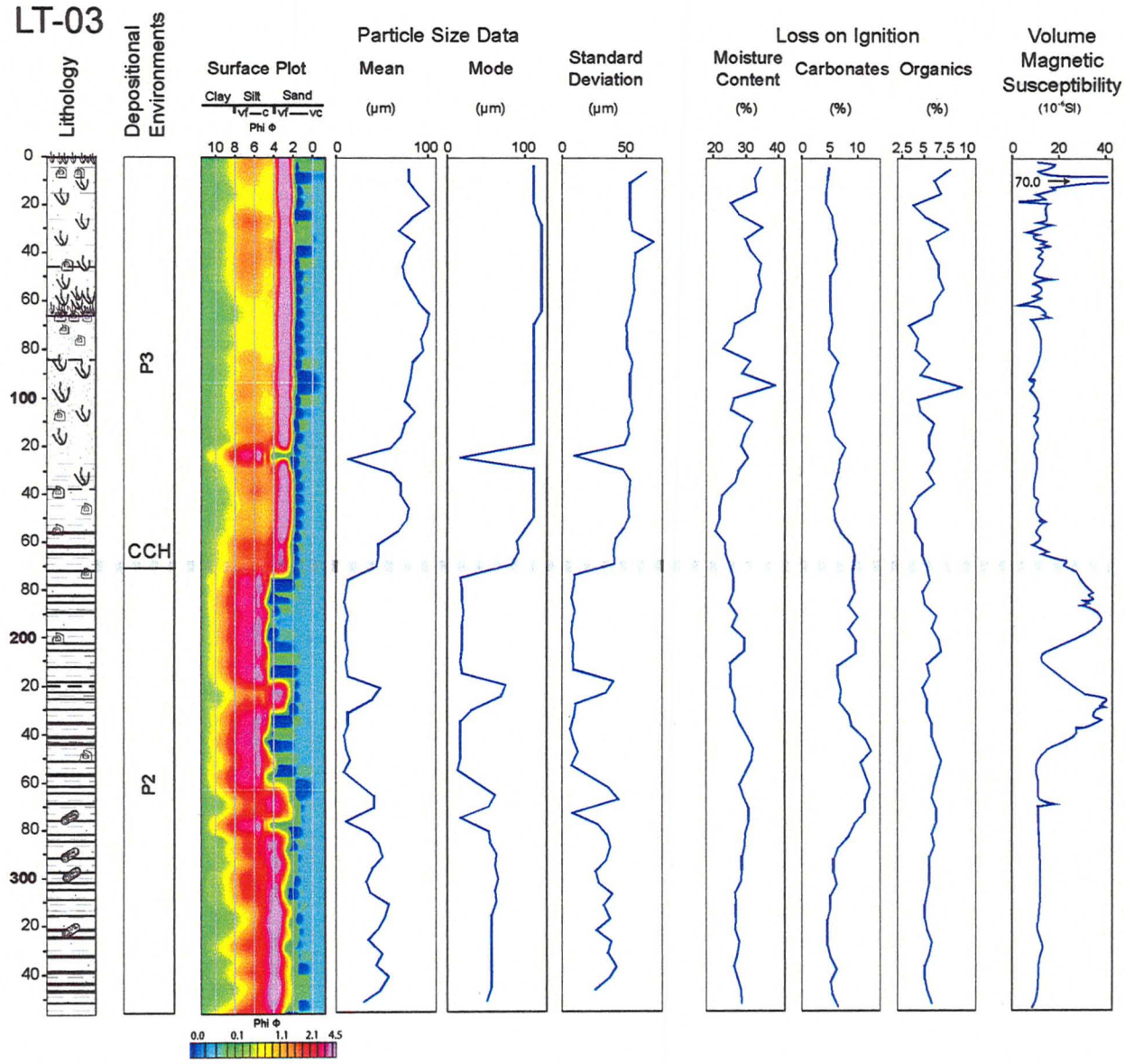

Figure B.4 Particle size and physical property data for core LT-03. P2: Pre-causeway Wetland/Lagoon,.: Post-causeway (334 BC) deposition. The causeway construction horizon (CCH) is indicated at ~70 cm depth by a shift in partile size from silt to coarser sand.

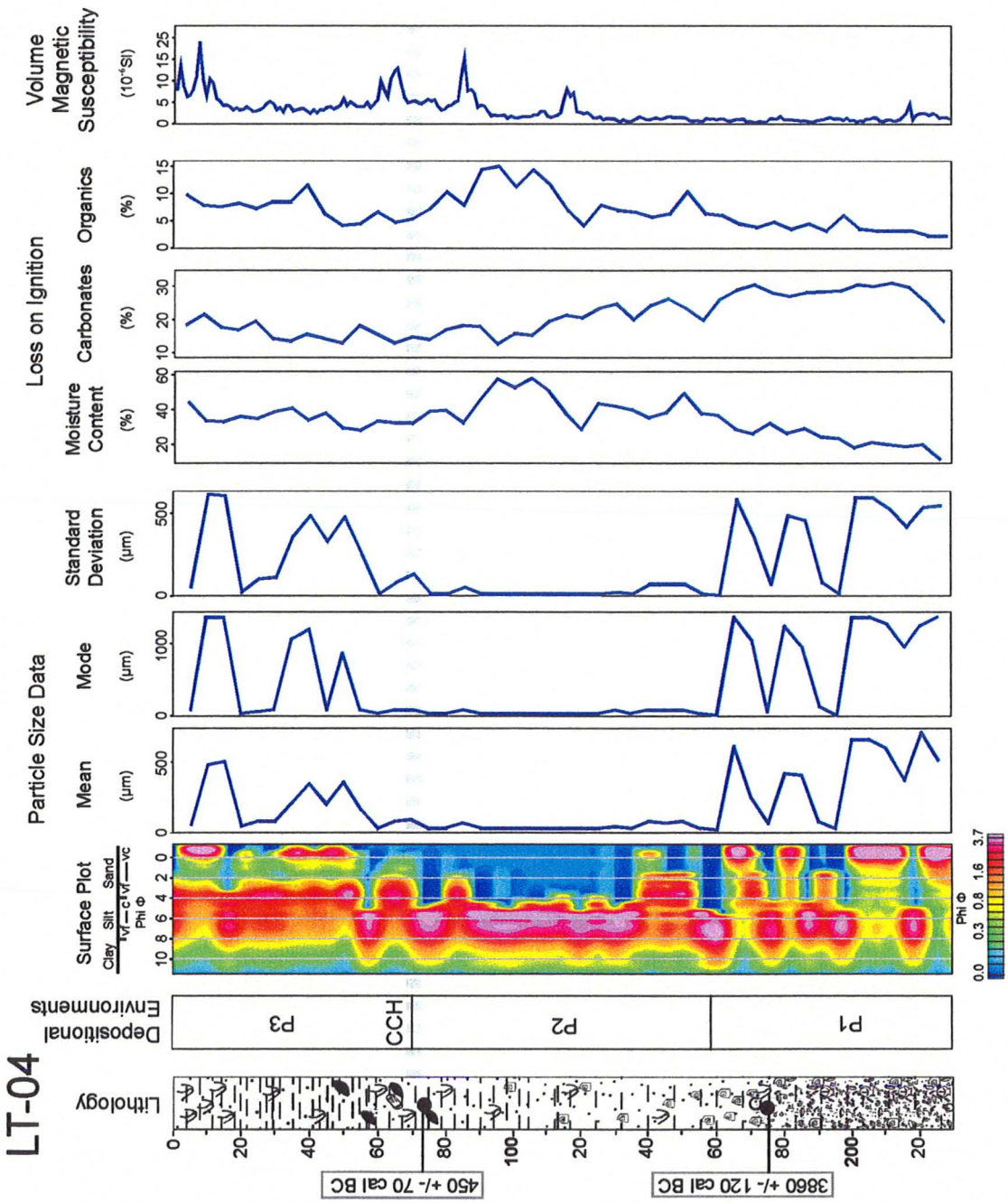

Figure B.5: Particle size and physical property data for core LT-04. The causeway construction horizon (CCH) is indicated at 70 cm by an abrupt shift to coarser grain size. A 14C date obtained on olive pits at 76-77 cm depth yielded an age of 450 +/- 70 cal BC, confirming the 4th c. age for the causeway.

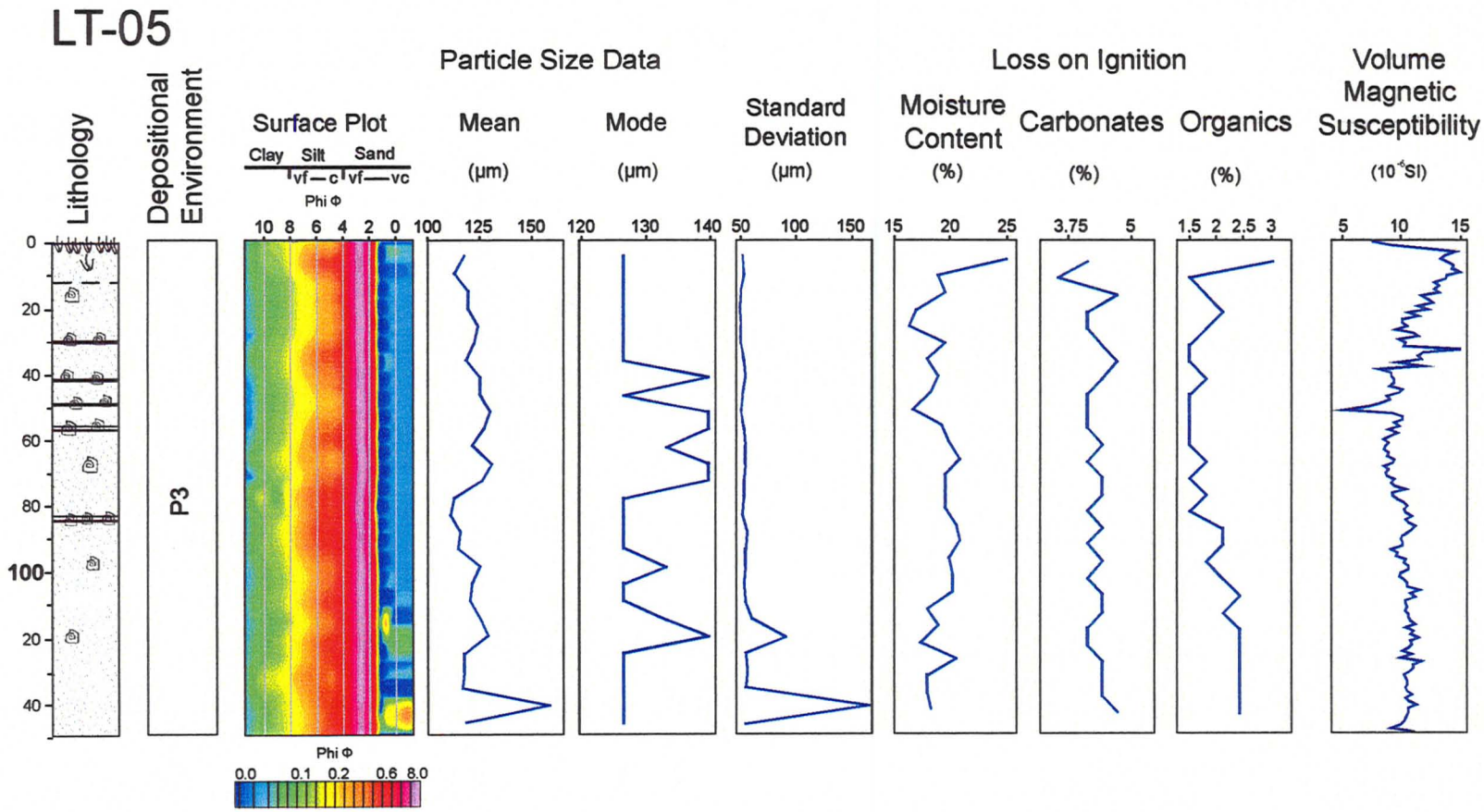

Figure B.6: Particle size and physical property data for core LT-05. P3: Post-causeway (334 BC) deposition.

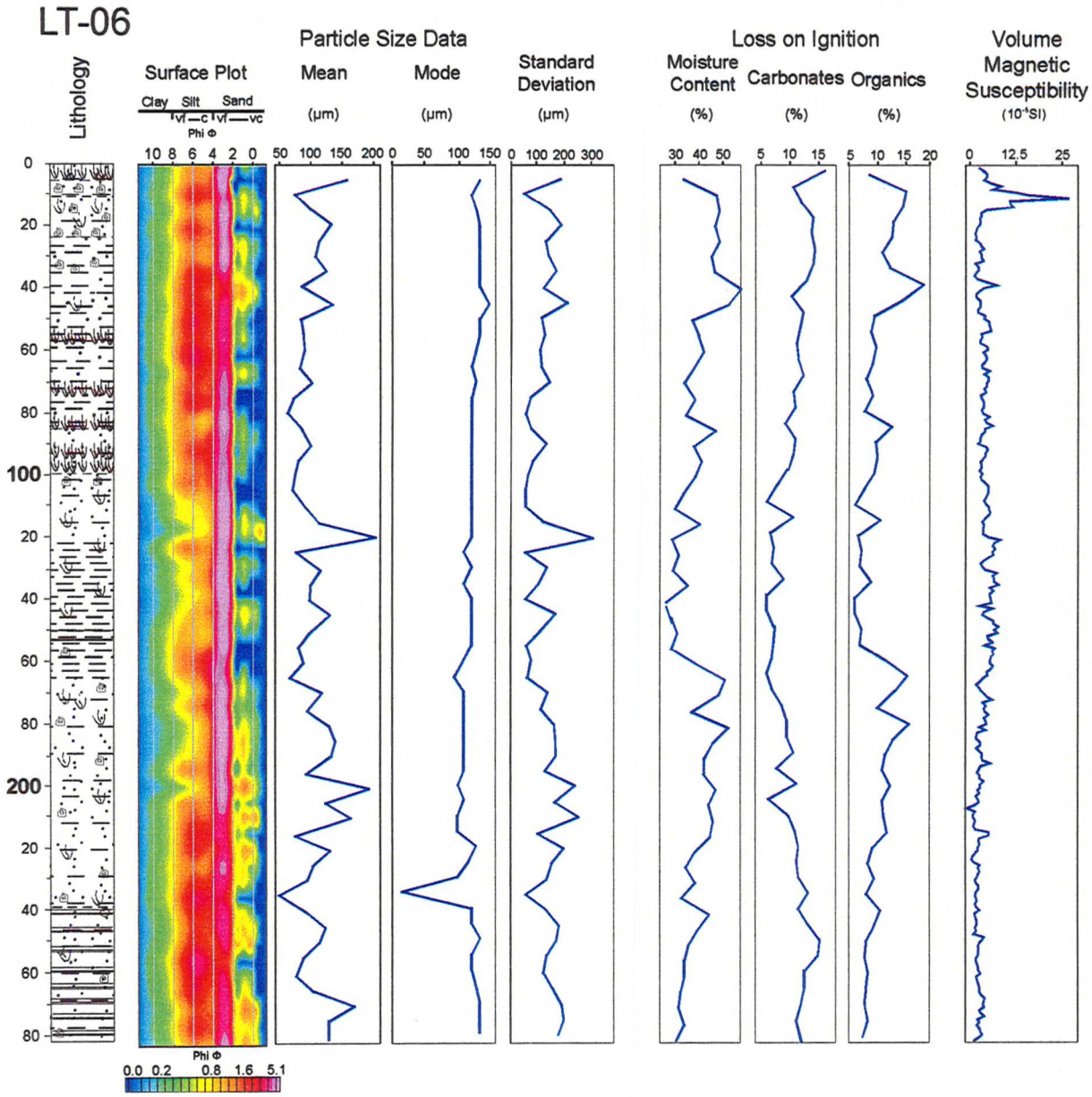

Figure B.7: Particle size and physical property data for core LT-06 (not discussed in this thesis).

Appendix B

Core Number	Water Depth (m)	Length (m)	Easting/Northing
LT2006_01	4.2	2.68	481099.2 / 4246518.3
LT2006_02	3.8	1.70	481046.1 / 4246355.3
LT2006_03	4.5	3.60	481049.8 / 4246349.6
LT2006_04	4.2	2.26	481271.4 / 4246692.0
LT2006_05	1.8	1.50	480977.9 / 4246289.4
LT2006_06	4.5	2.88	480579.7 / 4246240.2

Figure B.8: Liman Tepe/ Karantina Island marine core locations (UTM), depths and lengths.

Appendix C:
Statistics and Foraminifera counts, LT-04

Appendix C: Fractional abundance (%) and standard error (2σ) of LT-04 foraminifera at Liman Tepe/Clazomenae.

Core depth (cm)	**5.5**	**30.5**	**50.5**	**65.5**	**75.5**	**95.5**
Total Count	**267**	**774**	**491**	**240**	**462**	**465**
Specimens per 1cc	**854.4**	**1764.6**	**1301.1**	**384**	**1140.8**	**1488**
Phase	**3**	**3**	**3**	**3/2**	**2**	**2**
Elphidium sp.	*10.4%*	*10.1%*	*6.6%*	*20.4%*	*21.0%*	*11.1%*
Standard error	2.1%	1.4%	1.3%	4.0%	2.4%	1.6%
Ammonia sp.	*7.5%*	*6.5%*	*6.6%*	*15.4%*	*7.7%*	*7.5%*
Standard error	1.8%	1.1%	1.3%	3.6%	1.5%	1.3%
Rosalina sp.	*18.7%*	*14.5%*	*11.1%*	*17.9%*	*34.5%*	*29.2%*
Standard error	2.6%	1.6%	1.7%	3.8%	2.8%	2.3%
Haynesina sp.	*13.4%*	*12.2%*	*13.1%*	*17.5%*	*6.2%*	*15.9%*
Standard error	2.3%	1.5%	1.8%	3.8%	1.4%	1.8%
Asterigerinata sp.	*4.1%*	*3.8%*	*3.4%*	*2.9%*	*4.8%*	*8.6%*
Standard error	1.3%	0.9%	0.8%	1.7%	1.2%	1.4%
Cornuspira sp.	*0.7%*	*0.9%*	*1.4%*	*0.4%*	*0.7%*	*0.4%*
Standard error	0.6%	0.4%	0.6%	0.6%	0.5%	0.3%
Triloculina sp.	*0.8%*	*7.8%*	*7.0%*	*1.7%*	*2.2%*	*1.7%*
Standard error	1.8%	1.2%	1.4%	1.3%	0.9%	0.7%
Quinqueloculina sp.	*16.8%*	*16.7%*	*22.5%*	*7.1%*	*6.9%*	*3.9%*
Standard error	2.5%	1.7%	2.3%	2.6%	1.5%	1.0%
Miliolinella sp.	*4.5%*	*12.6%*	*12.8%*	*0.8%*	*2.1%*	*1.5%*
Standard error	1.4%	1.6%	1.8%	0.9%	0.8%	0.6%
Spiroloculina sp.	*1.5%*	*0.6%*	*0.4%*	-	*0.6%*	*0.0%*
Standard error	0.8%	0.4%	0.3%	-	0.4%	0.0%
Articulina sp.	*1.1%*	*1.4%*	*0.2%*	-	*0.3%*	*0.0%*
Standard error	0.7%	0.6%	0.2%	-	0.3%	0.0%
Vertebralina sp.	*4.1%*	*2.3%*	*1.6%*	-	*0.3%*	*0.4%*
Standard error	1.3%	0.7%	0.6%	-	0.3%	0.3%
Planorbuina sp.	*0.7%*	*2.1%*	*3.5%*	*1.3%*	*1.1%*	*0.0%*
Standard error	0.6%	0.7%	1.0%	1.1%	0.6%	0.0%
Bulimina sp.	*0.4%*	*0.4%*	*0.4%*	*1.7%*	*2.0%*	*2.2%*
Standard error	0.4%	0.3%	0.3%	1.3%	0.8%	0.7%
Bolovina sp.	*4.9%*	*3.5%*	*3.7%*	*8.3%*	*4.6%*	*11.1%*
Standard error	1.4%	0.9%	1.0%	2.8%	1.2%	1.6%
Textularina sp.	-	*0.5%*	*0.4%*	*0.8%*	-	*1.1%*
Standard error	-	0.3%	0.3%	0.9%	-	0.5%
Cibicides sp.	*3.0%*	*4.0%*	*7.2%*	*3.8%*	*5.0%*	*5.2%*
Standard error	1.1%	0.9%	1.4%	1.9%	1.3%	1.1%

Appendix B: Fractional abundance (%) and standard error (2σ) of LT-04 foraminifera continued.

Core depth (cm)	**110.5**	**120.5**	**140.5**	**160.5**	**180.5**	**210.5**	**Shannon**
Total Count	**260**	**390**	**753**	**352**	**448**	**369**	**Diversity**
Specimens per 1cc	**1664**	**2141.6**	**2400**	**1126.4**	**1433.6**	**1180.8**	**Index**
Phase	**2**	**2**	**2**	**1**	**1**	**1**	**-**
Elphidium sp.	*11.9%*	*6.7%*	*5.2%*	*1.7%*	*2.5%*	*2.4%*	*2.29*
Standard error	1.6%	1.4%	0.9%	0.8%	0.8%	0.9%	
Ammonia sp.	*4.6%*	*4.9%*	*4.7%*	*8.8%*	*6.3%*	*1.6%*	*2.436*
Standard error	1.0%	1.2%	0.8%	1.7%	1.3%	2.1%	
Rosalina sp.	*33.4%*	*26.3%*	*2.6%*	*26.7%*	*21.6%*	*14.6%*	*2.348*
Standard error	2.3%	2.4%	1.8%	2.6%	2.1%	2.0%	
Haynesina sp.	*8.5%*	*9.3%*	*8.1%*	*9.9%*	*10.0%*	*16.3%*	*2.423*
Standard error	1.3%	1.6%	1.1%	1.7%	1.6%	2.1%	
Asterigerinata sp.	*5.0%*	*2.8%*	*4.3%*	*4.5%*	*3.1%*	*5.4%*	*2.349*
Standard error	1.0%	0.9%	0.8%	1.2%	0.9%	1.3%	
Cornuspira sp.	-	*1.0%*	*0.7%*	*1.1%*	*0.9%*	*1.9%*	*2.314*
Standard error	-	0.6%	0.3%	0.6%	0.5%	0.8%	
Triloculina sp.	*6.5%*	*10.3%*	*12.5%*	*11.4%*	*14.3%*	*17.3%*	*2.231*
Standard error	1.2%	1.7%	1.3%	1.9%	1.8%	2.2%	
Quinqueloculina sp.	*1.5%*	*14.4%*	*11.7%*	*9.7%*	*17.6%*	*6.8%*	*2.314*
Standard error	1.7%	2.0%	1.3%	1.7%	2.0%	1.4%	
Miliolinella sp.	*3.5%*	*8.2%*	*11.6%*	*12.5%*	*14.7%*	*16.8%*	*2.18*
Standard error	0.9%	1.5%	1.3%	1.9%	1.8%	2.1%	
Spiroloculina sp.	*0.8%*	*2.6%*	*0.8%*	*22.7%*	*0.9%*	-	*2.092*
Standard error	0.4%	0.9%	0.4%	0.9%	0.5%	-	
Articulina sp.	*0.0%*	-	*0.4%*	*0.9%*	*0.2%*	-	*1.696*
Standard error	0.0%	-	0.3%	0.5%	0.2%	-	
Vertebralina sp.	-	*0.3%*	-	-	-	-	*1.425*
Standard error	-	0.3%	-	-	-	-	
Planorbuina sp.	*1.9%*	*3.9%*	*2.4%*	*1.4%*	*0.7%*	*0.3%*	*2.111*
Standard error	0.7%	1.1%	0.6%	0.7%	0.4%	0.3%	
Bulimina sp.	*1.2%*	*1.0%*	*1.1%*	*0.6%*	*0.4%*	*0.3%*	*2.329*
Standard error	0.5%	0.6%	0.4%	0.4%	0.3%	0.3%	
Bolovina sp.	*3.8%*	*5.7%*	*6.4%*	*3.7%*	*5.1%*	*2.2%*	*2.258*
Standard error	0.9%	1.3%	1.0%	1.1%	1.1%	0.8%	
Textularina sp.	*0.4%*	-	*0.7%*	-	*0.4%*	-	*1.826*
Standard error	0.3%	-	0.3%	-	0.3%	-	
Cibicides sp.	*3.5%*	*2.6%*	*3.1%*	*4.8%*	*0.1%*	-	*2.278*
Standard error	0.9%	0.9%	0.7%	1.3%	0.5%	-	

Appendix D:
Radiocarbon date information from Beta Analytic (Florida, USA)

Core	Depth	Beta Sample Number	Measured Radiocarbon Age (Raw date)	13C/12C Ratio	Conventional Radiocarbon Age (Libby Value)	Analysis	Material	2 Sigma Calibration
LT2006-01	84-85 cm	243245	1800 +/- 40 BP	-24.2 o/oo	1810 +/- 40 BP	AMS-Standard delivery	Plant organics	Cal AD 120-260 (Cal BP 1830-1680) AND Cal AD 280-330 (Cal BP 1670-1620)
LT2006-01	99-101 cm	243246	111.1 +/- 0.5 pMC	-13.7 o/oo	108.6 +/- 0.5 pMC	AMS-Standard delivery	Plant material	Age of 0 BP, material living within the last 50 years
LT2006-04	76-77 cm	234186	2330 +/- 40 BP	-23.4 o/oo	2360 +/- 40 BP	AMS-Standard delivery	Olive Pits	Cal BC 520 to 380 (Cal BP 2470-2330)
LT2006-04	171-172 cm	234187	4910 +/- 40 BP	-14.1 o/oo	5090 +/- 40 BP	AMS-Standard delivery	Plant organics	Cal BC 3970-3790 (Cal BP 5920 to 5740)

All dates provided by Beta Analytic, Miami, Florida